HETEROGENEOUSLY COUPLED NEURAL OSCILLATORS

A Thesis
Presented to
The Academic Faculty

by

Patrick J. Bradley

In Partial Fulfillment
of the Requirements for the Degree
Doctor of Philosophy in the
School of Physics

Georgia Institute of Technology
April 2010

HETEROGENEOUSLY COUPLED NEURAL OSCILLATORS

Approved by:

Professor Robert Butera, Advisor
School of Electrical and Computer Engineering
Georgia Institute of Technology

Professor Kurt Wiesenfeld, Co-Advisor
School of Physics
Georgia Institute of Technology

Professor Daniel Goldman
School of Physics
Georgia Institute of Technology

Professor Michael Schatz
School of Physics
Georgia Institute of Technology

Professor Robert Clewley
Department of Mathematics
Georgia State University

Date Approved: April 2, 2010

To my mother, her love gives my universe two constants.

PREFACE

There are a multitude of mathematical models of neurons today. Using these, countless predictions about network behavior have been made. Experimental verification of these predictions are far fewer in number. The main reason for this is the difficulty in performing experiments with real, living neurons and particularly with neural networks. There are also problems with the models, themselves. Physics is sometimes described as "the art of approximation." We physicists, hopefully, have been trained to seek out the most simple description of any system, removing any variables deemed "negligible" with respect to the information desired. In the field of biophysics this is a daunting task. The word *simple* in the sense that we physicists think seems to have no place in a description of a biological system. The theoretical physicist desires to bound (within an order of magnitude) every variable in a given model to identify exactly which one(s) he can "throw out." Then, he can explain to the experimenter which are the important processes to watch and control. This approach becomes derailed when he realizes that any variable in a remotely tractable neuron model is already a huge approximation of tens, hundreds or even thousands of individual, biological mechanisms.

What to do? We feel that qualitative predictions are extremely useful in neuroscience today. These are more robust and more easily verified by experiment than quantitative predictions. Bifurcation theory has grown in popularity in describing individual neurons as well as networks. Bifurcation theory lends itself to a qualitative understanding, which is not synonymous with a less fundamental understanding, of a system. Our main focus is to expand on previous bifurcation analysis of two-neuron networks, with identical neurons and identical coupling. Our expansion comes as

heterogeneity in the coupling between the neurons, which is not a negligible effect.

One of the ways the brain represents information is in phase differences between coupled neurons. It has been previously shown that these phase differences exhibit a dependence on synaptic rate constants. We have developed bifurcation diagrams of equilibrium phase difference versus the synaptic rate constant. We show heterogeneities in coupling break the symmetry of these bifurcation diagrams causing important qualitative changes to the dynamics of systems of coupled neurons.

The predictions we can make from our study are qualitative, but similar qualitative trends can be observed in experiments.

ACKNOWLEDGEMENTS

My first thanks is to my Mother, you have talked me down off of countless ledges throughout my years. I could not be any luckier than to have you in my life. My Step-Father, for bringing some calm into a family that is otherwise lacking. My brother Tom, for being more fatherly than brotherly, when it was needed. My brother Chris, for being the first influence in my life towards intellectual pursuits. And collectively I thank my family for believing in me, regardless of how little I believe in myself.

Thank you Professor Butera, for finally getting me to focus on a topic and graduate! Thank you for every time you were excited about an idea or result I showed you, those times were always revitalizing. Professor Wiesenfeld, thank you for attempting to get me to think and communicate clearly. You have helped me become a better scientist. I thank Professors Michael Schatz, Daniel Goldman and Robert Clewley for taking the time to be a part of my thesis committee. Dr. Jianxia Cui, you were the closest thing to a partner I had during this work. I am indebted to you for your assistance both scientifically and organizationally. Dr. Brandon Donehoo, you were my "Ambassador to the South" and you were always a positive influence on me both academically and spiritually. Dr.'s Jonathan Halcrow and Domenico Lipolis, I thank you for being good friends and for your always willingly provided mathematical assistance. And lastly, Dr. Zangwill, I entered your office a number of times over the years expecting for you to suggest I drop out of the program. Thank you for always pushing me forward.

To all my friends in Atlanta outside of the physics department, I am lucky to have you. I certainly could not have completed this work without your support and occasional reminders about how but for the grace of God...

TABLE OF CONTENTS

LIST OF TABLES

LIST OF FIGURES

SUMMARY

The work we present in this thesis is a series of studies of how heterogeneities in coupling affect the synchronization of coupled neural oscillators. We begin by examining how heterogeneity in coupling strength affects the equilibrium phase difference of a pair of coupled, spiking neurons when compared to the case of identical coupling. This study is performed using pairs of Hodgkin-Huxley and Wang-Buzsaki neurons. We find that heterogeneity in coupling strength breaks the symmetry of the bifurcation diagrams of equilibrium phase difference versus the synaptic rate constant for weakly coupled pairs of neurons. We observe important qualitative changes such as the loss of the ubiquitous in-phase and anti-phase solutions found when the coupling is identical and regions of parameter space where no phase locked solution exists.

Another type of heterogeneity can be found by having different types of coupling between oscillators. Synaptic coupling between neurons can either be exciting or inhibiting. We examine the synchronization dynamics when a pair of neurons is coupled with one excitatory and one inhibitory synapse. We also use coupled pairs of Hodgkin-Huxley neurons and Wang-Buzsaki neurons for this work. We then explore the existance of $1:n$ coupled states for a coupled pair of theta neurons. We do this in order to reproduce an observed effect called quantal slowing. Quantal slowing is the phenomena where jumping between different $1:n$ coupled states is observed instead of gradual changes in period as a parameter in the system is varied. All of these topics fall under the general heading of coupled, non-linear oscillators and specifically weakly coupled, neural oscillators.

The audience for this thesis is most likely going to be a mixed crowd as the research reported herein is interdisciplinary. Choosing the content for the introduction proved far more challenging than expected. It might be impossible to write a maximally useful introductory portion of a thesis when it could be read by a physicist, mathematician, engineer or biologist. Undoubtedly readers will find some portion of this introduction elementary. At the risk of boring some or all of my readers we decided it was best to proceed so that enough of the mathematical (biological) background is explained in the introduction so that a biologist (mathematician) is able to appreciate the motivations for the research and the results presented. We begin with a introduction in nonlinear dynamics explaining the mathematical tools we use to characterize the excitability of individual neurons, as well as oscillations and synchrony in neural networks. The next part of the introductory material is an overview of the biology of neurons. We then describe the neuron models used in this work and finally describe the techniques we employ to study coupled neurons.

CHAPTER I

INTRODUCTION TO NONLINEAR DYNAMICS

In this thesis we deal with systems of coupled non-linear ordinary differential equations ranging from 2 to 12 dimensions. The main tool we use to analyze the non-linear dynamics of these systems is bifurcation theory. Our goal is to describe behavior in a fundamental and general a way, but still be accurate.

The almost limitless complexity in biological networks and their constituent parts cries out for simplifying principles. Much analysis has been performed in the past which was mired in detailed discussions of the specific currents that were present in a given model. It has proved very difficult to make generalizable findings using this type of current analysis. Responses of systems with the same currents can vary and nearly identical responses can be found in neuron models comprised of different currents [16]. This is surprising until one analyzes the bifurcation structure of the models. Now more and more computational neuroscientists are using the tools of bifurcation theory to further explain the dynamics of neurons and neural networks. If you seek to explain a general or fundamental phenomena, a bifurcation analysis may prove more useful than investigating the dynamics of the various currents in the system. We will not provide a formal and complete introduction to bifurcation theory, rather we will attempt in as few formulas as possible to give the reader enough understanding of the theory to appreciate our work.

1.1 One-dimensional systems

Our work analyzes various systems of weakly coupled neurons. The topic of weakly coupled neurons will be covered in the next section in detail. The fact that the coupling is weak will allow us to use an approximation which reduces multidimensional

systems to one dimension.

Consider the smooth, continuous system:

$$\frac{dx}{dt} = \dot{x} = f(x), x \in \Re \tag{1}$$

A good starting point to analyze this system is to determine the equilibrium or fixed points. *Equilibria*, x_e, occur when $f(x_e) = 0$ (Fig. 1). If the initial condition of a one-dimensional system is x_e the system will remain at x_e for all time. The behavior of the system started near the equilibrium, $x_e+\epsilon$, depends on the stability of the equilibrium. We say that a fixed point is *asymptotically stable* if the system returns to x_e as $t \to \infty$. All of the stable fixed points we encounter in our work are asymptotically stable, so we will just call them stable. We call a fixed point *unstable* if the system never returns to x_e nor stays within a finite neighborhood of x_e as $t \to \infty$. We call $x(t)$, the path starting at the initial condition, the *trajectory*. We may also determine the stability of a fixed point from the sign of the derivative of $f(x_e)$. The slope of $f(x)$ at the fixed point is an eigenvalue of the equilibrium. When $f'(x_e) < 0$ the equilibrium is stable and when $f'(x_e) > 0$ the equilibrium is unstable. A fixed point is an attractor of the system. An *attractor* is the set of points which all near by trajectories converge [35]. There is some debate as to the definition of an attractor, but for our purposes the one given is sufficient. For one dimensional systems, stable fixed points are the only possible attractors. Conversely, unstable fixed points are *repellers* meaning that all trajectories starting near the unstable fixed point are driven away from it.

In a smooth, one dimensional system two stable fixed points must always be separated by an unstable fixed point and vice versa. Graphically it is easy to understand the reason. In Fig. 1 it is plain that two successive equilibria cannot have the same slope, only a discontinuity in $f(x)$ could produce that situation.

Now that we have determined the equilibria of $f(x)$, we can construct a phase-portrait of the system. This is a graphical tool which aids in understanding the

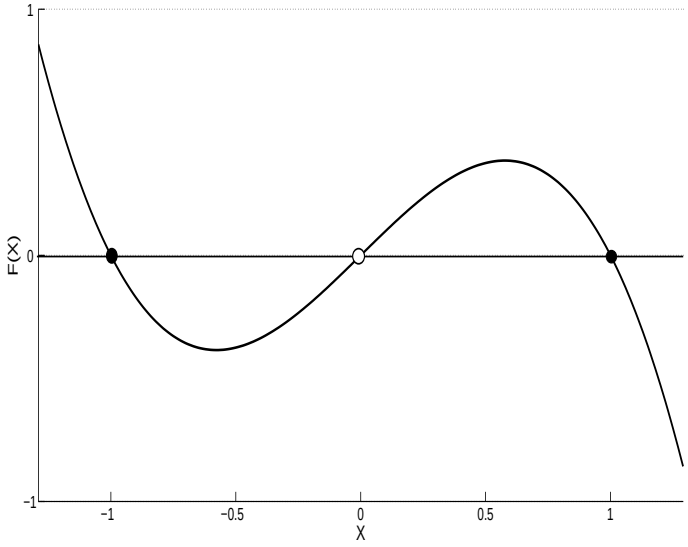

Figure 1: An example function of the right hand side of Eq. 1, $f(x) = x - x^3$ plotted versus x. There are 3 equilibria. The equilibrium at $x = 0$ (open circle) is unstable as $f'(0)$ is positive. The other two equilibria($x_e = -1, 1$) are stable (black circles) fixed points as the slope of $f(x)$ at those points is negative.

dynamics by showing the fixed points of a dynamical system in *phase space*, the set of all possible states for a system. The phase portrait allows us to predict the future of a trajectory given a starting position on the phase portrait. Figure 2 shows the phase portrait using the equilibria we found in Fig. 1. It is here that we first see the importance of finding unstable points. In one dimension the unstable fixed points completely partition the phase space. Although one could never observe the system at rest at an unstable fixed point in an experiment, they still are as important to the dynamics of the system as the stable fixed points. In one dimension, the location of the unstable points with respect to the initial condition determine where the trajectory will travel, as all neighboring trajectories will be driven away from it. One dimensional phase portraits are a good place to introduce the idea of topological equivalence. Two phase portraits are said to be *topologically equivalent* if they can be stretched or squeezed to look the same without changing the sequence or number of equilibria. If the number or sequence of fixed points in a phase portrait change, a

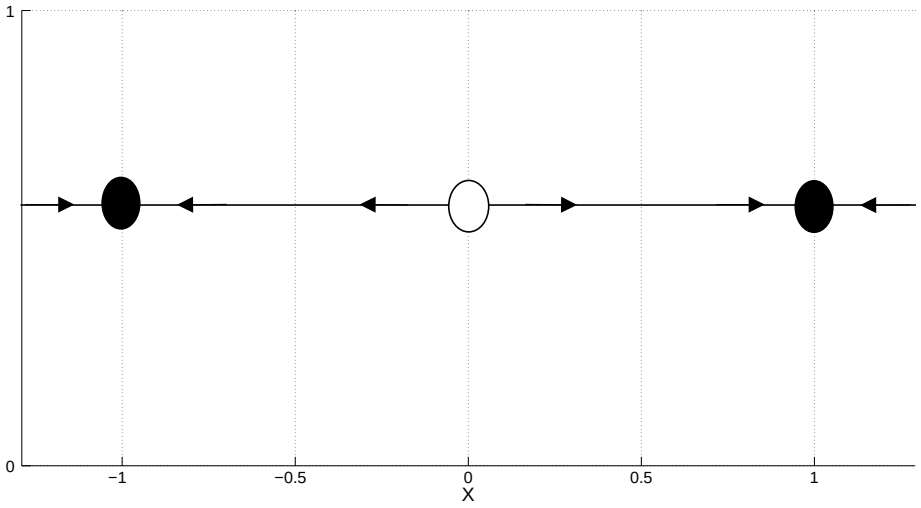

Figure 2: Phase portrait of the the system in Eq. 1.

bifurcation has occurred. We now consider a bifurcation as a qualitative change to the phase portrait of a dynamical system.

1.1.1 Saddle-node bifurcation

Let's consider the system in Eq. 1 with an added parameter b, called a *bifurcation parameter*. By changing the bifurcation parameter we can cause the system to undergo a topological change to the phase portrait.

$$\frac{dx}{dt} = x - x^3 + b = f(x, b), x \in \Re \tag{2}$$

When we change this parameter the curve in Fig. 1 shifts up and down, but does not deform as the parameter just an additive constant. We can consider Fig. 1 to be a plot of $f(x, b)$ when $b = 0$. As we increase b the curve moves upward bringing the stable fixed point at $x = -1$ and the unstable fixed point at $x = 0$ closer together on the $x - axis$. At some critical value of b these two equilibria will meet. This is an example of a *saddle-node bifurcation*. We need the value of the bifurcation parameter, b_{sn} and the variable, x_{sn} to specify the location of the saddle-node bifurcation. At this special point $f(x_{sn}, b_{sn}) = 0$ and $\frac{df(x_{sn}, b_{sn})}{dx} = 0$. Previously we considered the sign of

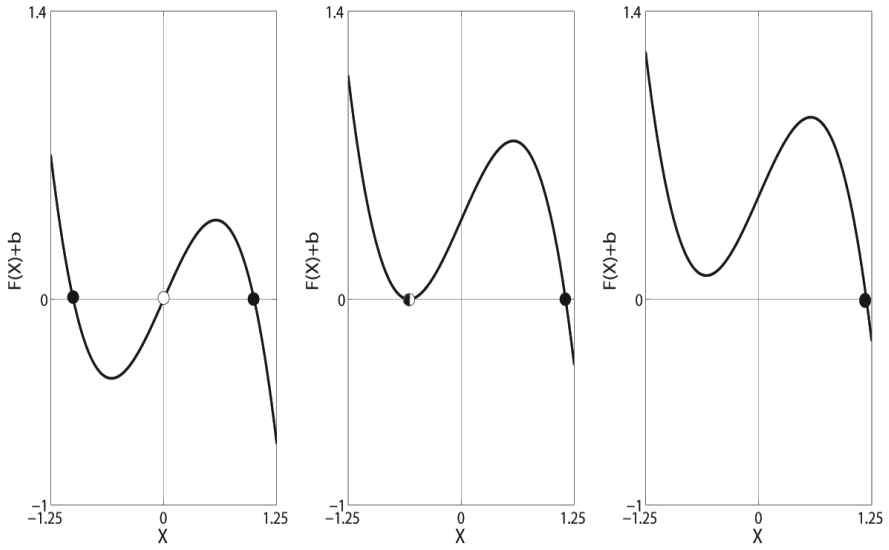

Figure 3: A local saddle-node bifurcation of the system described by Eq. 2. (a) Eq. 2 with $b = 0$. There are 3 fixed points where $f(x, b) = 0$. (b) A saddle-node bifurcation of Eq. 2 with $b \approx 0.384900179$. (c) As b is varied past the bifurcation point in panel (b) the two fixed points have annihilated leaving only a single stable fixed point.

the derivative of $f(x)$ to determine the stability, now this term becomes zero and the stability is called *marginal*. As we increase b further the two equilibria coalesce and annihilate, leaving us a single, stable fixed point. A saddle-node bifurcation either creates or destroys a pair (stable and unstable) of equilibria.

1.1.2 Local and normal

If we look at the plot of $f(x, b)$ near the region of the bifurcation it, looks like a parabola. In general, all saddle-node bifurcations look like parabolas near the bifurcation point. This observation brings up two important ideas: the bifurcation theory we are discussing in this section is *local*; and a general, functional representation of the dynamics exists near a bifurcation, called a *normal form*. The bifurcation theory we are describing is only applicable "in the neighborhood" of a bifurcation. It maybe true that a local bifurcation describes the global behavior of the system, but in general this cannot be assumed. There are techniques for explaining global bifurcation

structures; however, these are far more complex and we do not employ them in this work.

The saddle-node bifurcation is an intuitive place for us to explain the concept of a normal form. The normal form for a saddle-node bifurcation is a parabola with an additive parameter to move the curve up and down.

$$\frac{dx}{dt} = f_{sn}(x, b) = b \pm x^2 \tag{3}$$

Locally, the shape of a curve near a saddle-node bifurcation must be a parabola, as no other shape could provide the creation/annihilation of a stable and unstable fixed point. A Taylor expansion of $f(x, b)$ near the saddle-node bifurcation may be cast in the form of $f_{sn}(x, b)$ in Eq. 3. Figure 1 illustrates the concept of local bifurcation theory. Locally, the two fixed points at $x = -1, 0$ either annihilate one another or are created as a pair depending on the parameter b. We describe the dynamics near the bifurcation point using the normal form of the saddle-node bifurcation, Eq. 3. It is clear that all of this analysis ignores the third fixed point. The full equation has a cubic form which we cannot accurately approximate using a parabola.

A useful way for us to visualize a bifurcation is to plot the fixed points as a function of the variable and bifurcation parameter in a *bifurcation diagram*. Figure 4 shows the bifurcation diagram of the saddle-node bifurcation in Eq. 3.

1.1.3 Transcritical bifurcation

A *transcritical bifurcation* occurs when two fixed points exchange stability. Similar to the saddle-node bifurcation, as we vary the bifurcation parameter an unstable and stable fixed points approach each other and coalesce at a single point. The transcritical differs from the saddle-node in that the two points do not annihilate, rather the stabilities are exchanged and the fixed points separate away from one another as we continue to vary the bifurcation parameter (Fig. 5). The normal form

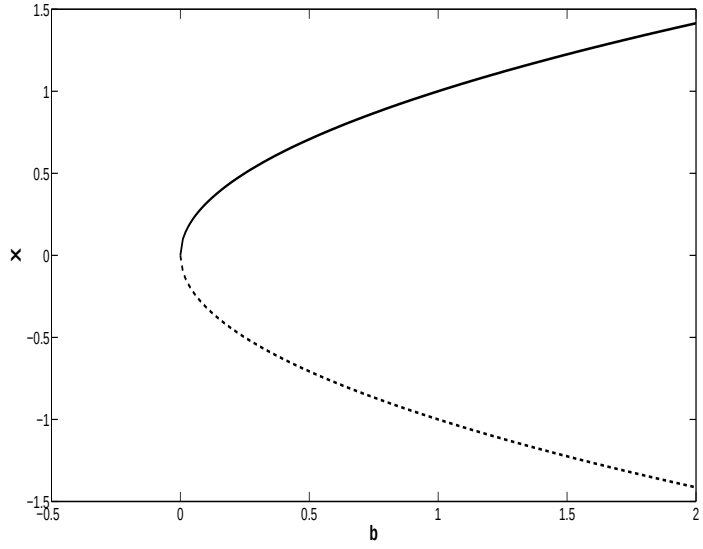

Figure 4: The bifurcation diagram of the saddle-node bifurcation, Eq. 3. The solid lines represent stable fixed points and the dashed lines are unstable. The two parabolic branches of stable fixed points are $x = \pm\sqrt{b}$.

for the transcritical bifurcation is

$$\frac{dx}{dt} = f_{tc}(x, b) = bx - x^2. \tag{4}$$

When we set b greater than or less than (but not equal) to zero, two fixed points exist at $x = 0, b$. The stability of the fixed point at $x = b$ is unstable for $b < 0$ and stable for $b > 0$ (Fig. 6). At the point $(x = 0, b = 0)$ a saddle point exists with marginal stability.

1.1.4 Pitchfork bifurcation

We encounter the pitchfork bifurcation numerous times in our work. A *pitchfork bifurcation* occurs when 3 fixed points are created out of one or vice versa. The stabilities of the various fixed points depend on whether the pitchfork is a sub- or super-critical. The sub-critical pitchfork bifurcation takes one stable fixed point and yields two stable fixed points straddling an unstable fixed point. The super-critical pitchfork bifurcation has one unstable fixed point yield two unstable fixed points

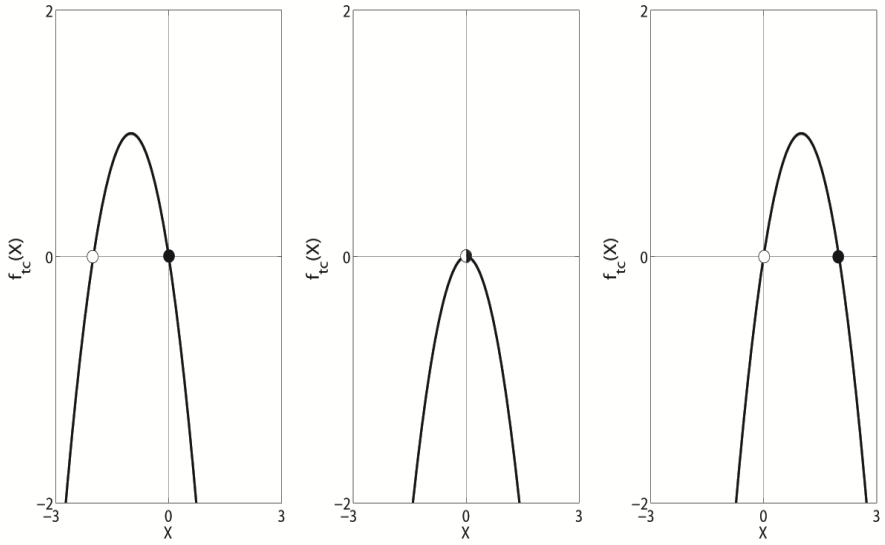

Figure 5: The normal form of the transcritical bifurcation plotted as b is varied through the bifurcation point. The number of fixed points do not change as a result of the bifurcation, but the situation can be interpreted as an "exchange" of stabilities between two fixed points. (a) Eq. 4 plotted with $b = -2$. (b) Eq. 4 plotted with $b = 0$. (c) Eq. 4 plotted with $b = 2$.

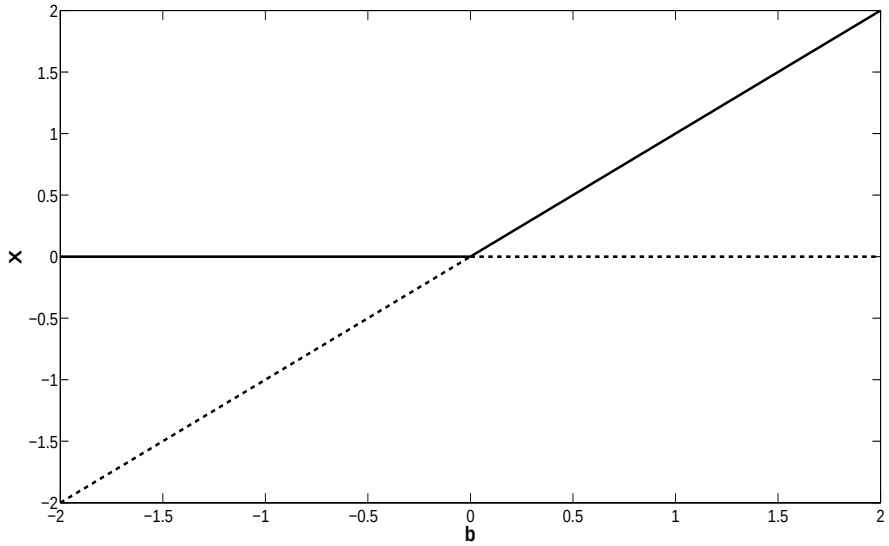

Figure 6: The bifurcation diagram of the transcritical bifurcation. There are two branches of solutions $x = 0$ and $x = b$ which intersect and exchange stabilities at the point $(X = 0, b = 0)$.

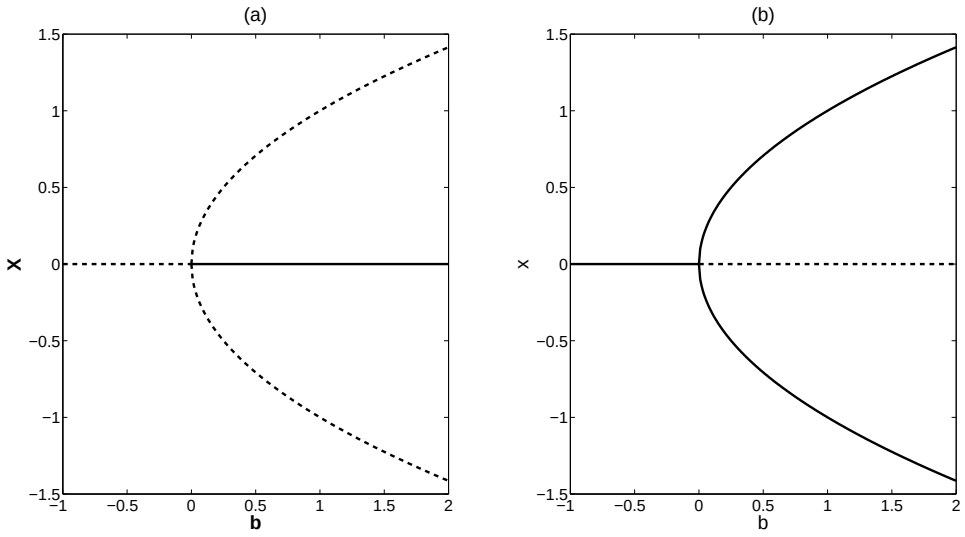

Figure 7: Plots of the two different normal forms of the pitchfork bifurcation Eq. 5. The solid lines are stable fixed points and the dashed lines are unstable. The two parabolic branches of fixed points are $x = \pm\sqrt{b}$. in both diagrams. (a) The subcritical pitchfork bifurcation with a positive cubic term in Eq. 5. (b) The subcritical pitchfork bifurcation with a negative cubic term in Eq. 5.

straddling a stable one.

The normal form for the pitchfork bifurcation is

$$\frac{dx}{dt} = f_{suppf}(x, b) = bx \pm x^3. \tag{5}$$

The sign of the cubic term determines whether the pitchfork is subcritical (+) or supercritical (-).

1.1.5 Imperfect bifurcations

Most of our work is studying how the introduction of heterogeneity to previously symmetric systems changes the resulting behavior. In the coupled pairs of neurons we study we observe both transcritical and pitchfork bifurcations. We can explore how heterogeneity effects the normal forms of these bifurcations by simply adding a heterogeneity parameter, h. For the identical case $h = 0$, any non-zero value of h results in a heterogeneous system.

For the transcritical bifurcation, the imperfect bifurcation has the form

$$\frac{dx}{dt} = f_{imptc}(x, b) = bx - x^2 + h. \tag{6}$$

When $h = 0$ you have the usual intersection of the two branches of fixed points at the transcritical bifurcation point. For $h > 0$ the branches of fixed points are shifted so that they never intersect (Fig. 8(a)). For $h < 0$ the branches of fixed points intersect and "pinch off" before they reach the location of the transcritical bifrucation, yielding two saddle-node bifurcations (Fig. 8(b)).

The existence of a pitchfork bifurcation implies that the system contains a symmetry. Symmetry and symmetry breaking (heterogeneity) are at the heart of this thesis. If we add a second parameter to Eq. 5 we can break the symmetry inherent in the pitchfork bifurcation.

$$\frac{dx}{dt} = f_{imppf}(x, b) = bx - x^3 + h. \tag{7}$$

We refer to Eq. 7 as the *imperfect pitchfork bifurcation*. For $h = 0$ the result is the symmetrical pitchfork bifurcation just discussed. For $h \neq 0$ the pitchfork bifurcation no longer occurs and is replaced by a saddle-node bifurcation and a branch of either stable or unstable solutions depending on the sign of the cubic term.

So far, we have dealt with bifurcations that were completely described by one variable and one parameter. The fact that the pitchfork bifurcation implies a symmetry also implies that there is a higher dimensionality to the bifurcation structure. A codimension 1 bifurcation is essentially a bifurcation that only requires one parameter to be varied in order to completely resolve the structure. A codimension 2 bifurcation needs 2 parameters to do this. The pitchfork bifurcation is a special case of a codimension 2 bifurcation called the *cusp bifurcation*.

1.1.6 Cusp bifurcation

A *cusp bifurcation* occurs at the point where two branches of saddle-node bifurcations intersect. Picture a surface in 3-dimensions (x, b, h) (where h is our second bifurcation

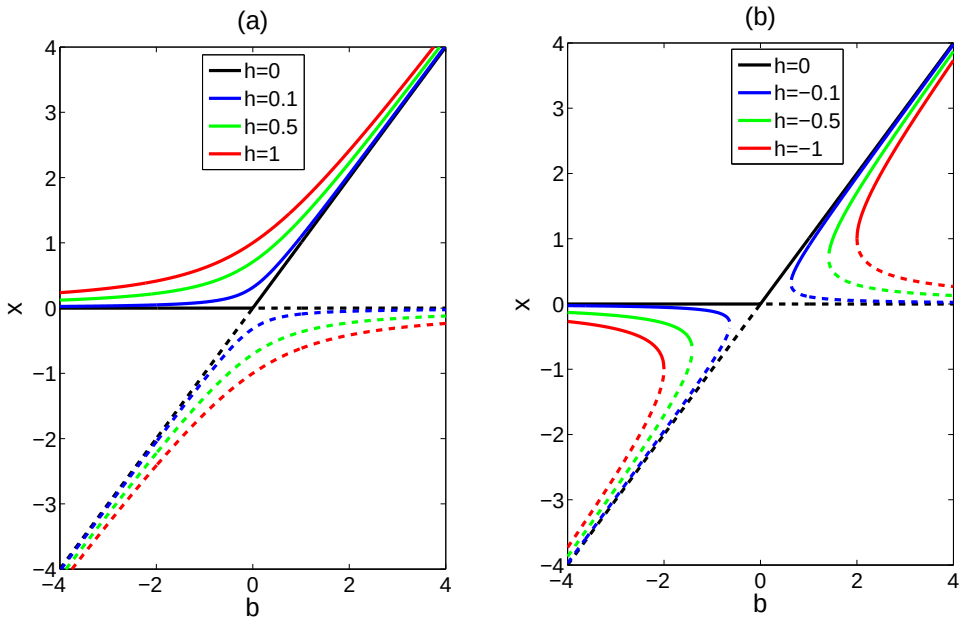

Figure 8: The imperfect Transcritical bifurcation. (a) For $h > 0$ the two branches of fixed points never intersect and no bifurcation occurs. (b) For $h < 1$ the two branches "pinch off" in separate locations causing two saddle-node bifurcations to occur.

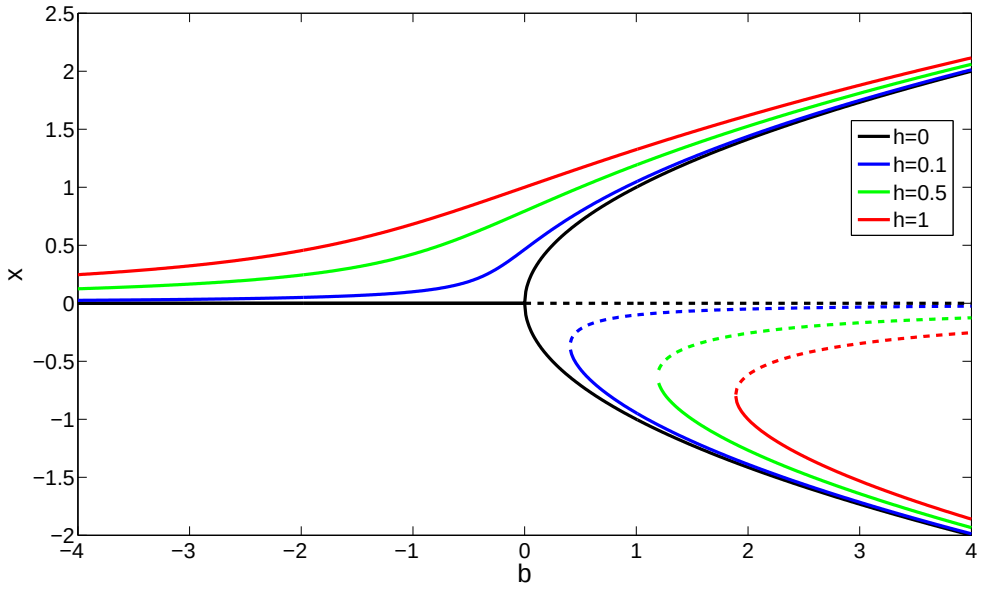

Figure 9: Plotting 4 examples of the imperfect pitchfork bifurcation with h=0 (identical), 0.1, 0.5 and 1. Note that the further from the location of the pitchfork bifurcation the more similar all of the cases become.

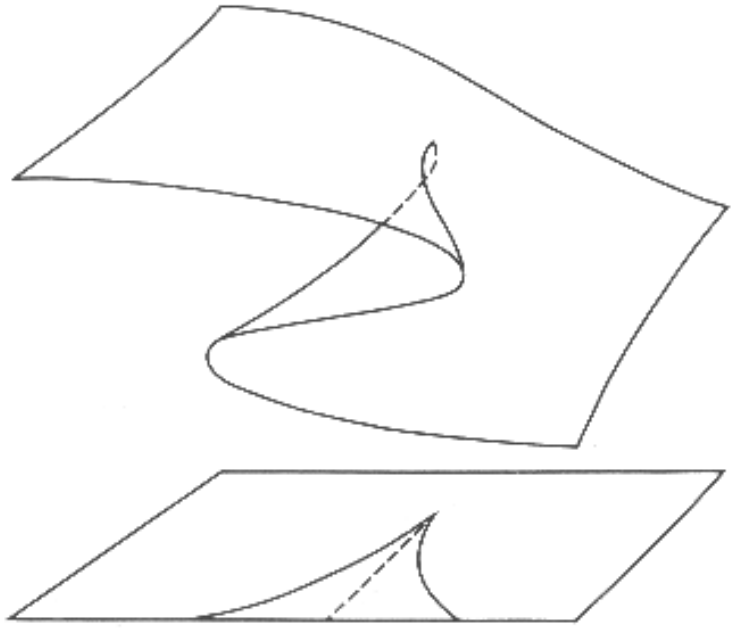

Figure 10: A cusp surface. The two folds represent branches of saddle-node bifurcations. These branches intersect at the cusp point. The branches of saddle-node points are projected down onto a two dimensional surface below the cusp surface. Fixed points are represented by the number of times a straight line in the z-direction pierces the surface. In the two dimensional region between the two branches of saddle-node points a straight line in the z-direction would pierce the surface three times. Outside of that region a straight line in the z-direction will pierce the surface once. (Image courtesy of Robert Gilmore http://lagrange.physics.drexel.edu)

parameter) with two different folds as you travel in the x direction (Fig. 10). The creases of these folds (branches of saddle-node bifurcations) are directed towards each other like a "V" and intersect at the cusp point. Mathematically, we describe the cusp point of the system

$$\frac{dx}{dt} = f(x, b, h) \tag{8}$$

to be when

$$f(x_{cusp}, b_{cusp}, h_{cusp}) = 0, \frac{df(x_{cusp}, b_{cusp}, h_{cusp})}{dx} = 0, \tag{9}$$

$$\frac{d^2 f(x_{cusp}, b_{cusp}, h_{cusp})}{dx^2} = 0, \text{ and } \frac{d^3 f(x_{cusp}, b_{cusp}, h_{cusp})}{dx^3} \neq 0. \tag{10}$$

The normal form of the cusp bifurcation is

$$\frac{dx}{dt} = c_1(b,h) + c_2(b,h)x + c_3 x^3 \tag{11}$$

where the constants can be calculated from the original equation (Eq. 8),

$$c_1(b,h) = f(x_{cusp}, b, h),\ c_2(b,h) = \frac{df(x_{cusp}, b, h)}{dx},\ c_3 = \frac{d^3 f(x_{cusp}, b_{cusp}, h_{cusp})}{6dx^3} \tag{12}$$

We can show that two branches of saddle-node bifurcations occur in the neighborhood of the cusp by setting the right hand side of Eq. 11 and it's first derivative equal to zero and solving the resulting system of equations for c_1. We find that $c_1 = \frac{2}{\sqrt{a}}(\frac{c_2}{3})^{3/2}$.

When considering the cusp bifurcation as the point of intersection of two branches of saddle-node bifurcations we can imagine encountering these branches at different places in the parameter space. The case of symmetrically passing through the cusp point is the pitchfork bifurcation described previously. In our example this would be the equivalent of having $h = 0$. For our example, the parameter h acts as a heterogeneity parameter. As we change h to a non-zero value and begin varying b we now encounter the branches of saddle-node points separately.

1.1.7 Periodic variable in one dimension

We can begin by defining *periodic* to describe behavior that repeats over a fixed interval, the *period*. The most simple system which can exhibit periodic behavior is a one dimensional system with a periodic variable. In general two or more dimensions

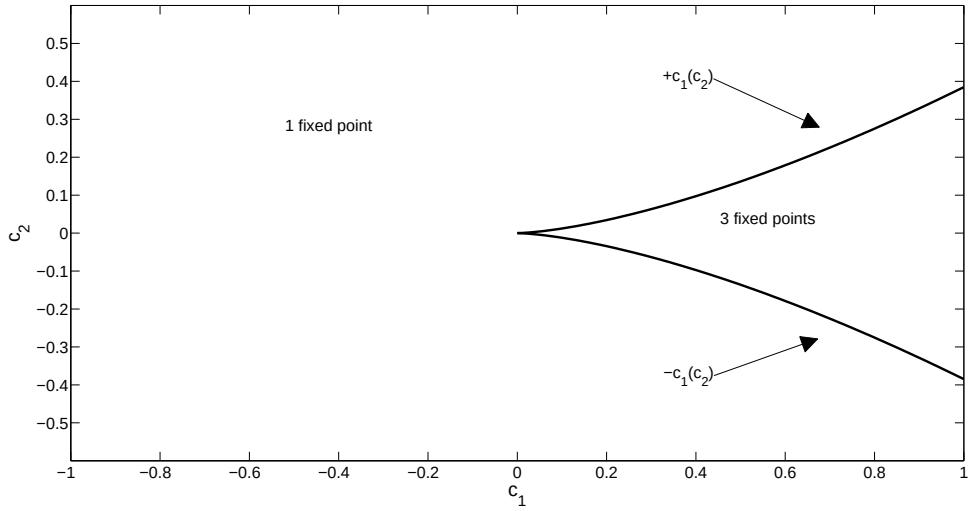

Figure 11: Plotting the two branches of saddle-node points which coalesce at the cusp bifurcation point. Between the two saddle-node branches there are 3 fixed points. Outside of that region there exists a single fixed point.

are required to have periodic motion, but the periodic variable allows this type of motion to exist even in one dimension. An intuitive periodic variable is angular position on a circle, θ. The angle is defined over the interval $0 \leq \theta \leq 2\pi$. If we imagine a bead constrained to move around a circular hoop, moving at a constant angular velocity, the dynamical system is described by

$$\frac{d\theta}{dt} = \omega. \tag{13}$$

The solution to the equation is $\theta(t) = \omega t + \theta_0$. The period of motion is $T = 2\pi/\omega$.

We can consider a more complicated system, where the motion is not uniform.

$$\frac{d\theta}{dt} = \omega - a\cos(\theta). \tag{14}$$

To find fixed points of our one dimensional system with a periodic variable we use the same recipe we used for our other one dimensional systems; calculating when $\dot{\theta} = 0$. We will assume both ω and a are positive constants. In our specific case since $-1 \leq \cos(\theta) \leq 1$, $\dot{\theta}$ can only equal zero if $a > \omega$. For values of $a < \omega$ the system

oscillates, at $a = \omega$ a saddle point appears and for $a > \omega$ there are two fixed points. The behavior of the system is different from the case of a non-periodic variable. No matter what value of θ is used as an initial condition, if $a > \omega$ the system will always come to rest at the stable fixed point. For cases where $a < \omega$ but still close in value to ω, you will see what is called the "ghost" of the attractor. Motion will slow down in the region where the saddle-node bifurcation occurred. Although $\dot{\theta}$ is no longer zero in that region, it is still small so that the motion will be slow. Since the motion is periodic, it will return to this point repeatedly for all time, having a strong effect on the behavior of the system. The ghost of the attractor also exists in the analogous situation in a one dimensional system when the variable is not periodic, but this region will at most be encountered once and will have no effect on the long term behavior of the system.

1.2 Multi-dimensional systems

We have established some basic ground work, but one dimensional dynamics are limited. One dimensional phase spaces can be sectioned off by fixed points. Stable fixed points act as attractors, unstable fixed points are repellers. In two dimensions fixed points still act as attractors and repellers, but they no longer completely partition regions of phase space. Motion is said to be periodic if started at an initial point in phase space $\vec{x}_0$ the system returns to that same point in a finite amount of time, T. A *periodic orbit* is the set of all the points that the trajectory passes through during this finite time. Another way to express it is that for any point on periodic orbit $\vec{x}(t) = \vec{x}(t + T)$. In two dimensions a periodic orbits are now possible and these can completely section off regions of phase space. *Limit cycles* will appear often in our work, these are isolated periodic orbits. This means that neighboring trajectories will either spiral towards (stable) or away (unstable) from the limit cycle. This is because any continuous function that is continuously differentiable will have a unique solution

over any time interval $(-\tau, \tau)$. This is called the existence and uniqueness theorem [35]. If this wasn't true then for a single given initial point there could be multiple solutions. Since every point has a unique solution two trajectories cannot share a point and therefore cannot cross.

1.2.1 Fixed points in two dimensions and beyond - linear stability analysis

Consider the two-dimensional system

$$\frac{dx}{dt} = f(x, y) \tag{15}$$

$$\frac{dy}{dt} = g(x, y). \tag{16}$$

A point(x_0, y_0) is a fixed point of the system if $f(x_0, y_0) = g(x_0, y_0) = 0$. The stability of this fixed point is determined by a similar method to that used to answer the same question in one-dimension. In multi-dimensional systems fixed points may be attractive in one direction while being repelling in another direction. In order to be a stable fixed point, the point needs to be an attractor in all directions. To check the stability we calculate the expansion about the fixed point. To first order the expansion is

$$\delta\dot{x} = \frac{\partial f(x_0, y_0)}{\partial x}\delta x + \frac{\partial f(x_0, y_0)}{\partial y}\delta y + ... \tag{17}$$

$$\delta\dot{y} = \frac{\partial g(x_0, y_0)}{\partial x}\delta x + \frac{\partial g(x_0, y_0)}{\partial y}\delta y + ... \tag{18}$$

This describes what happens when a small perturbation is made away from the equilibrium point. The dynamical equations describing the behavior of the system near the fixed point up to terms linear in x and y are

$$\frac{d}{dt}\begin{bmatrix} \delta x \\ \delta y \end{bmatrix} = \begin{bmatrix} \frac{\partial f(x_0,y_0)}{\partial x} & \frac{\partial f(x_0,y_0)}{\partial y} \\ \frac{\partial g(x_0,y_0)}{\partial x} & \frac{\partial g(x_0,y_0)}{\partial y} \end{bmatrix} \begin{bmatrix} \delta x \\ \delta y \end{bmatrix} \tag{19}$$

The 2×2 matrix of partial derivatives in Eq. 19 is called the *stability matrix* or *matrix of variations* [3]. For a fixed point the stability matrix is equivalent to another

mathematical structure called the *Jacobian*. For limit cycles the stability matrix and the Jacobian are distinct structures. We will discuss the Jacobian more when we examine limit cycles. The stability matrix is one of the most powerful and often used tools by the nonlinear dynamicist. Although this is the first time we encounter this object in name we actually calculated it back when we were only working in one dimension. In that case, we were able to deduce the slope of the zero crossing by looking at the function graphically. The sign of the slope at the fixed point identified the stability. The stability matrix is a generalized slope. In fact it is generalizable beyond two dimensions. If we rewrite Eq. 19 using vector notation we now have an equation for the dynamics near a fixed point for a system of N dimension.

$$\begin{aligned}
\frac{dx_1}{dt} &= f_1(x_1, x_2, ..., x_N) \\
\frac{dx_2}{dt} &= f_2(x_1, x_2, ..., x_N) \\
&... \\
\frac{dx_N}{dt} &= f_N(x_1, x_2, ..., x_N)
\end{aligned}$$

$$\delta\dot{\mathbf{X}} = \mathbf{A}\delta\mathbf{X} \tag{20}$$

where

$$A_{i,j} = \frac{\partial f_i(x_i, ..., x_N)}{\partial x_j} \tag{21}$$

To determine the stability of the fixed point we have to calculate the eigenvalues of $\mathbf{A}$ by a process called *diagonalization*. We accomplish this by calculating the determinant of the stability matrix minus a diagonal matrix with the desired eigenvalues as the diagonal entries. We equate this quantity to zero and solve the characteristic equation for the eigenvalues λ_i.

$$\det(\mathbf{A} - \lambda\mathbf{I}) = 0 \tag{22}$$

The solution to Eq. 20 is

$$\mathbf{x} = e^{\lambda_1 t}\mathbf{e_1} + e^{\lambda_2 t}\mathbf{e_2} + \dots \tag{23}$$

where $\mathbf{e_i}$ are the eigenvectors of $\mathbf{A}$. In general these eigenvalues can be real, imaginary or complex. The stability of the fixed point is determined by the sign of the real part of the eigenvalues. If all the real parts of the eigenvalues are negative the fixed point is stable, if all the real parts of the eigenvalues are positive the fixed point is unstable and if the real parts of the eigenvalues have both positive and negative values then the fixed point is a saddle. The imaginary part of the eigenvalue tells us something about the motion. If no imaginary part exists then a trajectory will fall directly toward or away from the fixed point. If the eigenvalues are complex trajectories will spiral toward or away from the fixed point depending on the sign of the real part.

1.2.2 Limit cycles

We defined limit cycles previously. A stable limit cycle is one which attracts neighboring trajectories, while unstable limit cycles repel the neighboring trajectories. The situation is quite analogous to fixed points. A great deal of information about the nature of the limit cycle can be found by calculating the Jacobian of the limit cycle. We calculate the Jacobian from the matrix of variations as the solution to

$$\frac{d}{dt}\mathbf{J} = \mathbf{A}\mathbf{J}\,, \mathbf{J}(0) = \mathbf{I} \tag{24}$$

integrated around the limit cycle. The task of solving Eq. 24 can be technically challenging. We only give it to show the theoretical underpinnings of what is observed numerically in this work. The eigenvalues of the Jacobian of the limit cycle invariants of the system which helps us determine the attributes of a given limit cycle. Being invariants of the system means that under a smooth change of coordinates these values remain unchanged. Limit cycles are very robust and useful structures in understanding the behavior of a dynamical system. And just as the unstable fixed points were of utmost important in one dimensional dynamics, so are unstable limit cycles in higher dimensional systems.

Periodic behavior (or at least quasi-periodic) is found all throughout the natural

world. Planets orbit stars, stars orbit in galaxies, oceans have currents, hearts beat, neurons spike, the list really goes ad infinitum. In the next section we describe some of the mathematical underpinnings of some of this behavior and set the stage for the techniques applied in the research presented in this thesis. Our work is focused on synchrony which requires multiple oscillating structures, but we have to walk before we can run, or jog at least.

In one dimensional systems the possible bifurcations all came from creating or destroying fixed points or changes of stability. In higher dimensional systems these bifurcations exist, but the possibilities grow as limit cycles can be created and destroyed and they can also interact with fixed points. Systems describing the dynamics of an individual neuron have both quiescent and oscillating states and pass through a bifurcation as the system changes from one state to the other. We will discuss four bifurcations that involve both fixed points and limit cycles. The bifurcations are important in the classification of individual neurons.

1.2.3 Saddle-node on an invariant circle bifurcation (SNIC)

We begin with the case of two fixed points existing on a limit cycle. We already encountered this situation when we examined a one dimensional system with a periodic variable. When we set the bifurcation parameter b less than some critical value, b_c, any initial point in phase space will wind up at a stable equilibrium point (Fig. 12(a)). As we increase b past the critical value the system will oscillate on a stable limit cycle (Fig. 12(c)). The amplitude of this limit cycle will hardly change as we vary b, but the system will begin oscillating with a zero frequency which will increase as we increase b further from b_c. When the two fixed points are "on the limit cycle" what we really have are two heteroclinic trajectories. A *heteroclinic trajectory* is one that starts from an unstable fixed point and ends at a stable fixed point. At the point $b = b_c$ there is a limit cycle with zero frequency (Fig. 12(b)). As we increase b the

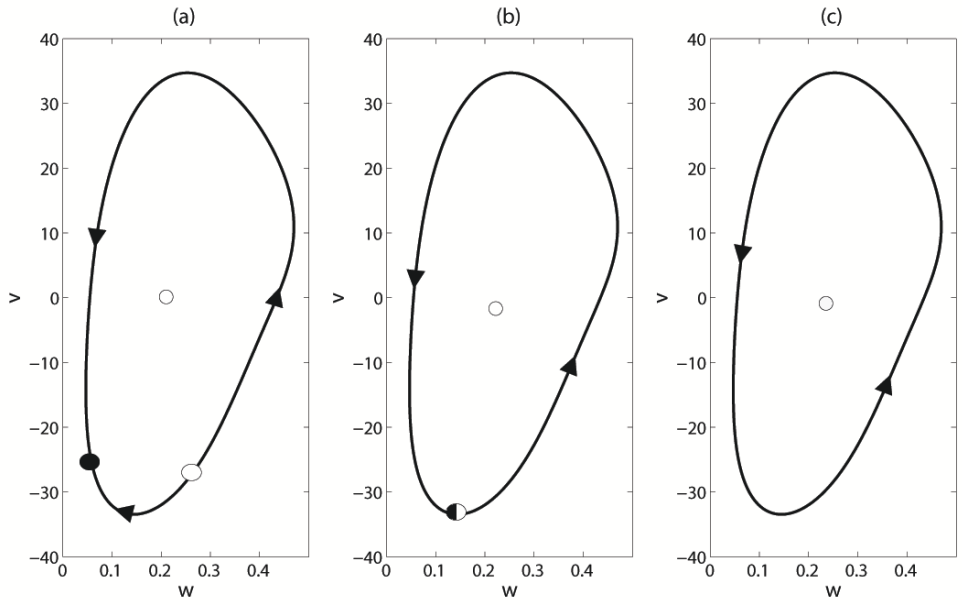

Figure 12: Example of a saddle-node on an invariant circle bifurcation. (a) For $b < b_c$ a pair of fixed points are connected by two heteroclinic trajectories. (b) As the bifurcation parameter, b is increased to $b = b_c$ the fixed points coalesce as a saddle-node and one of the heteroclinic trajectories disappears. (c) For $b > b_c$ there are no fixed points and all that is left is the limit cycle.

frequency will increase. The velocity of the trajectory will slow down as it passes through the region where the saddle-node bifurcation occurred. Just as in the case of the periodic variable in one dimension, the trajectory is passing through the "ghost of the attractor" which dissipates as b is increased further from b_c.

1.2.4 Saddle-node off of an invariant circle

A saddle-node off an invariant circle bifurcation has a stable limit cycle and a pair of fixed points which lie outside of the limit cycle when $b < b_c$ (Fig. 13(a)). This system has a bistability. The system can either be at rest at the stable fixed point or oscillating on a stable limit cycle. When we set $b = b_c$ the two fixed points coalesce as a saddle-node (Fig. 13(b)). If we increase $b > b_c$ only the stable limit cycle remains and all trajectories are attracted to it (Fig. 13(c)). In this situation, the "ghost of the attractor" does not lie on the limit cycle like the SNIC situation, so oscillations begin

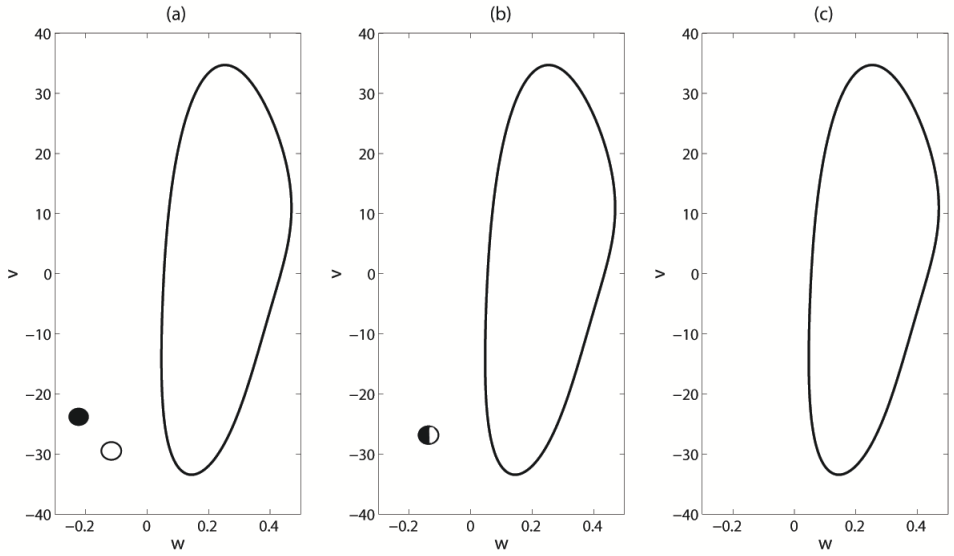

Figure 13: Example of a saddle-node off of an invariant circle bifurcation. (a) For $b < b_c$ a stable and unstable pair of fixed points exist outside of a stable limit cycle. (b) When $b = b_c$ the fixed points coalesce as a saddle-node. (c) For $b > b_c$ there are no fixed points and all that is left is the limit cycle. The "ghost of the attractor" does not lie on the limit cycle, so when oscillations first appear they occur at a finite frequency.

at a non-zero frequency. This is an important, qualitative difference when compared to the SNIC bifurcation.

1.2.5 Andronov-Hopf bifurcation

In Andronov-Hopf bifurcations (HB) a limit cycle is either created or destroyed at a fixed point and the fixed point changes stability in the process. A subcritical HB begins a stable fixed point inside an unstable limit cycle which is itself inside a stable limit cycle (Fig. 14(a)). As we increase b, the unstable limit cycle decreases in amplitude until it is reduced to a point on top of the stable fixed point (Fig. 14(b)). The unstable limit cycle no longer exists and the fixed point becomes unstable. This leaves a stable limit cycle surrounding an unstable fixed point (Fig. 14(c)). Dynamically, if the system was at rest at the stable fixed point and we increased b beyond the bifurcation point, the system would then begin to oscillate on the stable limit

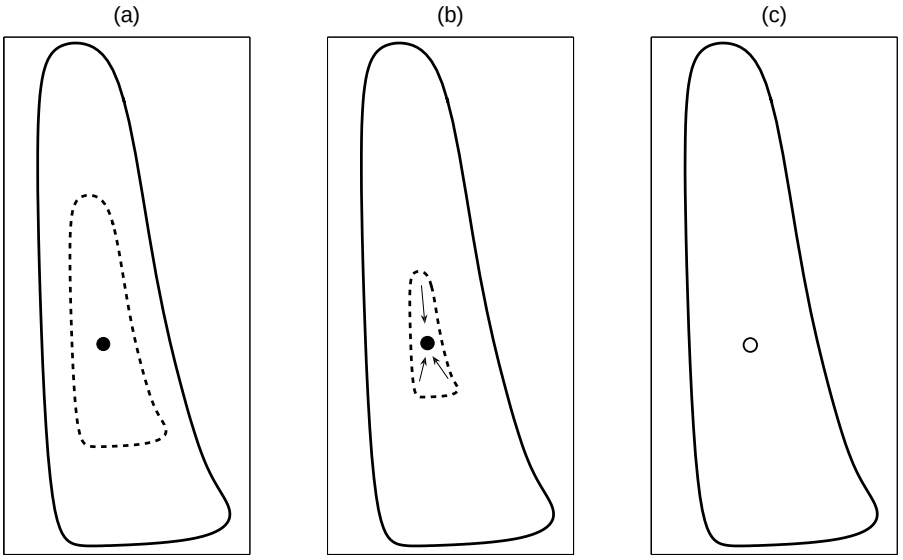

Figure 14: Example of a sub-critical Andronov-Hopf bifurcation. (a) $b < b_c$ a stable fixed point exists inside an unstable limit cycle which is itself inside a stable limit cycle. (b) As we increase b the amplitude of the unstable limit cycle decreases until it collapses on the stable fixed point. At the bifurcation point, $b = b_c$ the fixed point becomes unstable and the limit cycle disappears. (c) For $b > b_c$ a stable limit cycle exists with an unstable fixed point inside.

cycle with a finite amplitude and non-zero frequency. The frequency would not vary significantly as we continued to increase b.

The second HB is the supercritical HB. This bifurcation occurs when a stable fixed point (Fig. 15(a)) changes stability and a stable limit cycle begins to expand out of it (Fig. 15(b)). As we increase b further the amplitude of the stable limit cycle increases (Fig. 15(c)). A system which begins to oscillate after passing through a supercritical HB will begin oscillating with an arbitrarily small amplitude but non-zero frequency.

1.2.6 How do we find periodic orbits?

If someone gives us a set of equations and asks us to find the periodic orbits (if there are any) how do we proceed? There are some analytic techniques, mostly for proving that periodic orbits do not exist. We can consult [35] for an introductory review of these analytic techniques or [3] if we want to get serious about dealing with periodic

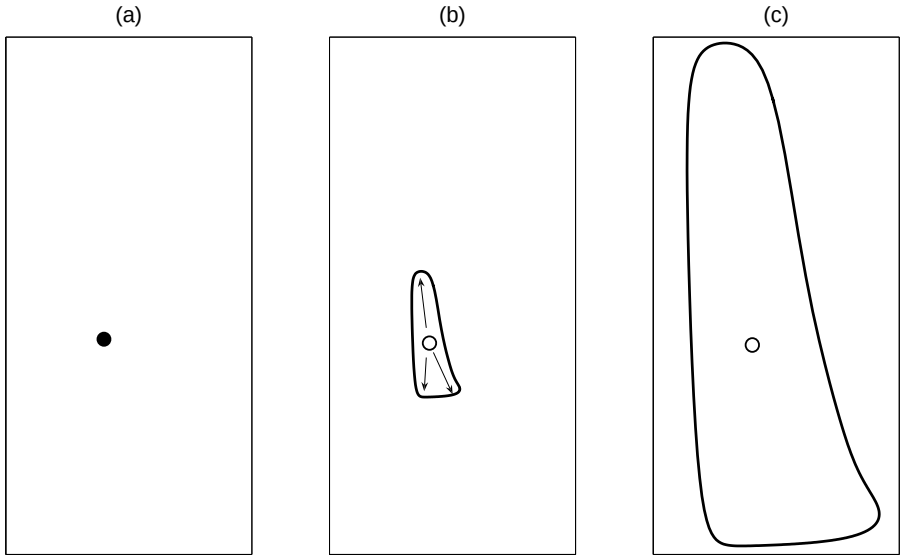

Figure 15: Example of a super-critical Andronov-Hopf bifurcation. (a) $b < b_c$ a single stable fixed point exists. (b) When $b > b_c$ a stable limit cycle appears from the fixed point and the fixed point turns unstable. (c) As we increase b further the amplitude of the stable limit cycle increases.

orbits and...*chaos*!

In our work we deal with periodic orbits in a couple of ways. The first method is to try and avoid them! We use a phase reduction to reduce our problem down to one dimension. This phase reduction method is limited in what information it can provide about the system, but it happens to be very useful when we want to know about synchronization properties of coupled oscillators. When a phase reduction will not work we use a technique involving return maps to find periodic orbits.

1.2.7 Return maps

Up to this point we have been exclusively discussing *flows*, dynamical systems with continuous time. *Maps* are dynamical systems with discrete time. There is no one rule to the discretization of time in a map. A discrete map can be derived from a continuous system. For example, we can strobe the system at fixed intervals of time or we can record values only when specific events occur. The choice of the type of

discretization depends on the job we want to do.

For our purposes we use return maps. To create a return map we must choose a *Poincaré section*, an $N-1$ dimensional surface in an N dimensional phase space. The choice of exactly what section we use is quite arbitrary and is somewhat of an art form. The main idea is that we create a surface, the Poincaré section, and start with an initial condition on the surface. Next, we integrate the equations forward in time until the trajectory intersects the surface again, traveling in the same direction as the initial point left the surface. If the trajectory intersects the surface at the same point as the initial point, we have found a point on a periodic orbit! Note the importance of the direction. In order to make this calculation we need to define a Poincaré section and a direction. This also implies that the flow cannot be parallel to the section or you will have an ambiguous result.

This sounds simple enough, but there are an infinite number of initial conditions, so finding that one special point takes a little care. The following example will show how find a periodic orbit in a two dimensional system.

Example: Driven nonlinear oscillator Given the system

$$\dot{x} = -\mu x - x^3 + A\sin t \tag{25}$$

find the periodic orbits as a function of μ.

Because the system is driven we can search for periodic orbits with the same period as the driving force, $T = 2\pi$. We begin our integration at $t = 0$ and continue until $t = 2\pi$. Our Poincaré section is at $t = 2\pi$. This seems to contradict my previous characterization of using a Poincaré section where I said that we begin with an initial condition on the section and integrate until the section is intersected again by the trajectory. Since we know the period of the motion in this example, $t = 0$ and $t = T$ are the same point. We start with a window of N initial conditions

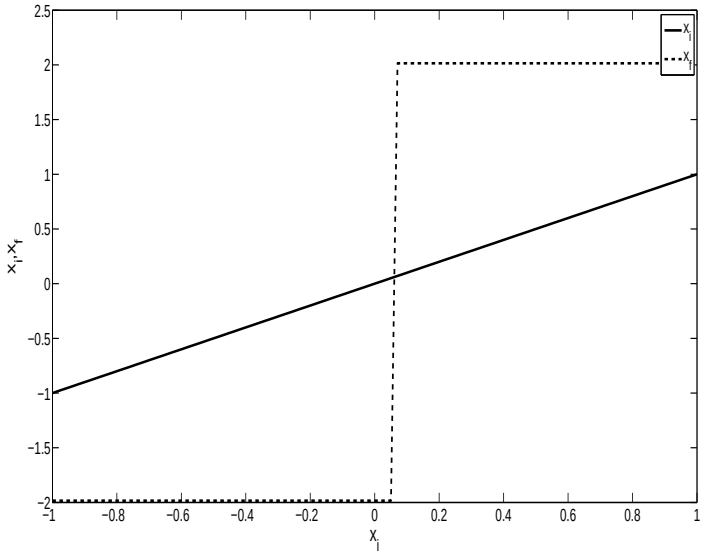

Figure 16: Example return map for the driven nonlinear oscillator with $A = 0.1$ and $\mu = -4$.

$\vec{x}_i = [x(t=0)_1, x(t=0)_2, ..., x(t=0)_N]$ which contain the initial condition for the unstable periodic orbit. We create a return map with the final state of each initial condition after one period, $\vec{x}_f = [x(t=T)_1, x(t=T)_2, ..., x(t=T)_N]$ (Fig. 16). The point at which the line of final positions crosses the line of initial conditions with a positive slope is the initial condition for the unstable periodic orbit. It is likely that we were not lucky enough to have chosen one of our initial conditions as the periodic point. We will have one initial condition which yielded a final position "above" the initial condition and the subsequent initial condition will have a corresponding final value which lies "below" the initial condition. We choose these two values of $\vec{x}_i$ as the boundaries of a new window of initial conditions. We then integrate forward another period and repeat the process. Using this process we iteratively zoom in on the actual value of the initial condition for the unstable periodic orbit to arbitrary accuracy. We then vary the parameter μ and create a bifurcation diagram of the initial condition of the periodic orbit(s) for each value of μ in Eq. 25. The resulting bifurcation diagram is a supercritical pitchfork bifurcation (Fig. 17).

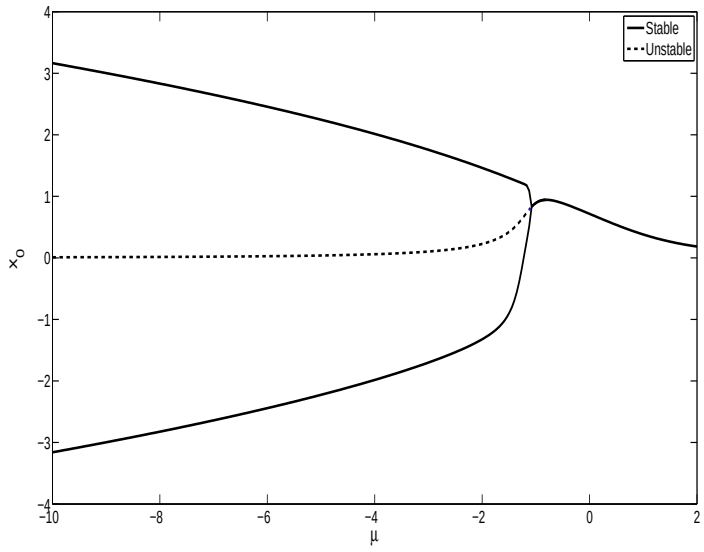

Figure 17: Bifurcation diagram for the driven nonlinear oscillator showing the pitchfork bifurcation of periodic orbits.

CHAPTER II

NEURONS AND NETWORKS

In this chapter we will provide some background about the physiology of individual neurons and the different mathematical models which we use in our work. We will then describe how neurons can be coupled together and how we model neural networks. We will conclude this chapter by describing a technique called the weak coupling approximation, which we employ simplify calculations easier while still yielding accurate results.

2.1 The neuron

Neurons are the fundamental cellular constituent of the nervous system. Neurons are also the fundamental computational unit in the brain. There is a large variation in the morphology and dynamical properties of neurons. Despite this, we can still make reasonable generalizations about the electrical properties of the neuron. The basic neuron structure consists of a soma, an axon, dendrites and terminal buttons. There is a membranous system which surrounds and defines different cell compartments, including the outer cell membrane called the *plasmalemma*. The mathematical models we use in this thesis simulate the dynamics of the voltage across the plasmalemma and various conductances which determine the flow of transmembrane currents in and out of the neuron. These currents are ions moving through the voltage dependent ion gates of the membrane. The *soma* is the central cell body which holds the nucleus, most of the structures for genomic expression and protein synthesis. We stop here in describing the inner-workings of the soma as that information would be superfluous for understanding our work. The *dendrites* are the "input" poles of the neuron and the *axon* is the "output" pole. The branching structure of the dendrites can be very

extensive. Dendrites usually emanate from the soma for vertebrates. In the case of invertebrates, the branches generally arise from the axon. An electrochemical signal called an action potential propagates down the axon away from the soma. Neural networks can be vast and complex having thousands of connections for every neuron. *Terminal boutons* are found at the ends of the branches of the axon. There are several ways which neurons can couple to one another and to other structures. In our work we study chemical coupling. Terminal boutons may form chemical synapses with other neurons and secrete chemicals called neurotransmitters across the synaptic connections. There are many types of *neurotransmitters*, chemicals which either excite or inhibit the post-synaptic cell with regards to the firing of an action potential. The *chemical synapse* is the junction between the terminal bouton of the pre-synaptic cell and the membrane of the post-synaptic cell. We will only study synapses of this type, so from here on we will drop the "chemical" descriptor and just refer to the junctions as synapses.

2.2 The action potential

The production and transmission of action potentials are the basis of the information in a neural network. An *action potential* is a disproportionately large, non-linear voltage response to input signals which are amplified by the voltage dependent ionic currents. The action potential is seen as a large deviation from the resting potential of the membrane. We will often refer to the action potential as a *spike*, referring to the rapid rise and fall from the resting voltage associated with it. The action potential is the fundamental excitable response of the neuron.

2.3 Excitability

Neurons are excitable media. They exhibit highly non-linear responses to inputs which we observe as action potentials. Neurons may also exhibit periodically spiking behavior and may also exhibit what we call bursting. Bursting is when there are

periods of spiking followed by periods of quiescence. When dealing with neurons that spike, but not burst, there are two basic types of excitability into which neurons we classify neurons. These classifications were originally identified by Alan Hodgkin in 1948 [9]. Actually, Hodgkin identified three types, but the third type was essentially characterized by it's lack of excitability. We will only concern ourselves with the first two types. The classification of Type I excitability is typically given to a neuron that enters the oscillating regime of parameter space with a zero frequency and Type II classification is typically given when a neuron begins spiking with a non-zero frequency [29]. Generally, the oscillating regime is entered through an increase in the external applied current to the cell. The reason for these different behaviors is the type of bifurcation which the neuron undergoes as it moves from a resting to a spiking state [31]. The Type I neuron undergoes a saddle-node on an invariant circle bifurcation at this transition. Recall that when the bifurcation parameter (in this case an external applied current) is close to but greater than the critical value near an SNIC bifurcation, the system will oscillate but at an arbitrarily low frequency because of the "ghost of the attractor." The Type II neuron can either go through a sub- or super-critical Andronov-Hopf bifurcation or a saddle-node off of an invariant circle bifurcation. Since none of these bifurcations have the annihilation of fixed points occurring on the limit cycle, the systems begin spiking with a finite, non-zero frequency. The excitability of a neuron will be very important when we begin to consider how neurons respond to external perturbations when in the spiking regime.

2.4 Neuron models

All of the neuron models we use in this thesis can be traced back to their experimental origins. When tracing backward to these origins all the paths will converge to the Hodgkin-Huxley model. The Hodgkin-Huxley model was developed from analysis of Alan Hodgkin and Andrew Huxley's experimental data along with some initial

insights of the two; impressive results that have remained in use for over 50 years and garnered them a Nobel prize. We use both Hodgkin-Huxley and Wang-Buzsaki models in our work. Both of these models describe the dynamics of the transmembrane voltage of a neuron. This voltage depends on the total of the different ionic currents, I_{ionic}, which pass through the membrane through the voltage gated, ion specific, ion channels and any external applied current, I_{stim}. These models have a common form consisting of a voltage balance equation

$$C\frac{dV}{dt} = I_{ionic} + I_{stim} \tag{26}$$

and additional equations which describe the dynamics of *gating variables* which represent the fraction of ion channels of a specific type which are open at a given instant. Gating variables are modeled as both instantaneous functions of the voltage and as functions of voltage with time-dependent dynamics. This second type requires additional differential equations to determine the time dependent nature for these non-instantaneous gating variables. The choice of gating variables and their dependencies is a complex undertaking, there are thousands of these types of models currently in existence.

The last model we introduce described is a different type called a phase model. *Phase models* describe the dynamics of the phase of an oscillator and ignore amplitude changes. These types of models are useful when dealing with weak perturbations which generally only affect the phase of an oscillator and not its amplitude.

2.4.1 Hodgkin-Huxley model

People often hear people refer to a model as being "Hodgkin-Huxley like." Hodgkin and Huxley's landmark work on the giant squid axon revolutionized the field of computational neuroscience. They published a series of 5 papers in 1952 which described the key properties of the ionic conductances underlying the action potential [14, 11, 10, 12, 13] in a giant squid axon. The Hodgkin-Huxley model neuron has

Type II excitability.

The equations for the Hodgkin-Huxley model are:

$$C_m \frac{dV}{dt} = -g_K n^4 (V - E_K) - g_{Na} m^3 h (V - E_{Na}) - g_L (V - E_L) + I_{stim} \tag{27}$$

$$\frac{dn}{dt} = \alpha_n (1 - n) - \beta_n n \tag{28}$$

$$\frac{dm}{dt} = \alpha_m (1 - m) - \beta_m m \tag{29}$$

$$\frac{dh}{dt} = \alpha_h (1 - h) - \beta_h h \tag{30}$$

$$\alpha_n = 0.01 \frac{V + 55}{1 - \exp \frac{-(V+55)}{10}} \tag{31}$$

$$\beta_n = 0.125 \exp \frac{-(V + 65)}{80} \tag{32}$$

$$\alpha_m = 0.1 \frac{V + 40}{1 - \exp \frac{-(V+40)}{10}} \tag{33}$$

$$\beta_m = 4.0 \exp \frac{-(V + 65)}{18} \tag{34}$$

$$\alpha_h = 0.07 \exp \frac{-(V + 65)}{20} \tag{35}$$

$$\beta_h = \frac{1}{1 - \exp \frac{-(V+35)}{10}} \tag{36}$$

With $g_{Na} = 120 \frac{\text{mS}}{\text{cm}^2}, g_K = 36 \frac{\text{mS}}{\text{cm}^2}, g_L = 0.3 \frac{\text{mS}}{\text{cm}^2}, E_{Na} = 50\text{mV}, E_K = -77\text{mV}, V_L = -54.6\,\text{mV}, C_m = 1 \frac{\mu\text{F}}{\text{cm}^2}, I_{stim} = 10 \frac{\mu\text{A}}{\text{cm}^2}$

2.4.2 Wang-Buzsaki model

The Wang-Buzsaki model was created during a study of fast oscillations in the neocortex and hippocampus and has Type I excitability [38]. The equations for the Wang-Buzsaki model are :

$$C_m \frac{dV}{dt} = -g_K n^4 (V - E_K) - g_{Na} m_\infty^3 h (V - E_{Na}) - g_L (V - E_L) + I_{stim} \tag{37}$$

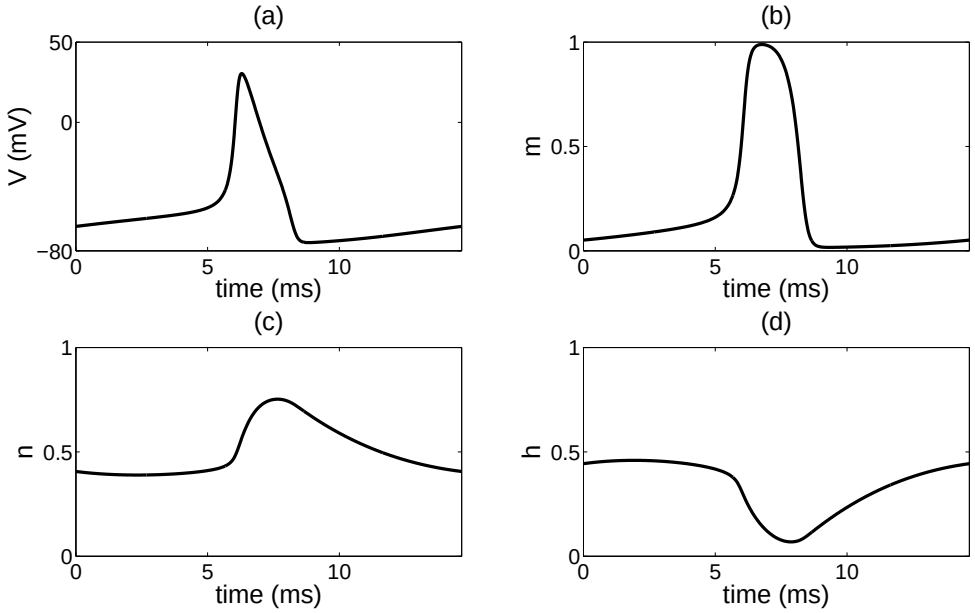

Figure 18: Example (a) voltage, (b) m sodium channel gating variable, (c) n potassium channel gating variable and (d) h sodium channel gating variable trajectories for the Hodgkin-Huxley model on a stable limit cycle with $I_{stim} = 10\frac{\mu\text{A}}{\text{cm}^2}$.

$$\frac{dn}{dt} = \phi(\alpha_n(1-n) - \beta_n n) \tag{38}$$

$$\frac{dh}{dt} = \phi(\alpha_h(1-h) - \beta_h h) \tag{39}$$

$$m_\infty = \frac{\alpha_m}{\alpha_m + \beta_m} \tag{40}$$

$$\alpha_m = \frac{-0.1(V+35)}{\exp -0.1(V+35) - 1} \tag{41}$$

$$\beta_m = 4\exp -(V+60)/18 \tag{42}$$

$$\alpha_h = 0.07\exp -(V+58)/20 \tag{43}$$

$$\beta_h = \frac{1}{\exp -0.1(V+28) + 1} \tag{44}$$

$$\alpha_n = \frac{-0.1(V+34)}{\exp -0.1(V+34) - 1} \tag{45}$$

$$\beta_n = 0.125\exp -(V+44)/80 \tag{46}$$

With $g_{Na} = 35\frac{\text{mS}}{\text{cm}^2}, g_K = 9\frac{\text{mS}}{\text{cm}^2}, g_L = 0.1\frac{\text{mS}}{\text{cm}^2}, E_{Na} = 55\text{mV}, E_K = -90\text{mV}, V_L = -65\text{ mV}, C_m = 1\ \frac{\mu\text{F}}{\text{cm}^2}, I_{stim} = 10\ \frac{\mu\text{A}}{\text{cm}^2}, \phi = 5$

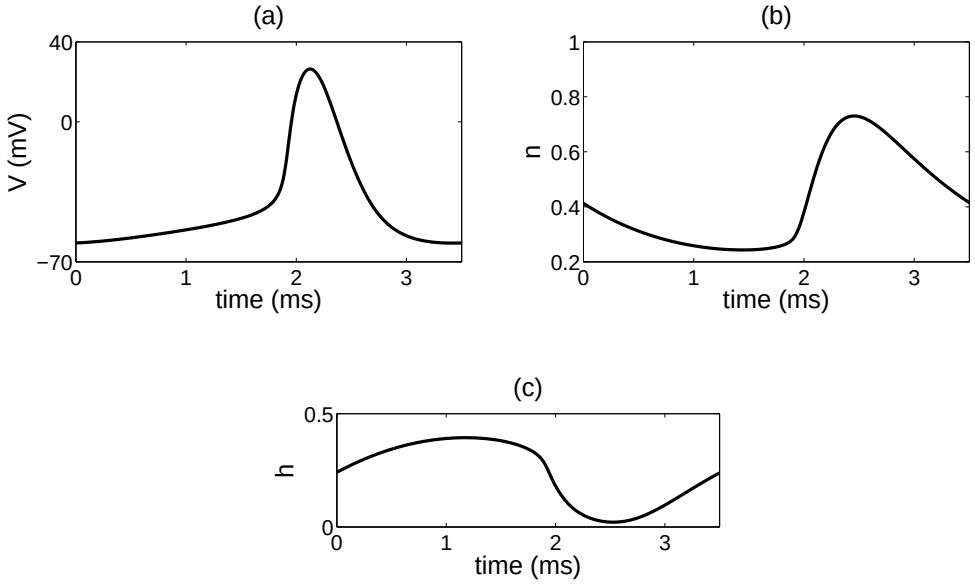

Figure 19: Example (a) voltage, (b) n potassium channel gating variable, (c) h sodium channel gating variable trajectories for the Wang-Buzsaki model on a stable limit cycle with $I_{stim} = 10\ \frac{\mu\text{A}}{\text{cm}^2}$.

2.4.3 Theta model

The theta model is a simple one-dimensional, phase model for a neuron.

$$\frac{d\theta}{dt} = 1 - \cos\theta + (1 + \cos\theta)I(t) \tag{47}$$

The theta model has type I excitability and is in fact the normal form of the saddle-node on an invariant circle bifurcation described earlier. The theta model is the most simple and generic neuron model with Type I excitability.

2.5 Neural networks

In this thesis we focus on two types of networks, pairs of weakly coupled neurons and coupled complexes of neurons. The complexes of neurons in the latter problem, collectively, have a periodic bursting behavior. We study the interaction between these two bursting groups of neurons by representing each by a one dimensional phase model.

2.5.1 Coupled neurons

We model synaptically coupled neurons by adding a new current term into the voltage balance equations of the coupled, model neurons.

$$I_{syn,i}(V_i, t) = g_{syn,i}(V_i - V_{syn})\alpha^2(t - t_{spike})e^{-\alpha(t-t_{spike})} \tag{48}$$

The factor of α^2 normalizes the integral of the alpha function over time. This synaptic current is the result of a single spike, a series of spikes would be a summation of Eq. 48. The alpha function causes these terms to decay to zero as $t \to \infty$. If the coupling is sufficiently weak, predictions can be made only considering the synaptic current resulting from the most recent spike. In our full numerical simulations we use a an additional pair of coupled ODE's which have as their solution the desired alpha function.

$$\dot{a} = -2\alpha a - \alpha^2 b \tag{49}$$

$$\dot{b} = a \tag{50}$$

These ODE's are a second order, critically damped system with the alpha function in Eq. 48 being the corresponding analytic response in this case. A similar pair of ODE's must be added for every synaptic connection. For a pair of mutually coupled neurons this means that two pairs, or four ODE's, will be added to the system to model the coupling. In this way we avoid having any explicit time dependence in our system. In a system of a mutually coupled pair of neurons, neuron 1 would have a synaptic current which depended on V_1 and b_2.

$$I_{syn,i}(V_i, b_j) = g_{syn,i}(V_i - V_{syn})b_j \tag{51}$$

When neuron 2 fired an action potential we set $b_2 = \alpha$ and $a_2 = 0$. The dynamics would then take over and b_2 will have the same behavior as the explicit time dependent alpha function in Eq. 48. With this technique we are only considering the effect from

the most recent spike in the synaptic current. This will only be accurate if the coupling is weak enough, or the effect decays quickly enough, that contribution to synaptic current from a single spike has dissipated after one period.

2.5.1.1 Types of coupling

Synaptic coupling is traditionally classified as excitatory or inhibitory. This classification is based off of the relative value of V_{syn} to the resting potential of the neuron, V_{eq}. If $V_{syn} > V_{eq}$ the coupling is *excitatory*, if $V_{syn} < V_{eq}$ the coupling is *inhibitory*.

2.5.2 Phase reduction and the weak coupling approximation

We begin with a dynamical system $\dot{\vec{x}} = \vec{f}(\vec{x})$ which is on a strongly attracting limit cycle. If left undisturbed, the trajectory will stay on this one dimensional path. We could parameterize this trajectory with a phase variable, $\Phi(t)$. There exist mathematics which can calculate $\Phi(t)$ from $\vec{x}(t)$ [5] but we may achieve useful results just from knowing that this is possible. This phase variable will then proceed uniformly in time

$$\frac{d\Phi}{dt} = \omega \tag{52}$$

at a constant frequency ω.

This may seem like a useless bit of semantics as Eq. 52 could literally be representing any system on a limit cycle. The true usefulness of a phase reduction comes when we have two such "phase reduced" oscillators which are coupled together. In this case we will need to know some information about how an oscillator reacts to small perturbations from it's stable limit cycle. To first order if we multiply the perturbation by the gradient of the phase (Fig. 20, 21) we can continue to describe our system in this phase reduced format.

We define the phase gradient

$$Z(\Phi) = \lim_{\Delta V \to 0} \frac{\Delta \Phi}{\Delta V} = \frac{\partial \Phi}{\partial V}. \tag{53}$$

Calculating the gradient of the phase is not a simple matter. This calculation has to be performed numerically. [7] describes their method of calculating the phase gradient as

> The derivative of the phase was evaluated by computing the dephasing induced at large time by small initial perturbations.

To perform this calculation we first must obtain the limit cycle data for all the variables in the neuron model. Next, for each point on the limit cycle we first add a small perturbation to the voltage variable then start the integration again. We simultaneously integrate forward in time the unperturbed equations starting at the same point. The simultaneous integrations are stopped when the initially perturbed neuron has returned to it's limit cycle. Once this has occurred we calculate the phase-difference between the perturbed and unperturbed limit cycles. The phase-difference divided by the initial perturbation yields an approximate value for $\frac{\partial \Phi}{\partial V}$. This method is somewhat brute force, but it turns out to be equivalent to solving the adjoint equation from Malkin's theorem.

Malkin's theorem. For an oscillator with a stable limit cycle, $\vec{x}_0$, its phase is described by the equation

$$\dot{\Phi} = 1 + \epsilon \mathbf{Q}(\Phi) \cdot \vec{p}(t). \tag{54}$$

Malkin found [22, 23] that $\mathbf{Q}$ is the solution to

$$\dot{\mathbf{Q}} = -\mathbf{A}^T \mathbf{Q}(t), \;\; \mathbf{Q}(0) \cdot \vec{f}(\vec{x}(0) = 1, \tag{55}$$

Izhikevich applies Malkin's theorem to coupled relaxation oscillators [18]. When the coupling perturbation $\vec{p}(t)$ is solely in voltage, then only the voltage component of $\mathbf{Q}$ survives the dot product with $\vec{p}$ and $\mathbf{Q}$ is equivalent to the phase gradient. The averaging procedure in the software package XPP solves Eq. 55 in its adjoint calculation [4].

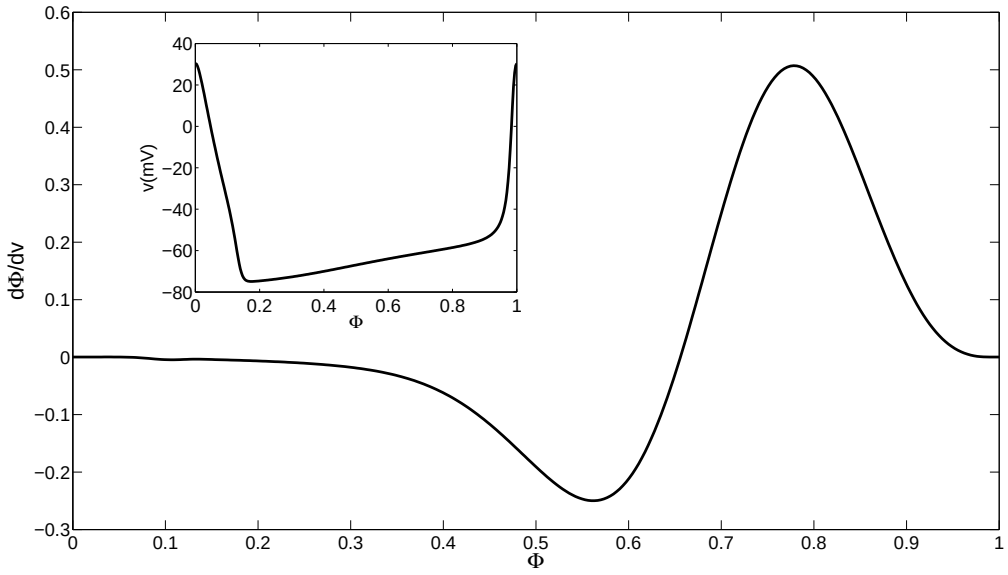

Figure 20: The phase gradient for the Hodgkin-Huxley model shown with a subplot of the voltage.

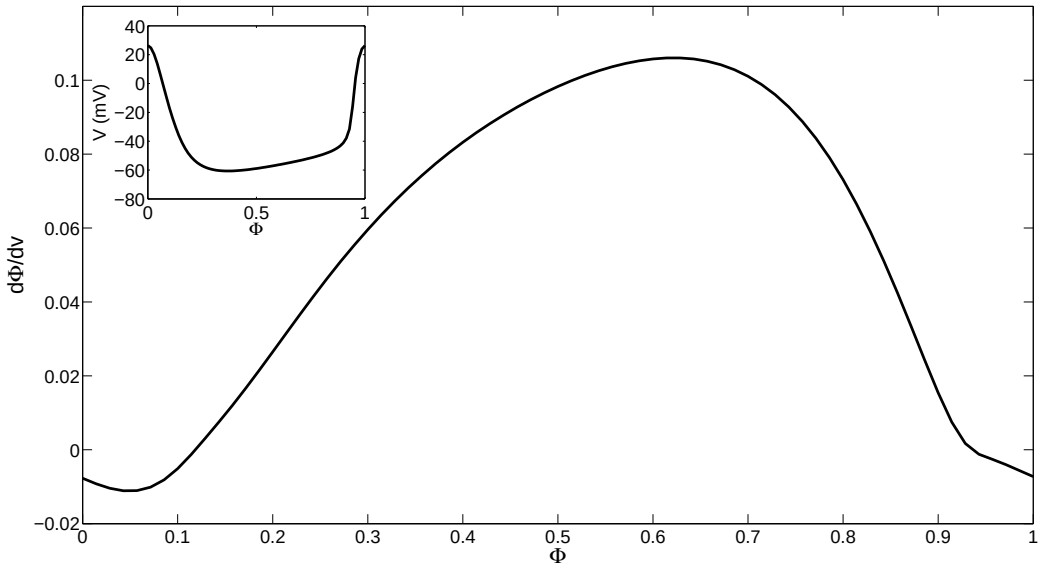

Figure 21: The phase gradient for the Hodgkin-Huxley model shown with a subplot of the voltage.

We now have just two equations which describe the phase dynamics of a weakly coupled pair of neurons.

$$\frac{d\Phi_i}{dt} = \omega_i + \frac{\partial \Phi_i}{\partial V_i} I_{syn,i}(\Phi_i, \Phi_j),\ i \neq j \tag{56}$$

To first order, $I_{syn,i}$ can be evaluated on the unperturbed trajectories $I_{syn,i}(\Phi_i, \Phi_j) = g_{syn,i}(V_i(\Phi_i) - E_{syn}) \sum_{spikes} F_c(\Phi_j - t_{spike})$. $F_c(\Phi_j - t_{spike})$ is the coupling function. We chose $E_{syn} = -77$ mV (inhibitory) and 35 mV (excitatory) for the Hodgkin-Huxley Model and -90 mV (inhibitory) and 0 mV (excitatory) for the Wang-Buzsaki Model. The excitatory value we selected for E_{syn} for the Hodgkin-Huxley model is an intermediate value between the two more common values of $E_{syn} = 0$ mV or $E_{syn} = E_{Na}$; however the results remain qualitatively the same in this region [7]. As we previously described, we model the synaptic coupling using alpha functions.

$$F_c(\Phi_j - t_{spike}) = \alpha^2(\Phi_j - t_{spike}) \exp(-\alpha(\Phi_j - t_{spike})). \tag{57}$$

We define $\Phi = \Phi_1 - \Phi_2$ as the phase-difference between the two neurons yielding:

$$\frac{d\Phi}{dt} = H_1(\Phi) - H_2(-\Phi) = G(\Phi). \tag{58}$$

Thus, we have reduced the problem of a mutually coupled pair of neurons to a single differential equations. Since the perturbation is small we can averaged its effects over one period.

$$H_i(\Phi) = \int_0^T \frac{\partial \Phi_i}{\partial V_i} I_{syn}(\Phi_i, \Phi_j) dt. \tag{59}$$

The zeros of $G(\Phi)$ are the equilibrium points of phase-difference for the system. We will use this technique to produce bifurcation diagrams examining the dependence of the equilibrium phase-difference between a pair of mutually coupled neurons on the synaptic rate constant for many different systems.

CHAPTER III

IDENTICALLY COUPLED NEURONS

The main product of our work with mutually coupled pairs of neurons are bifurcation diagrams of equilibrium phase-difference, Φ, versus the synaptic rate constant α. These diagrams allow us to make predictions about the dynamics of the coupled pairs of neurons studied. From the diagrams we can predict if a phase locked state exists for the parameter set at a given value of α and the value of the phase-difference as a function of α.

We study pairs of both Hodgkin-Huxley or Wang-Buzsaki neurons. In both cases we consider mutually excitatory and inhibitory coupling. Hodgkin-Huxley and Wang-Buzsaki neurons were chosen because they have Type II and Type I excitability, respectively. In this way we simulate all the general coupling and excitability combinations. In this chapter we examine the cases with identical neurons coupled with identical values of synaptic conductance.

3.1 Hodgkin-Huxley model

We first begin by examining the case of identically coupled Hodgkin-Huxley neurons, identically coupled through alpha functions. An analysis of these Hodgkin-Huxley systems was previously given in [37], although they did not show numerical verification of the results of the weak coupling approximation using simulations of the full set of equations, as we will show at the end of the chapter.

As we vary the synaptic rate constant, α for an excitatory coupled pair of Hodgkin-Huxley neurons we observe a series of 3 pitchfork bifurcations (Fig. 22). For small values of α, phase locking in anti-phase ($\Phi = 0.5$) is the stable solution and in-phase ($\Phi = 0, 1$) phase locking is the unstable solution. As we increase α, the first pitchfork

bifurcation is encountered at ($\alpha = 0.12\text{ms}^{-1}, \Phi = 0.5$). At this super-critical pitchfork bifurcation the $\Phi = 0.5$ solution loses stability and two new, symmetric branches of stable solutions appear. These branches are intermediate values of Φ. We define *intermediate* values of Φ to be $0.5 < \Phi < 1$ or $0 < \Phi < 0.5$. Because the neurons are identical there is a reflection symmetry about the $\Phi = 0.5$ axis. The system is symmetric under an exchange of neurons. The branches of stable solutions created at the first pitchfork bifurcation terminate at the second pitchfork bifurcation at ($\alpha = 0.27\,\text{ms}^{-1}, \Phi = 0, 1$), intersecting the $\Phi = 0, 1$ branch of unstable solutions. The second pitchfork is also a super-critical pitchfork bifurcation oriented in the opposite direction of the first pitchfork. At the second pitchfork the branch of solutions at $\Phi = 0, 1$ becomes stable for the rest of the values of α that we studied. The region of values of α between the two pitchfork bifurcations has a stable in-phase solution and an unstable anti-phase solution. The unstable branch of solutions at $\Phi = 0.5$ becomes stable at the third pitchfork bifurcation at ($\alpha = 1.0\,\text{ms}^{-1}, \Phi = 0.5$). The third bifurcation is a sub-critical bifurcation and yields a stable branch of solutions at $\Phi = 0.5$ and two symmetric branches of stable solutions at intermediate values of Φ. The region of parameter space of values of α greater than the location of the third pitchfork bifurcation has a bistability of in-phase and anti-phase solutions.

The bifurcation diagram of inhibitory coupled Hodgkin-Huxley neurons (Fig. 23) is qualitatively very similar to the excitatory coupled case with the stabilities reversed. In addition to the 3 pitchfork bifurcations we also see a pair of saddle-node bifurcations. As we increase α from $0.1\,\text{ms}^{-1}$ toward the first pitchfork bifurcation the in-phase ($\Phi = 0, 1$) solution is stable and the anti-phase ($\Phi = 0.5$) solution is unstable. The first pitchfork bifurcation is a sub-critical bifurcation at ($\alpha = 0.2\,\text{ms}^{-1}, \Phi = 0.5$), causing the $\Phi = 0.5$ state to become stable and a symmetric pair of unstable fixed points appear at intermediate values of Φ. As we continue to increase α the unstable branches of intermediate values approach the $\Phi = 0, 1$ axis and the stable

$\Phi = 0.5$ branch continues undisturbed. Before the intermediate solution branches intersect the stable $\Phi = 0, 1$ branch a saddle-node bifurcation occurs on each branch at $(\alpha = 0.45\,\mathrm{ms}^{-1}, \Phi = 0.05, 0.95)$. This changes the stability of the intermediate solutions from unstable to stable. The intermediate solutions, now stable as a result of the saddle-node bifurcation, now intersect the stable, in-phase ($\Phi = 0, 1$) branch of solutions at the second pitchfork bifurcation. This bifurcation is a super-critical pitchfork bifurcation at $(\alpha = 0.45\,\mathrm{ms}^{-1}, \Phi = 0, 1)$, which results in the termination of the intermediate branches of solutions created at the first pitchfork bifurcation and the loss of stability of the in-phase ($\Phi = 0, 1$) branch of solutions. The region of parameter space between the second and third pitchfork bifurcations has a stable anti-phase ($\Phi = 0.5$) branch of solutions and an unstable, in-phase ($\Phi = 0, 1$) branch of solutions. The third pitchfork bifurcation at $(\alpha = 2.13\,\mathrm{ms}^{-1}, \Phi = 0.5)$ is also super-critical and results in the creation of a symmetric pair of branches of stable solutions of intermediate phase-difference and the loss of stability of the anti-phase ($\Phi = 0.5$) branch of solutions.

3.1.1 Full numerical simulation results

We verified the predicted stable fixed points from the weak coupling approximation study by solving the full set of equations for the coupled system in the Matlab environment [25]. The integration of the equations were performed by Matlab's "ode45" integrator. The "ode45" integrator is a Runga-Kutta style integrator. Using Matlab's event location function inside the "ode45" integrator options we track the times of threshold crossings of voltage for each neuron. We chose a value of 20 mV as the threshold. There is nothing special about this choice of threshold other than it *only* occurs during an action potential. Since the shape and magnitude of the action potential is essentially unchanged in a weakly coupled system, tracking the times of these threshold crossings allows us to accurately calculate periods and phase-differences.

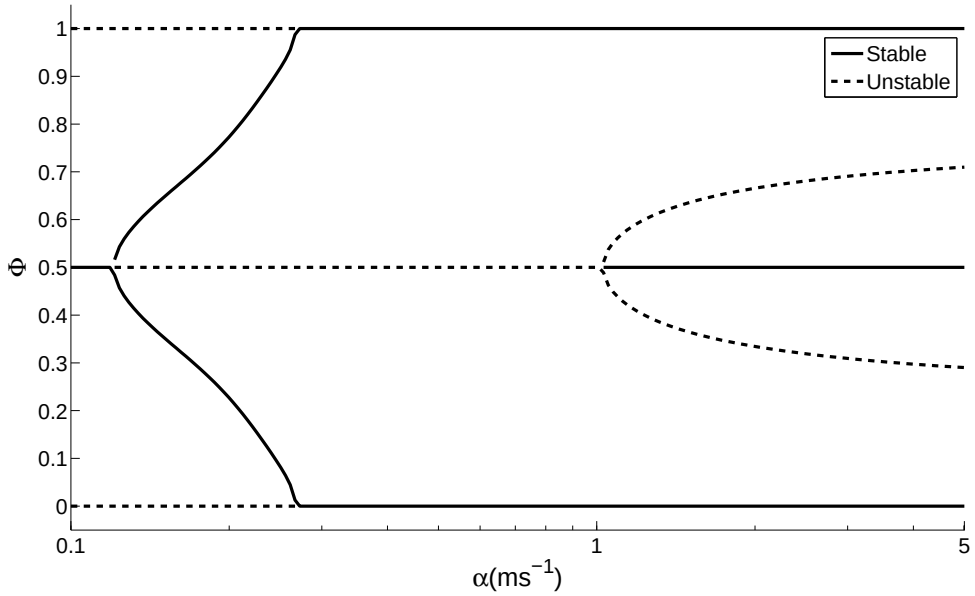

Figure 22: Bifurcation diagram of equilibrium phase-difference versus the synaptic time constant for identically, excitatory coupled Hodgkin-Huxley neurons.

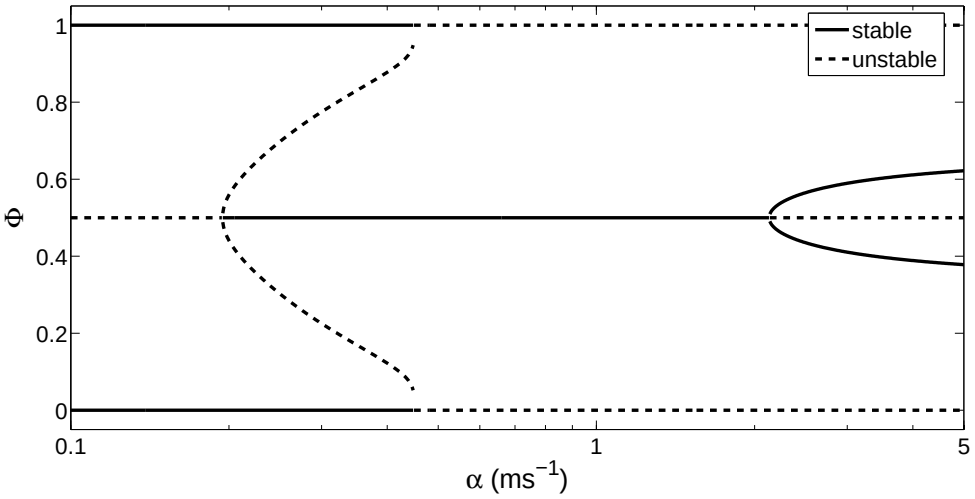

Figure 23: Bifurcation diagram of equilibrium phase-difference versus the synaptic time constant for identically, inhibitory coupled Hodgkin-Huxley neurons.

We calculate the phase-difference and the change in the phase-difference from period to period. Once the phase-difference has become stable and nearly unchanged from period to period the simulation stops and the phase-difference as a function of α is saved and plotted as a point on a bifurcation diagram. We developed no rule for determining an acceptable tolerance in the change of phase-difference from period to period to accurately identify the stable phase-difference. We found the tolerance to be model and parameter dependent. In order to check for bistable cases we began ran multiple simulations initial conditions that were nearly in-phase or nearly anti-phase. The basins of attraction of the states are high dimensional structures. Our approach is certainly not a complete method to find different states in systems that are bistable, but sufficed to verify the predicted bistable states.

Using a value of $g_{syn} = 0.1\ \frac{\text{mS}}{\text{cm}^2}$, we found very good qualitative agreement between the results of the weak coupling approximation and those of the full numerical simulations for both the excitatory (Fig. 24) and inhibitory (Fig. 25) cases. In both cases we saw some slight shifting of where the various bifurcations occurred in the numerical results compared with the weak coupling approximation results, but topologically they are the same.

3.2 Wang-Buzsaki model

The structure of the bifurcation diagrams of equilibrium phase-difference, Φ, versus the synaptic rate constant, α, for identically coupled Wang-Buzsaki neurons are qualitatively similar to those of identically coupled Hodgkin-Huxley neurons with the type of coupling (excitatory or inhibitory) swapped.

For identically, excitatory coupled Wang-Buzsaki neurons (Fig. 26), we find an unstable branch of anti-phase solutions for small values of α which continues until the first of three pitchfork bifurcations, a sub-critical pitchfork bifurcation occurring at $(\alpha = 0.54\,\text{ms}^{-1}, \Phi = 0.5)$. The sub-critical pitchfork bifurcation causes the branch

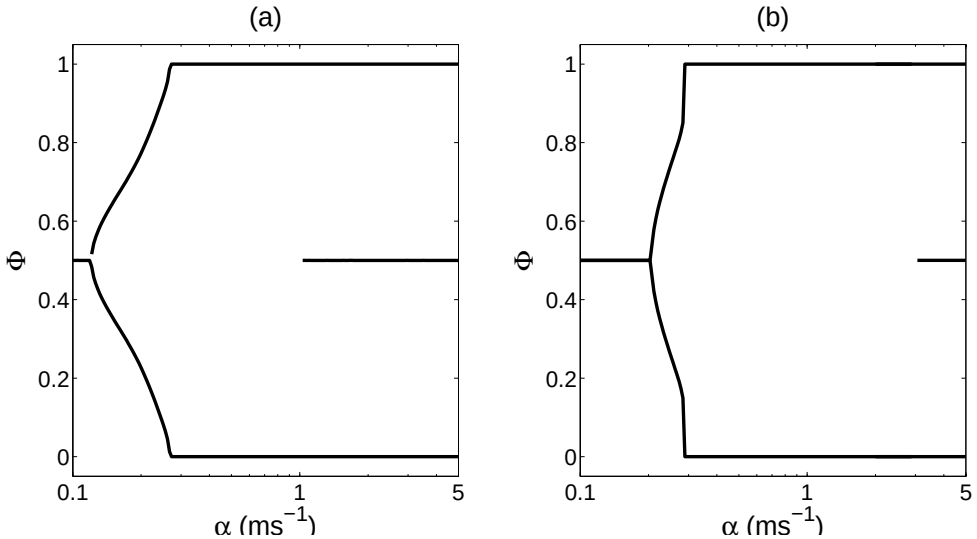

Figure 24: Comparison of the bifurcation diagrams of equilibrium phase-difference versus the synaptic time constant for identically, excitatory coupled Hodgkin-Huxley neurons calculated using (a) the weak coupling approximation (b) full numerical simulations.

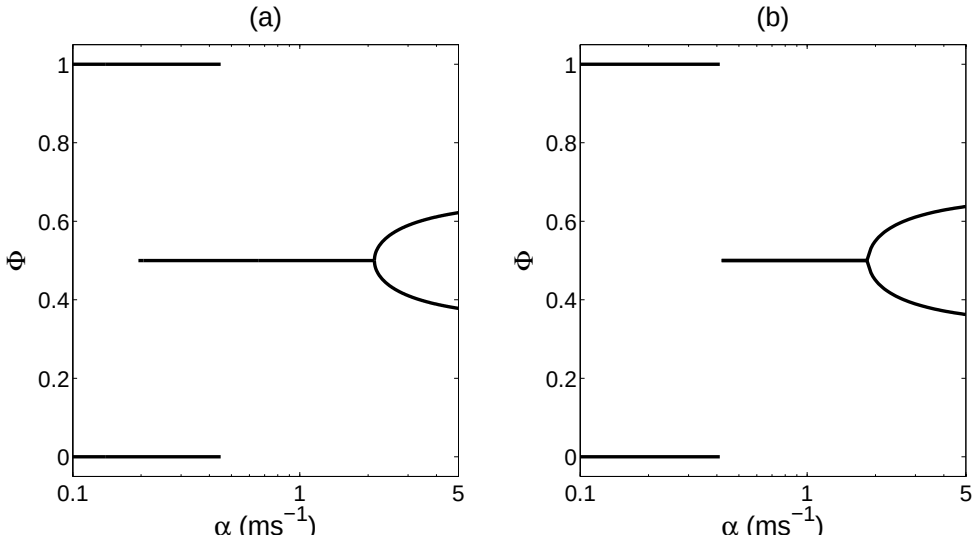

Figure 25: Comparison of the bifurcation diagrams of equilibrium phase-difference versus the synaptic time constant for identically, excitatory coupled Hodgkin-Huxley neurons calculated using (a) the weak coupling approximation (b) full numerical simulations.

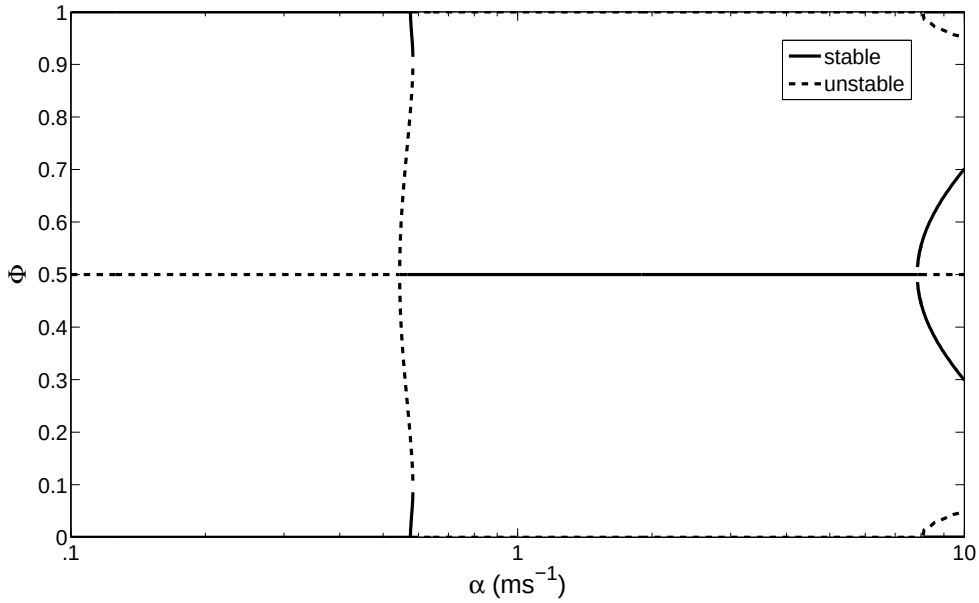

Figure 26: Bifurcation diagram of equilibrium phase-difference versus the synaptic time constant for identically, excitatory coupled Wang-Buzsaki neurons.

of anti-phase solutions to become stable and creates a pair of unstable branches of solutions with intermediate values of Φ. These intermediate branches change stability at a pair of saddle-node bifurcations symmetric about the $\Phi = 0.5$ axis at $(\alpha = 0.58\,\mathrm{ms}^{-1}, \Phi = 0.09, 0.91)$. The branches of intermediate solutions intersect and terminate at the second pitchfork bifurcation at $(\alpha = 0.58\,\mathrm{ms}^{-1}, \Phi = 0, 1)$. This, sub-critical pitchfork bifurcation causes the branch of in-phase solutions to become unstable. The stable branch of anti-phase solutions continues until the third pitchfork bifurcation at $(\alpha = 7.9\,\mathrm{ms}^{-1}, \Phi = 0.5)$. This super-critical pitchfork bifurcation causes the branch of anti-phase solutions to become unstable and creates two symmetric branches of stable fixed points at intermediate values of Φ. A qualitatively new feature of the excitatory coupled Wang-Buzsaki case is a fourth pitchfork bifurcation occurring at $(\alpha = 8.13\,\mathrm{ms}^{-1}, \Phi = 0, 1)$. This is a sub-critical pitchfork bifurcation which causes the in-phase branch of solutions to become stable and creates two branches of unstable solutions which are symmetric about the $\Phi = 0, 1$ in-phase axis.

For the case of identically, inhibitory coupled Wang-Buzsaki neurons (Fig. 27) we find a stable branch of anti-phase solutions at small values of α. This branch of stable, anti-phase solutions continues until the first pitchfork bifurcation at ($\alpha = 0.43\,\mathrm{ms}^{-1}, \Phi = 0.5$). This super-critical pitchfork bifurcation causes the branch of anti-phase solutions to become unstable and creates two, stable branches of solutions at intermediate values of Φ. The stable branches of intermediate solutions changes stability at a pair of saddle-node bifurcations, located symmetrically about the anti-phase axis at ($\alpha = 0.58\,\mathrm{ms}^{-1}, \Phi = 0.07, 0.93$). The intermediate branches then intersect and terminate into the unstable branch of in-phase solutions at the second pitchfork bifurcation at ($\alpha = 0.58\,\mathrm{ms}^{-1}, \Phi = 0, 1$). This sub-critical pitchfork bifurcation causes the branch of in-phase solutions to become stable and remain stable for all $\alpha > 0.58\,\mathrm{ms}^{-1}$ shown. The unstable branch of anti-phase solutions resulting from the first pitchfork bifurcation continues as we increase α until it meets the third pitchfork bifurcation at ($\alpha = 3.88\,\mathrm{ms}^{-1}, \Phi = 0.5$). This sub-critical pitchfork bifurcation causes the branch of anti-phase solutions to lose stability and creates two branches of unstable solutions at intermediate values of Φ which are symmetric about the anti-phase axis.

3.2.1 Full numerical simulation results

We used the same numerical method to verify the predictions made using weak coupling approximation for the coupled Wang-Buzsaki system as the coupled Hodgkin-Huxley system which we previously described. Compared to the Hodgkin-Huxley system, we found that higher error tolerances in the "ode45" integrator were required to achieve a similar accuracy of results for the Wang-Buzsaki system. With the higher error tolerances we achieved very good qualitative agreement between the weak coupling approximations results and those obtained through the numerical procedure solving the full system of equations for both the exciatory (Fig. 28) and inhibitory

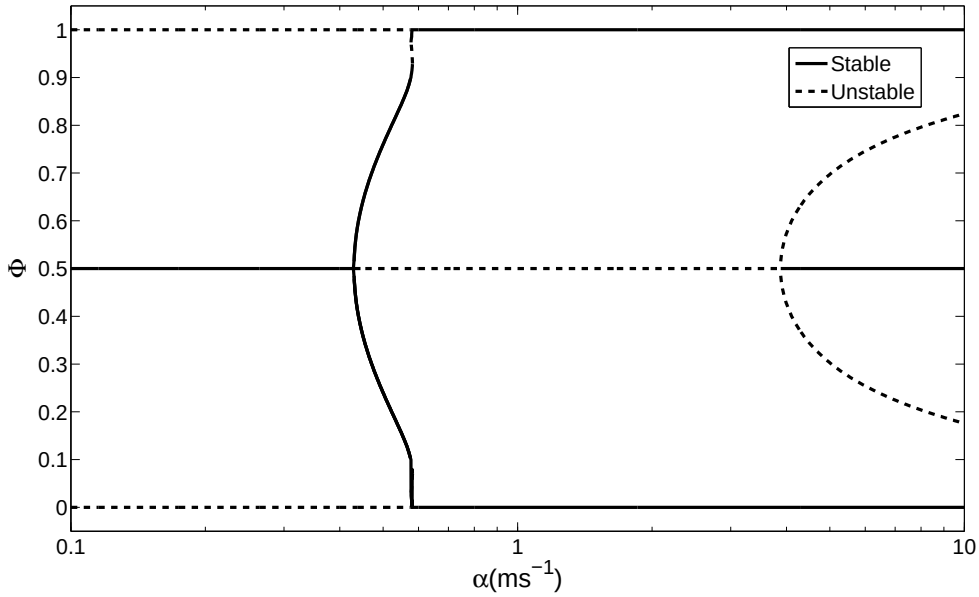

Figure 27: Bifurcation diagram of equilibrium phase-difference versus the synaptic time constant for identically, inhibitory coupled Wang-Buzsaki neurons.

(Fig. 29) cases. The only qualitative difference is that neither of the bifurcation diagrams from the full numerical simulations show the stable branch (or appropriate break in the stable branch) of solutions which would result from the saddle-node bifurcations observed in the weak coupling approximation results.

3.3 Discussion

We see that a multiple pitchfork bifurcation structure is common to all the cases examined in this section. The pitchfork bifurcation occurs when there are symmetries in the system. In these systems both the neurons and the coupling are identical.

Topologically, the bifurcation diagrams for the excitatory and inhibitory cases for either the Hodgkin-Huxley or Wang-Buzaki systems are nearly the same with the stabilities reversed. This could be intuitive to some readers since, roughly, you could consider excitatory coupling to be "positive" and inhibitory coupling to be "negative." Thinking in this manner one might expect that changing the sign of the coupling would change the sign of the slope at a zero crossing. Another interesting

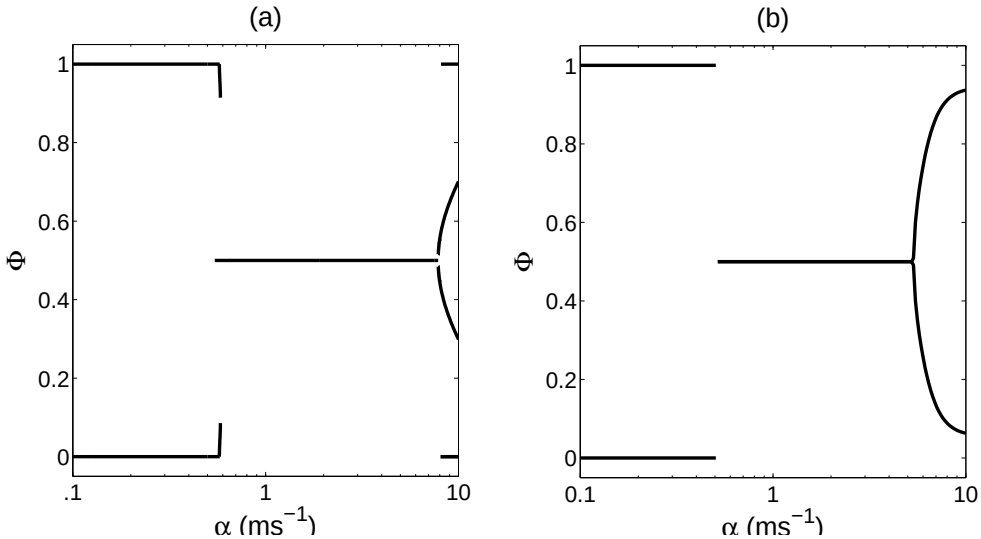

Figure 28: Comparison of the bifurcation diagrams of equilibrium phase-difference versus the synaptic time constant for identically, excitatory coupled Wang-Buzsaki neurons calculated using (a) the weak coupling approximation (b) full numerical simulations.

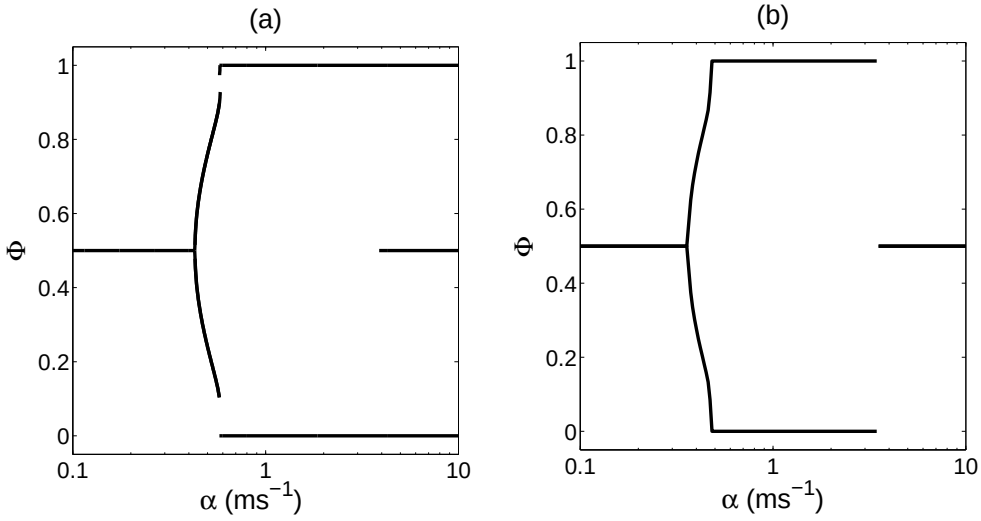

Figure 29: Comparison of the bifurcation diagrams of equilibrium phase-difference versus the synaptic time constant for identically, inhibitory coupled Wang-Buzsaki neurons calculated using (a) the weak coupling approximation (b) full numerical simulations.

observation is that, topologically, comparing the Hodgkin-Huxley and Wang-Buzsaki results in this section you again see them to be nearly the same with the stabilities reversed. Combining these two we have the result that excitatory coupled pairs of Hodgkin-Huxley neurons have very similar equilibrium phase dynamics when compared with inhibitory coupled pairs of Wang-Buzsaki neurons. The same can be said for inhibitory coupled Hodgkin-Huxley neurons and excitatory coupled Wang-Buzsaki neurons. We speculate that this type of symmetry is present when comparing any coupled pair of Type II neurons to a coupled pair of Type I neurons. This symmetry is less intuitive than the swapping of stabilities when changing the type of coupling. In the weak coupling approximation, the phase gradient is the structure which contains all the intrinsic information about the neuron. In general Type II phase gradients have regions of both positive and negative responses where Type I neurons tend to have phase gradients that are almost purely positive. It was surprising to see mirror image type symmetry resulting from objects that don't themselves have that type of symmetry.

CHAPTER IV

HETEROGENEOUS SYNAPTIC CONDUCTANCE BETWEEN WEAKLY COUPLED NEURONS

There has been a great deal of research developing a theory of weakly coupled neural oscillators. The studies have typically looked at identically coupled neurons [7, 37, 8, 36, 1]. Some have considered heterogeneous neurons, particularly with heterogeneities in the external, applied current [6, 39]. In vivo and in vitro, significant heterogeneities in cellular properties exist [34]. Furthermore, in dynamic clamp experiments coupling two real, biological neurons or a biological neuron and a model neuron, heterogeneity is typically observed in the synaptic conductances [32]. [21] studied the effects of heterogeneous synaptic coupling on clustering in small networks, but the mutual coupling between any pair of neurons in their study was identical.

We examine the symmetry breaking effects that heterogeneity has on the bifurcation diagrams of equilibrium phase-difference, Φ versus the synaptic rate constant, α for weakly coupled pairs of neurons. We use Hodgkin-Huxley and Wang-Buzsaki model neurons which have Type II and Type I excitability, respectively, mutually coupled with either a pair of excitatory or inhibitory synapses. We implement the heterogeneity through differences in the synaptic conductance between the mutually coupled pair of neurons, parameterized by a dimensionless parameter,

$$h = \frac{g_{syn,1}}{g_{syn,2}}. \tag{60}$$

For consistency we choose the same values for the heterogeneity parameter throughout this section $h = 1, 2/3, 1/3, 1/10$.

4.1 Effects of heterogeneity on $G(\Phi)$

When the coupling is identical $G(\Phi)$ in Eq. 58 is guaranteed to have zeros at $\Phi = 0, 0.5$ and 1, representing the in-phase and anti-phase solutions (Fig. 30(a)). They can either be stable or unstable fixed points, depending on the slope of $G(\Phi)$ at the zero crossing. For the identical case $G(\Phi)$ is the odd part of the $H(\Phi)$ and the periodicity of $H(\Phi)$ guarantees $G(\Phi)$ will be zero at $\Phi = 0$ and 1. $\Phi = 0.5$ is the axis about which $H(\Phi)$ is flipped so $G(\Phi = 0.5) = 0$ always. It is also possible to have other intermediate values of phase-difference for fixed points with identical coupling, but these are always in addition to $\Phi = 0, 0.5$ and 1. In the case of identical neurons coupled with heterogeneous values of synaptic conductance, in-phase and anti-phase are in general not solutions (Fig. 30(b)). In the weak coupling approximation heterogeneous values of g_{syn} result in differences in scaling of $H(\Phi)$ for the respective neurons. Graphically we can see the differences between the identical and heterogeneous cases easily by noting how the intersections of $H_1(\Phi)$ and $H_2(-\Phi)$ change with heterogeneity. These intersections are the fixed points of the system. Heterogeneous values of synaptic conductance also can cause the appearance of regions of α where no fixed points exist. If we choose the heterogeneous, linear scalings of $g_{syn,i}$ which result in $H_1(\Phi)$ never intersecting $H_2(-\Phi)$, then $G(\Phi)$ will have no zeros over the entire period (Fig. 31). When we examine $G(\Phi)$ for different amounts of heterogeneity but the same value of α, the effects are seen as a smooth "sliding" of the zeros of the function and thereby the fixed points for the system (Fig. 32). Even a slight amount of heterogeneity in synaptic coupling removes the ubiquitous in-phase and anti-phase solutions.

4.2 Hodgkin-Huxley model

We begin with the case of excitatory coupled Hodgkin-Huxley neurons with $h = 2/3$ (Fig. 33). When we set $\alpha = 0.1\ \mathrm{ms}^{-1}$ there is a stable solution at $\Phi \approx 0.4$ and a nearly in-phase, unstable solution $\Phi \approx 0.04$. As α is increased the stable branch

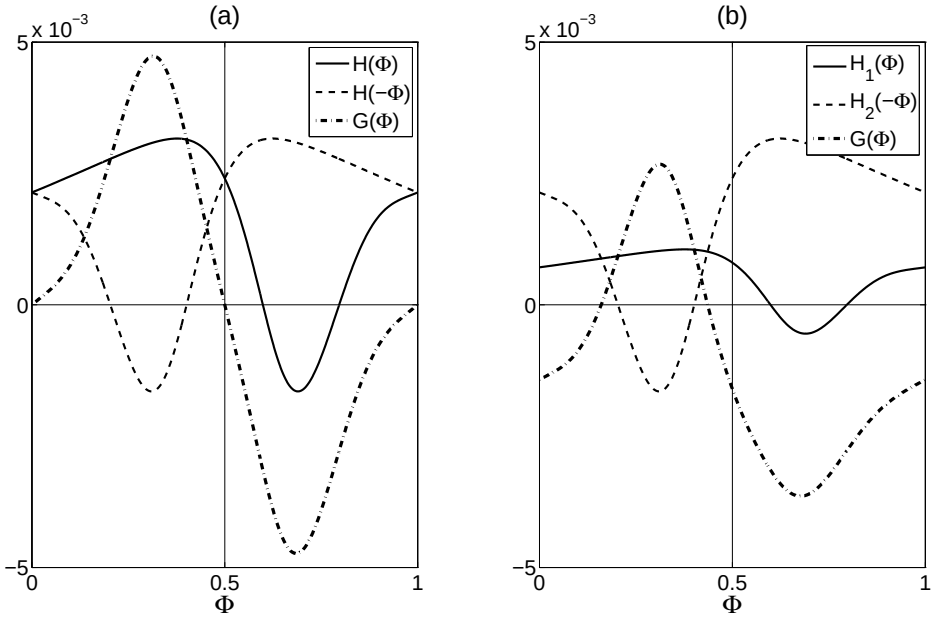

Figure 30: (a) $G(\Phi)$ with identical values of g_{syn} and excitatory coupling. In this case $H_1(\Phi) = H_2(\Phi)$ so we need only calculate $H(\Phi)$ once. $G(\Phi) = H(\Phi) - H(-\Phi)$ which is simply the "odd part" of $H(\Phi)$. For identical coupling at least 3 solutions are guaranteed, $\Phi = 0, 0.5$ and 1. (b) $G(\Phi)$ calculated from $H_1(\Phi)$ and $H_2(-\Phi)$ with heterogeneous synaptic conductance, $g_{syn,1} = 0.1\ \frac{\text{mS}}{\text{cm}^2}$ and $g_{syn,2} = 0.3\ \frac{\text{mS}}{\text{cm}^2}$, and excitatory coupling. When the coupling is not identical in-phase and anti-phase are no longer general solutions. The solutions occur when $H_1(\Phi) = H_2(-\Phi)$.

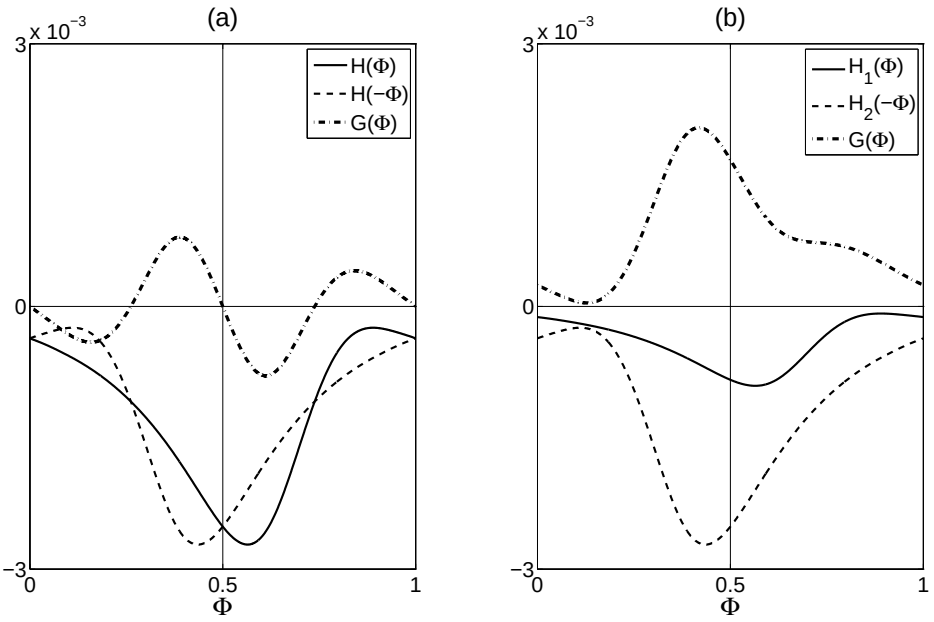

Figure 31: (a) $G(\Phi)$ with identical values of g_{syn} and excitatory coupling with $\alpha = 0.28\,\mathrm{ms}^{-1}$. (b) $G(\Phi)$ calculated from $H_1(\Phi)$ and $H_2(-\Phi)$ with heterogeneous synaptic conductance, $g_{syn,1} = 0.1\,\frac{\mathrm{mS}}{\mathrm{cm}^2}$ and $g_{syn,2} = 0.3\,\frac{\mathrm{mS}}{\mathrm{cm}^2}$, and excitatory coupling with $\alpha = 0.28\,\mathrm{ms}^{-1}$. The heterogeneous values of synaptic conductance scale $H_1(\Phi)$ and $H_2(\Phi)$ so that $G(\Phi)$ does not equal zero for the entire period, predicting no fixed points for equilibrium phase at these parameters.

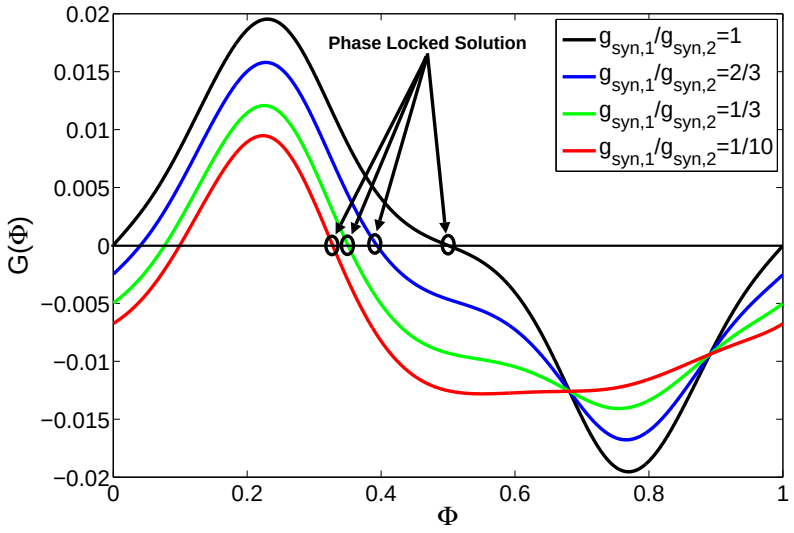

Figure 32: The effect of various amounts of heterogeneity on the function $G(\Phi)$ with $\alpha = 0.1\,\mathrm{ms}^{-1}$, calculated for the Hodgkin-Huxley model with excitatory coupling.

of solutions gradually decreases, intersecting the stable branch of solutions from the identical case at ($\alpha = 0.23\,\mathrm{ms}^{-1}, \Phi = 0.15$). The stable branch continues to decrease as α is increased intersecting a branch of stable solutions for the identical case again at ($\alpha = 0.93\,\mathrm{ms}^{-1}, \Phi = 0, 1$). After this second intersection the stable branch appears to asymptotically approach a value of Φ very close to 1. As we increase α the unstable branch starting at ($\alpha = 0.1\,\mathrm{ms}^{-1}, \Phi = 0.04$) decreases in Φ and intersects an unstable branch of solutions for the identical case at ($\alpha = 0.19\mathrm{ms}^{-1}, \Phi = 0, 1$). We continue to track this branch of solutions, we see it changes stability twice at a pair of saddle-node bifurcations. The first occurs at ($\alpha = 0.23\,\mathrm{ms}^{-1}, \Phi = 0.95$) and the second at ($\alpha = 0.17\,\mathrm{ms}^{-1}, \Phi = 0.65$). In between the two saddle-node bifurcations (while the solutions are stable) this branch of solutions intersects a stable branch from the identical case at ($\alpha = 0.23\,\mathrm{ms}^{-1}, \Phi = 0.85$). After the second saddle-node bifurcation this branch of solutions is once again unstable and intersects an unstable branch of anti-phase solutions for the identical case at ($\alpha = 0.48\,\mathrm{ms}^{-1}, \Phi = 0.5$). After the intersection we continue to increase α and the branch decreases in Φ until it asymptotically approaches the lower unstable branch of solutions resulting from the third pitchfork bifurcation in the identical case. Finally at ($\alpha = 1.39\,\mathrm{ms}^{-1}, \Phi = 0.56$) where we observe another saddle-node bifurcation. This bifurcation creates a stable and unstable pair of solution branches. The stable branch decreases in Φ as α is increased, asymptotically approaching the stable branch of anti-phase solutions from the identical case and the newly created unstable branch increases in Φ as α is increased asymptotically approaching the upper unstable branch of solutions emanating from the third pitchfork bifurcation in the identical coupling case.

Qualitatively, we see some significant differences between the case of Hodgkin-Huxley neurons coupled identically ($h = 1$) and with $h = 2/3$. First, the in-phase and anti-phase solutions are not guaranteed to be solutions when $h = 2/3$. Second, the $h = 2/3$ case has several saddle-node bifurcations and no pitchfork bifurcations. The

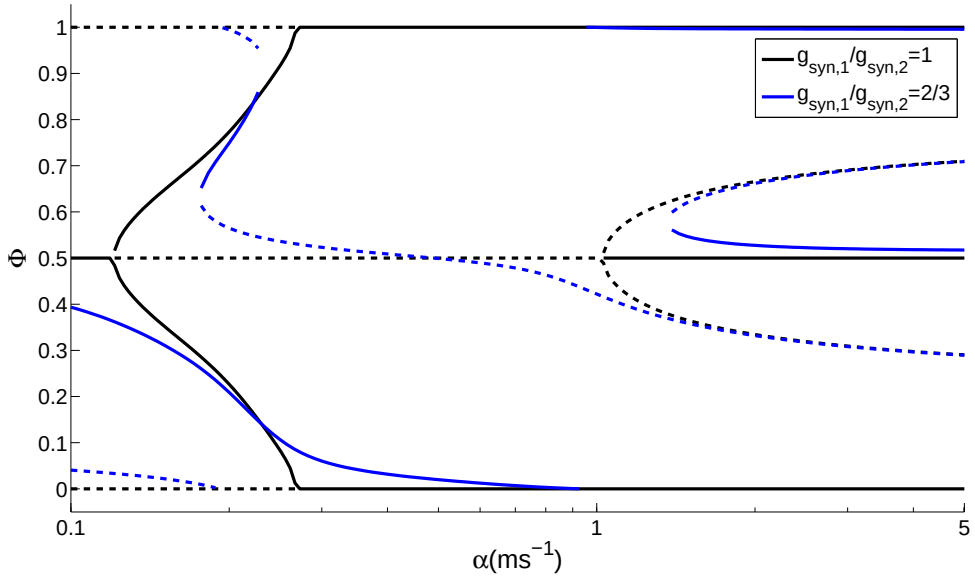

Figure 33: Bifurcation diagram of equilibrium phase-difference versus the synaptic time constant for excitatory coupled Hodgkin-Huxley neurons. The black curve is the identical case, the blue is the case when $h = 2/3$.

qualitative difference between the identical and $h = 2/3$ cases are more pronounced in the neighborhood of the pitchfork bifurcations. As you move away from the pitchfork bifurcations the identical and heterogeneous cases become nearly indistinguishable.

When we compare all 3 cases of heterogeneously, excitatory coupled Hodgkin-Huxley neurons we see little qualitative difference between them (Fig. 34). Branches of solutions of the $h = 1/3$ and $h = 1/10$ cases intersect branches of solutions from the identical case at the same locations as the $h = 2/3$ case. The branch of unstable solutions starting at $(\alpha = 0.1\ \text{ms}^{-1}, \Phi = 0.08)$ also has two saddle-node bifurcations at $(\alpha = 0.23\ \text{ms}^{-1}, \Phi = 0.92)$ and $(\alpha = 0.21\ \text{ms}^{-1}, \Phi = 0.67)$ which are separated by an intersection with a stable branch of solutions from the identical case. The corresponding unstable branch for the $h = 1/10$ case starting at $(\alpha = 0.1\ \text{ms}^{-1}, \Phi = 0.33)$ does not have any saddle-node bifurcations and remains unstable before and after it intersects the stable branch of solutions from the identical case. The third saddle-node bifurcation for the $h = 2/3$ case also occurs for the other heterogeneous cases, but is

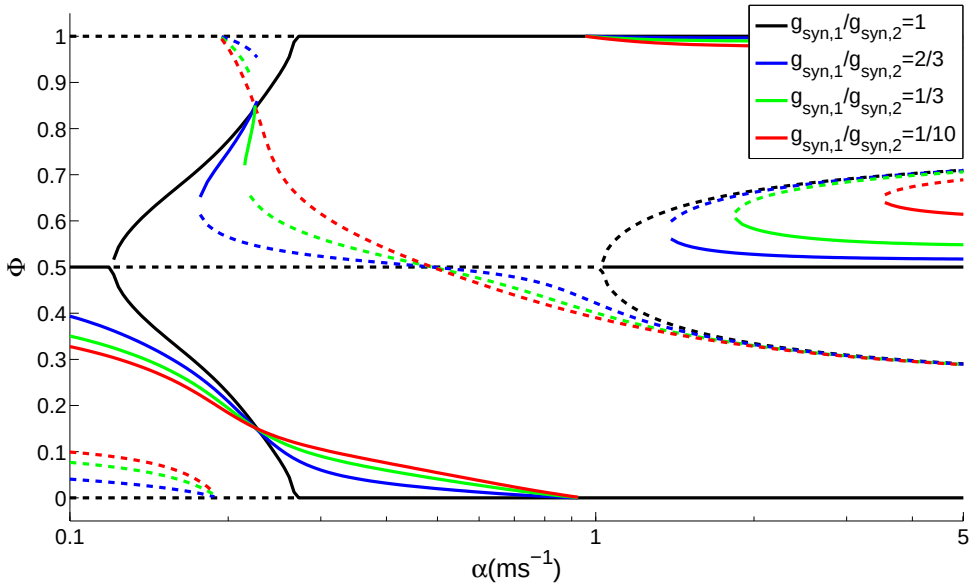

Figure 34: (a) Bifurcation diagram of equilibrium phase-difference versus the synaptic time constant for excitatory coupled Hodgkin-Huxley neurons. As heterogeneity is introduced immediately it is seen that the in-phase solution ($\Phi = 0, 1$) only occurs for a single value of α and the anti-phase solution ($\Phi = \frac{1}{2}$) is completely lost. For larger amounts of heterogeneity the pitchfork bifurcation at about $\alpha = 0.12\,\mathrm{ms}^{-1}$ has completely disappeared and it's remnants can only be seen as changes in curvature in stable line in that region.

shifted to ($\alpha = 1.83\,\mathrm{ms}^{-1}, \Phi = 0.61$) for $h = 1/3$ and to ($\alpha = 3.55\,\mathrm{ms}^{-1}, \Phi = 0.64$) for $h = 1/10$.

Imperfect pitchfork. When we examine the effects that heterogeneities in synaptic conductance had on the third pitchfork bifurcation ($\alpha = 1.0\,\mathrm{ms}^{-1}, \Phi = 0.5$) for excitatory coupled Hodgkin-Huxley neurons (Fig. 34), we see very similar results to the effects of varying the parameter h in the imperfect pitchfork bifurcation (Fig. 9) in the introductory section. The criticality of the bifurcation is reversed, but otherwise the plots are nearly identical. This is not surprising since we have reduced our equations to one dimension and even have a single parameter describing the amount of heterogeneity in our system. The effects of the heterogeneity we introduce has a

less familiar result when we look at the other two pitchfork bifurcations. The imperfect pitchfork breaks a pitchfork bifurcation into a saddle-node bifurcation and a separate branch of solutions which have no bifurcation. Because the other two bifurcations occur in somewhat close proximity in α they wind up interacting with each other. In this case we see that two saddle-node bifurcations resulting from the symmetry breaking when $h = 1/3, 2/3$ but these coalesce eventually yielding just two branches of solutions with no bifurcations when $h = 1/10$. If these two bifurcations were sufficiently separated in α, we presume that we would see the standard imperfect pitchfork scenario occur with the first two pitchforks as we do for the third pitchfork bifurcation.

The bifurcation diagram for inhibitory coupled Hodgkin-Huxley neurons with heterogeneity in coupling strength, $h = 2/3$ (Fig. 35), is qualitatively the same as the excitatory case with the same amount of heterogeneity with the stabilities reversed. A stable branch of solutions starts at $(\alpha = 0.1\,\mathrm{ms}^{-1}, \Phi = 0.14)$. As we increase α the stable branch intersects the stable branch of solutions for the identical case at $(\alpha = 0.4\,\mathrm{ms}^{-1}, \Phi = 0, 1)$. The branch then undergoes the first of two saddle-node bifurcations at $(\alpha = 0.43\,\mathrm{ms}^{-1}, \Phi = 0.94)$ in close proximity to an intersection with an unstable branch of solutions emanating from the first pitchfork bifurcation in the identically coupled case. If we continue to follow this solution branch it changes direction and α decreases as we follow it to the second saddle-node bifurcation at $(\alpha = 0.28\,\mathrm{ms}^{-1}, \Phi = 0.63)$. The branch then turns again and α once again increases. The branch then intersects the stable branch of anti-phase solutions at $(\alpha = 0.98\,\mathrm{ms}^{-1}, \Phi = 0.5)$. The branch decreases in Φ and asymptotically approaches the lower branch of stable solutions resulting from the third pitchfork bifurcation from the identical case. An unstable branch of solutions starts at $(\alpha = 0.1\,\mathrm{ms}^{-1}, \Phi = 0.44)$. As we increase α the values of Φ on the branch decrease and it intersects the unstable branch of solutions emanating from the first pitchfork bifurcation for the identical

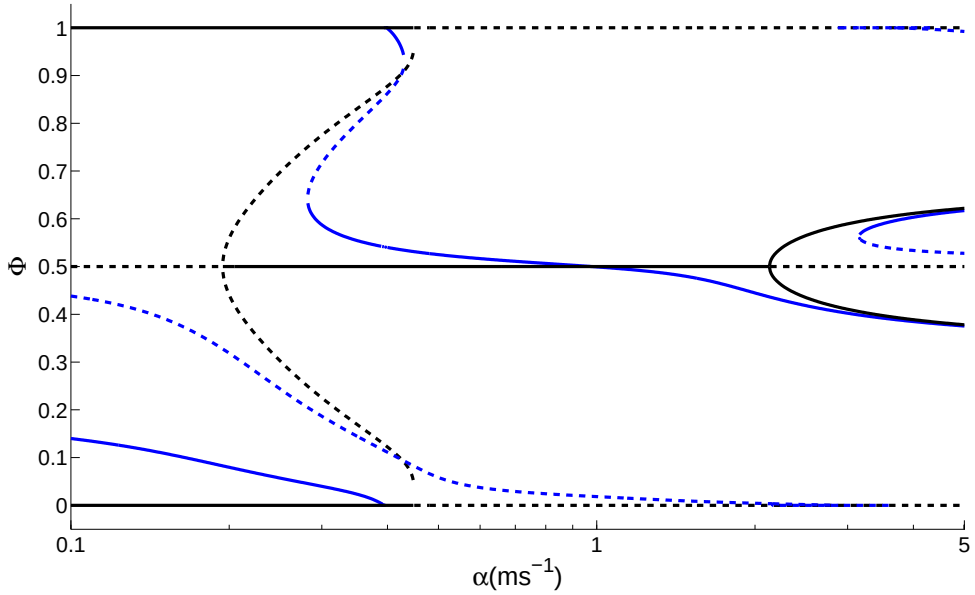

Figure 35: Bifurcation diagram of equilibrium phase-difference versus synaptic rate constant for inhibitory coupled Hodgkin-Huxley neurons. The black curve is for identical ($h = 1$) coupling and the blue curve is for heterogeneous coupling ($h = 2/3$).

case at ($\alpha = 0.43\,\mathrm{ms}^{-1}, \Phi = 0.1$). The branch continues to have decreasing values of Φ until it intersects the unstable branch of in-phase solutions for the identical case at approximately ($\alpha = 2.89\,\mathrm{ms}^{-1}, \Phi = 0, 1$). After it crosses the solution branch for the identical case the branch of unstable solutions asymptotically approaches a nearly in-phase solution at a value of Φ slightly less than 1.

When we increase the heterogeneity to $h = 1/3$ (Fig. 36), we see another significant qualitative change from both the identical and $h = 2/3$ cases for inhibitory coupled Hodgkin-Huxley neurons. This is the first time we encounter a system where there are regions of parameter space where no phase locking occurs. A stable branch starting at ($\alpha = 0.1\,\mathrm{ms}^{-1}, \Phi = 0.2$) and an unstable branch starting at ($\alpha = 0.1\,\mathrm{ms}^{-1}, \Phi = 0.38$) meet at a saddle-node bifurcation at ($\alpha = 0.2\mathrm{ms}^{-1}, \Phi = 0.2$). A second saddle-node bifurcation occurs at ($\alpha = 0.35\,\mathrm{ms}^{-1}, \Phi = 0.08$) from which a stable-unstable pair of solution branches are created. This results in a region of space $0.2\mathrm{ms}^{-1} \leq \alpha \leq 0.35\mathrm{ms}^{-1}$ where no phase-locked solution is predicted. The stable branches crosses the

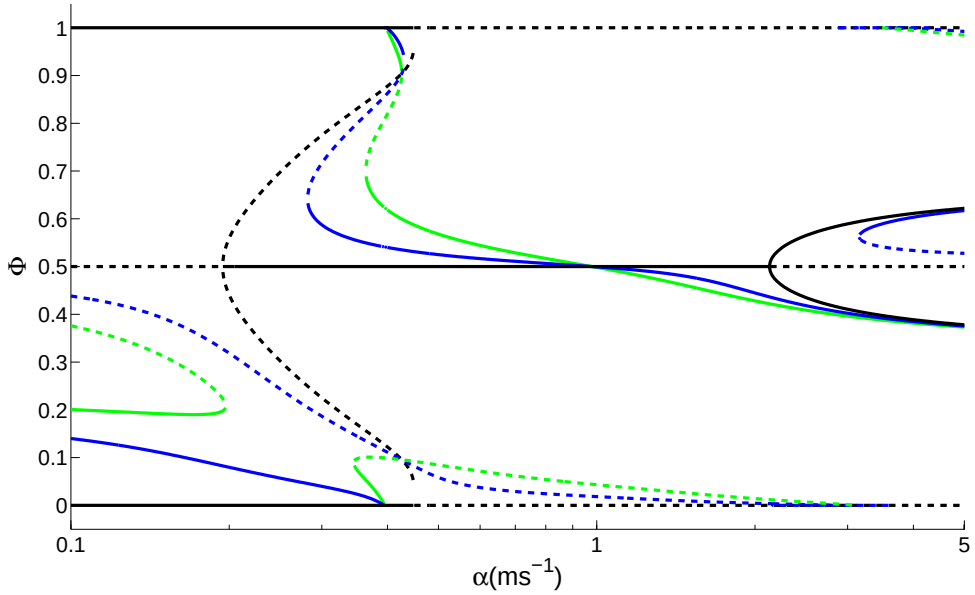

Figure 36: Bifurcation diagram of equilibrium phase-difference versus synaptic rate constant for inhibitory coupled Hodgkin-Huxley neurons. The black curve is for identical ($h = 1$) coupling, the blue and green curves are for heterogeneous couplings ($h = 2/3$ and $1/3$ respectively).

a stable branch of solutions from the identical case at the same point as the $h = 2/3$ case, then crosses the unstable branch of solutions emanating from the first pitch fork bifurcation from the identical case also at the same point that the $h = 2/3$ case crossed. The branch of solutions then changes stability twice through two saddle-node bifurcations occurring at ($\alpha = 0.43\,\mathrm{ms}^{-1}, \Phi = 0.9$) and ($\alpha = 0.36\,\mathrm{ms}^{-1}, \Phi = 0.71$). As we increase α further the branch remains stable, crossing the stable branch of anti-phase solutions from the identical case at the same point as the $h = 2/3$ crossed and then asymptotically approaches the lower branch emanating from the third pitchfork bifurcation in the identical case.

The only qualitative difference between the $h = 1/3$ case and the $h = 1/10$ case (Fig. 37) for inhibitory coupled Hodgkin-Huxley neurons is that the stable branch of solutions resulting from the saddle-node bifurcation which ends the region of no phase-locking occurs does not undergo any saddle-node bifurcations and remains stable

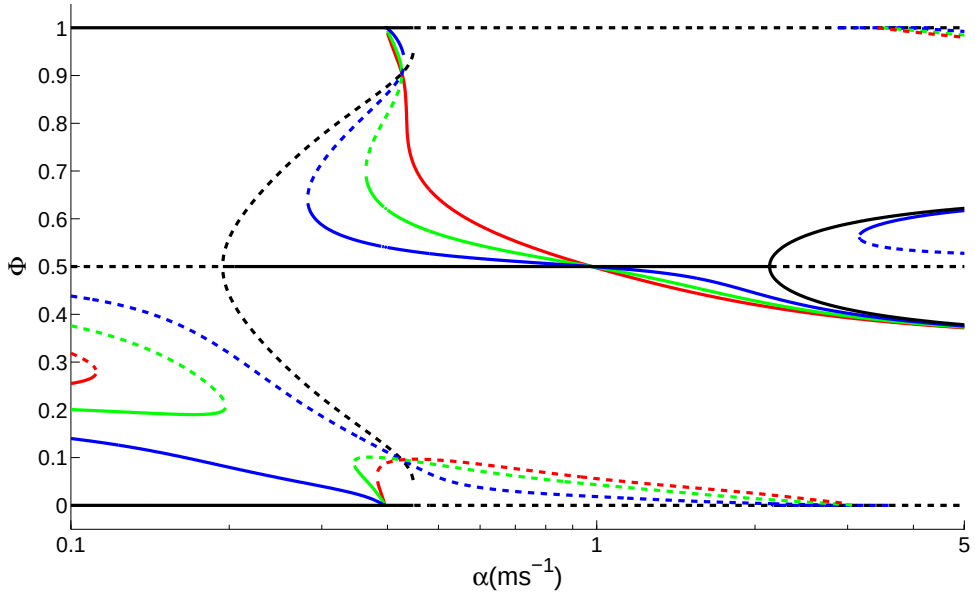

Figure 37: Bifurcation diagram of equilibrium phase-difference versus synaptic rate constant for inhibitory coupled Hodgkin-Huxley neurons. The black curve is for identical ($h = 1$) coupling, the blue, green and red curves are for heterogeneous couplings ($h = 2/3$, $1/3$ and $1/10$ respectively).

throughout. The stable branch of solutions starting at ($\alpha = 0.1\ \mathrm{ms}^{-1}, \Phi = 0.26$) intersects the unstable branch starting at ($\alpha = 0.1\ \mathrm{ms}^{-1}, \Phi = 0.32$) at a saddle-node bifurcation at ($\alpha = 0.11\ \mathrm{ms}^{-1}, \Phi = 0.28$). The is the beginning of a region from $0.11\ \mathrm{ms}^{-1} \leq \alpha \leq 0.38\ \mathrm{ms}^{-1}$ where no phase locking occurs. The second saddle-node bifurcation which ends the region of no phase-locking occurs at ($\alpha = 0.38\ \mathrm{ms}^{-1}, \Phi = 0.07$). For $\alpha > 0.38\ \mathrm{ms}^{-1}$ there is little difference between the $h = 1/3$ and the $h = 1/10$ cases.

Coupling Hodgkin-Huxley neurons with heterogeneous values of synaptic conductance causes the loss of the in-phase and anti-phase solutions that are guaranteed to exist in the identical case of identical coupling. This effect was observed for both types of coupling and all the values of h studied. Heterogeneous coupling above a certain level also caused regions where no phase-locked solution to appear. We only observed this effect in the inhibitory coupled case.

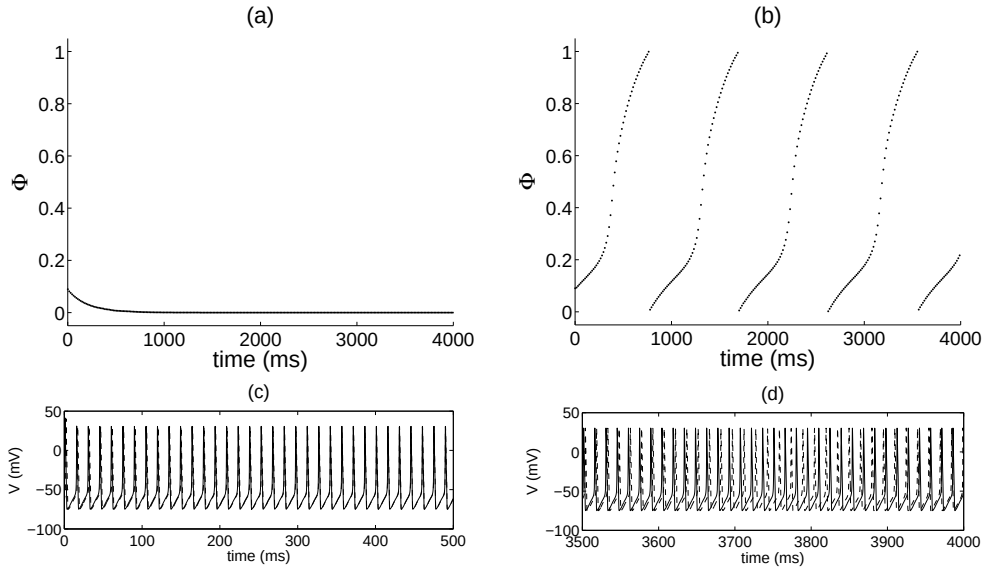

Figure 38: Panels (a) and (b) show the phase-difference, Φ, vs. time for inhibitory coupled Hodgkin-Huxley neurons with $\alpha = 0.25\,\mathrm{ms}^{-1}$. (a) In-phase synchrony with identical values of synaptic conductance, $g_{syn,1} = g_{syn,2} = 0.1\,\frac{\mathrm{mS}}{\mathrm{cm}^2}$ (b) A region of phase space where no phase locking occurs with heterogeneous values of synaptic conductance, $g_{syn,1} = 0.01\frac{\mathrm{mS}}{\mathrm{cm}^2}$ and $g_{syn,2} = 0.1\,\frac{\mathrm{mS}}{\mathrm{cm}^2}$. (c) Voltage trace for same coupling as panel (a) showing in-phase synchrony. (d) Voltage trace for the same coupling as panel (b) showing no phase locking. In panels (c) and (d) solid lines are the voltage traces for neuron 1 and dashed lines are the voltage traces for neuron 2.

4.2.1 Full numerical simulation results

We sought verification of the results of the weak coupling approximation by solving the full equations numerically in the Matlab environment using a fourth order Runga-Kutta integrator. We discussed the details of our numerical methods in the previous section investigating the case of identical coupling. Unlike the identical cases we now have predicted regions where no phase locked state exists. We used a two part criteria for concluding that there was no stable, phase-locked state: the phase-difference changed by more than a factor of 10^{-10} from period to period and the phase-difference was not steadily decreasing from period to period. We chose different example parameter sets in these regions and examined the voltage traces to get an idea of the behavior (Fig. 38). We observed regions where there was no phase-locking

but there were distinct regions of parameter space where the period to period change in phase-difference always slowed down. This occurred in regions of parameter space near where saddle-node bifurcations occurred at values of h close to the one being examined. In these cases, the system is passing through the "ghost of the attractor". We do not suggest that all the behavior in regions with no phase-locking is captured by this description, this is meant to be an example. A more complete, future study should be undertaken to understand the dynamics.

In general we found qualitative agreement between the weak coupling approximation and the results from the full numerical simulations (Fig. 39, 40). Although the weak coupling approximation results only depend on the relative values of synaptic conductance, the full numerical simulations also depend on the individual magnitude. The numerical simulations were calculated with $g_{syn} \leq 0.1 \frac{\text{mS}}{\text{cm}^2}$. This value of synaptic conductance remains within the valid region of weak coupling as shown in [7] where network frequency as a function of synaptic conductance predicted by the weak coupling approximation was compared to that quantity observed in full numerical simulations. For the $h = 2/3$ case we used the values $g_{syn,1} = 0.04 \frac{\text{mS}}{\text{cm}^2}$ and $g_{syn,2} = 0.06 \frac{\text{mS}}{\text{cm}^2}$. For the $h = 1/3$ case we used the values $g_{syn,1} = 0.02 \frac{\text{mS}}{\text{cm}^2}$ and $g_{syn,2} = 0.06 \frac{\text{mS}}{\text{cm}^2}$. For the $h = 1/10$ case we used the values $g_{syn,1} = 0.01 \frac{\text{mS}}{\text{cm}^2}$ and $g_{syn,1} = 0.1 \frac{\text{mS}}{\text{cm}^2}$. Qualitatively the numerical results and the weak coupling results are nearly identical.

4.3 Wang-Buzsaki Model

We found Wang-Buzsaki neurons have greater sensitivity to heterogeneities in synaptic conductances compared with Hodgkin-Huxley neurons. The bifurcation diagrams of equilibrium phase-difference versus the synaptic rate constant we calculated show regions of no phase locking for all values of heterogeneity studied.

For excitatory coupled Wang-Buzsaki neurons (Fig. 41), when $h = 2/3$ a stable

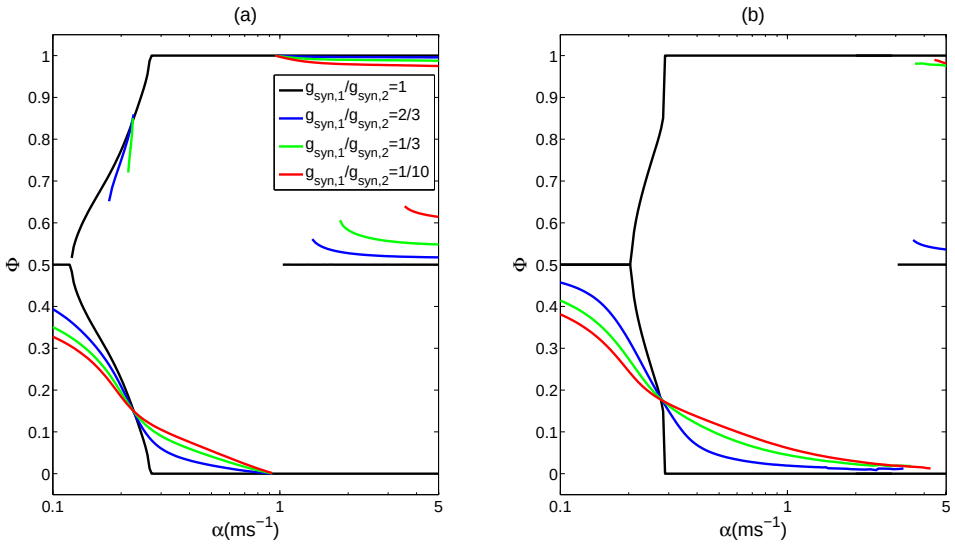

Figure 39: Bifurcation diagrams of equilibrium phase-difference versus synaptic time constant for excitatory coupled Hodgkin-Huxley neurons calculated (a) using the weak coupling approximation and (b) by solving the full set of equations numerically. Only stable fixed points are plotted.

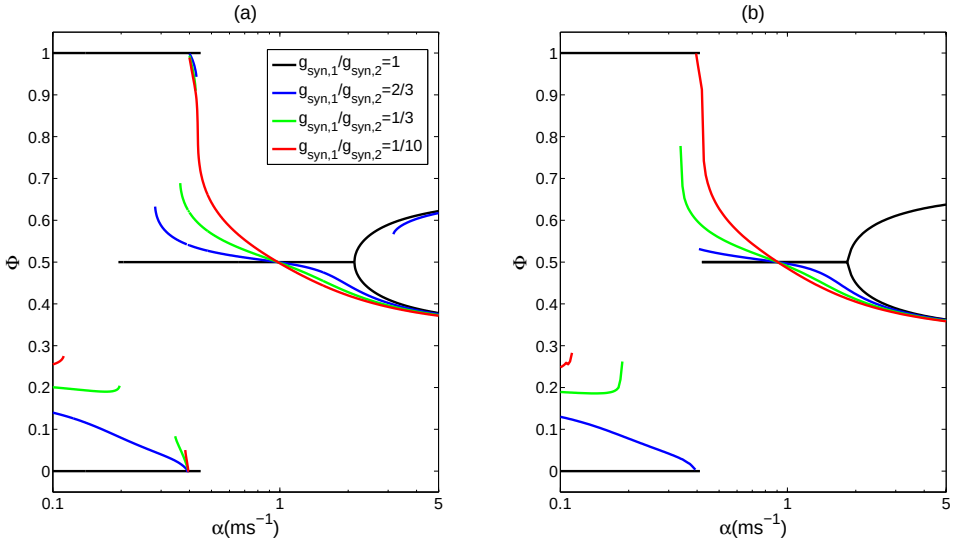

Figure 40: Bifurcation diagrams of equilibrium phase-difference versus synaptic time constant for inhibitory coupled Hodgkin-Huxley neurons calculated (a) using the weak coupling approximation and (b) by solving the full set of equations numerically. Only stable fixed points are plotted.

branch of solutions starts at ($\alpha = 0.1\,\mathrm{ms}^{-1}, \Phi = 0.86$) and an unstable branch of solutions starts at ($\alpha = 0.1\mathrm{ms}^{-1}, \Phi = 0.64$). As we increase α, these branches intersect and annihilate each other at saddle-node bifurcation at ($\alpha = 0.22\mathrm{ms}^{-1}, \Phi = 0.75$). At ($\alpha = 0.92\,\mathrm{ms}^{-1}, \Phi = 0.29$) a second, saddle-node bifurcation occurs creating a stable and unstable pair of solution branches. A region of no phase locked solution exists from $0.22\,\mathrm{ms}^{-1} < \alpha < 0.92\mathrm{ms}^{-1}$. As we continue to increase α the stable branch increases in Φ approaching, but never reaching $\Phi = 0.5$. The branch then begins to decrease in Φ and seemingly asymptotically approaches the lower stable branch of solutions emanating from the third pitchfork bifurcation from the identical case. The unstable branch of solutions, created at the second saddle-node bifurcation, decreases in Φ as we increase α, approaching but never reaching $\Phi = 0, 1$. The unstable branch begins to increase in Φ as we follow it to the fourth pitchfork bifurcation from the identical case and has values very close to the unstable branch created from that pitchfork bifurcation. When $h = 1/3$ we see a region with no phase locked solutions from $0.1\,\mathrm{ms}^{-1} < \alpha < 1.68\mathrm{ms}^{-1}$. At ($\alpha = 1.68\,\mathrm{ms}^{-1}, \Phi = 0.23$) a saddle-node bifurcation occurs creating a stable and unstable pair of solution branches. When $h = 1/10$ there are no phase locked solutions for the entire region of α that we studied.

Inhibitory coupled Wang-Buzsaki neurons (Fig. 42) with $h = 2/3$ has a stable branch of solutions starting at ($\alpha = 0.1\,\mathrm{ms}^{-1}, \Phi = 0.67$) and an unstable branch of solutions starting at ($\alpha = 0.1\,\mathrm{ms}^{-1}, \Phi = 0.9$). These two branches intersect and annihilate at a saddle node bifurcation at ($\alpha = 0.20\,\mathrm{ms}^{-1}, \Phi = 0.80$). At ($\alpha = 0.81\mathrm{ms}^{-1}, \Phi = 0.27$) a second saddle-node bifurcation occurs creating a stable and unstable pair of solution branches. There is a region of no phase locked solution from $0.20\mathrm{ms}^{-1} < \alpha < 0.81\mathrm{ms}^{-1}$. As we increase α, the unstable branch of solutions increases in Φ approaching, but never reaching $\Phi = 0.5$ then decreases in Φ as it approaches the lower, unstable branch from the third pitchfork bifurcation from the

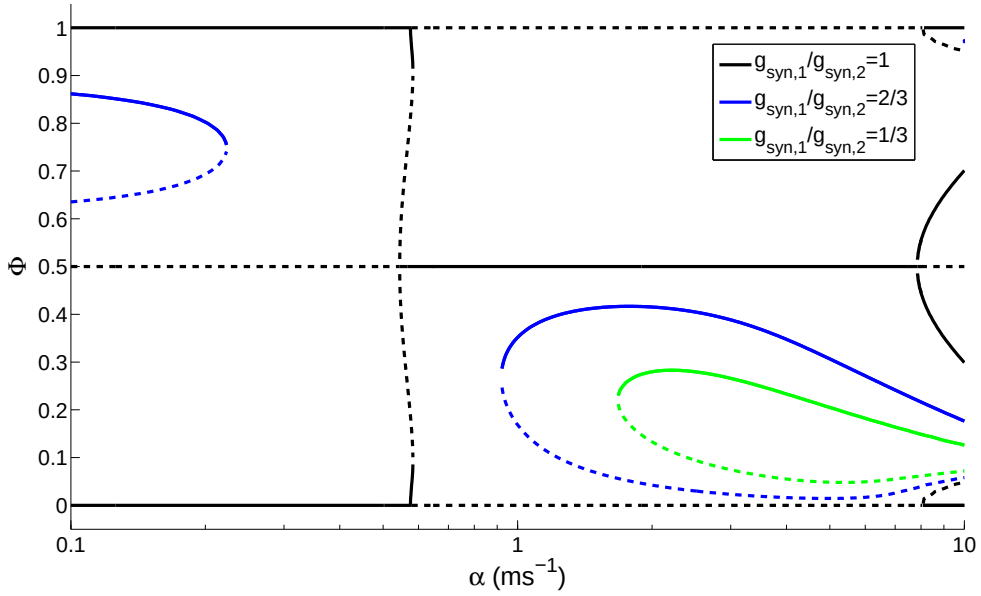

Figure 41: Bifurcation diagram of equilibrium phase-difference versus the synaptic time constant for excitatory coupled Wang-Buzsaki neurons, calculated using the weak coupling approximation. Solid lines indicate stable solutions and dashed lines unstable solutions.

identical case. The stable branch of solutions created at the second saddle-node bifurcation decreases in Φ as we increase α until it intersects the stable branch of in-phase solutions at $(\alpha = 3.76\,\mathrm{ms}^{-1}, \Phi = 0, 1)$. The branch of stable solutions decreases from a value of $\Phi = 1$ until $\alpha = 10\mathrm{ms}^{-1}$, the upper boundary of the region of α studied. A third saddle-node bifurcation occurs at $(\alpha = 9.63\,\mathrm{ms}^{-1}, \Phi = 0.69)$ creating a stable and unstable pair of solution branches. For $h = 1/3$ there is a region of no phase locked solutions from $0.1\ \mathrm{ms}^{-1} < \alpha < 1.46\ \mathrm{ms}^{-1}$. At $(\alpha = 1.46\ \mathrm{ms}^{-1}, \Phi = 0.20)$ a saddle-node bifurcation occurs creating a stable and unstable pair of solution branches. For $h = 1/10$ there is a region of no phase locked solutions from $0.1\mathrm{ms}^{-1} < \alpha < 2.34\mathrm{ms}^{-1}$. At $(\alpha = 2.34\ \mathrm{ms}^{-1}, \Phi = 0.13)$ a saddle-node bifurcation occurs creating a stable and unstable pair of solution branches.

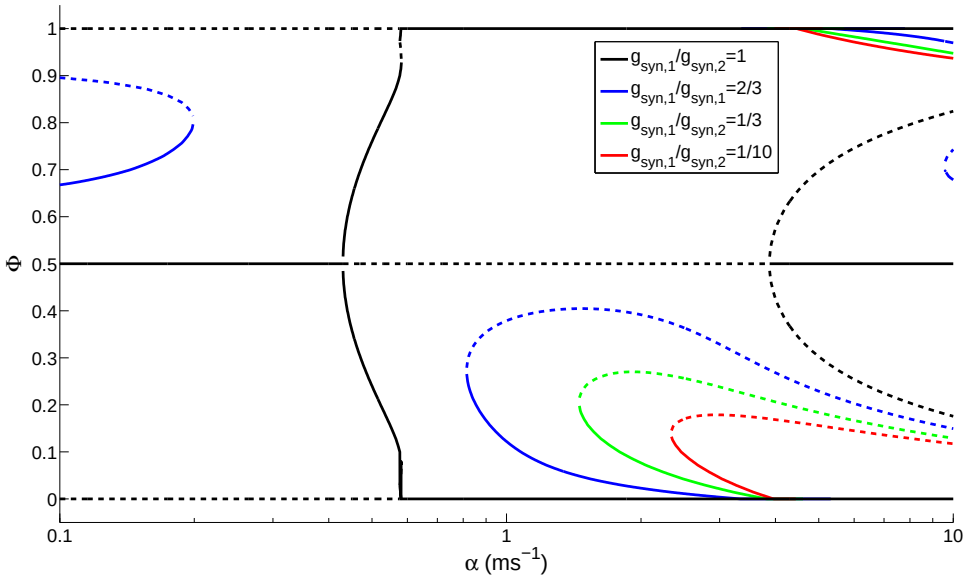

Figure 42: Bifurcation diagram of equilibrium phase-difference versus the synaptic time constant for inhibitory coupled Wang-Buzsaki neurons, calculated using the weak coupling approximation. Solid lines indicate stable solutions and dashed lines unstable solutions.

4.3.1 Full numerical simulation results

Using the same numerical procedure for solving the full set of equations for the system of coupled Wang-Buzsaki neurons described previously, we verified the bifurcation diagrams of equilibrium phase-difference versus the synaptic rate constant calculated using the weak coupling approximation (Fig. 43, 44). The values chosen as the synaptic conductances are the same as those chosen for the numerically calculated Hodgkin-Huxley bifurcation diagrams. We see very good qualitative agreement between the results from the weak coupling approximation and those calculated using the full set of equations.

4.4 Bifurcation analysis

We have shown only results for $h \leq 1$ thus far. Despite the heterogeneous coupling there is still a symmetry present in our system. The neurons in our system are

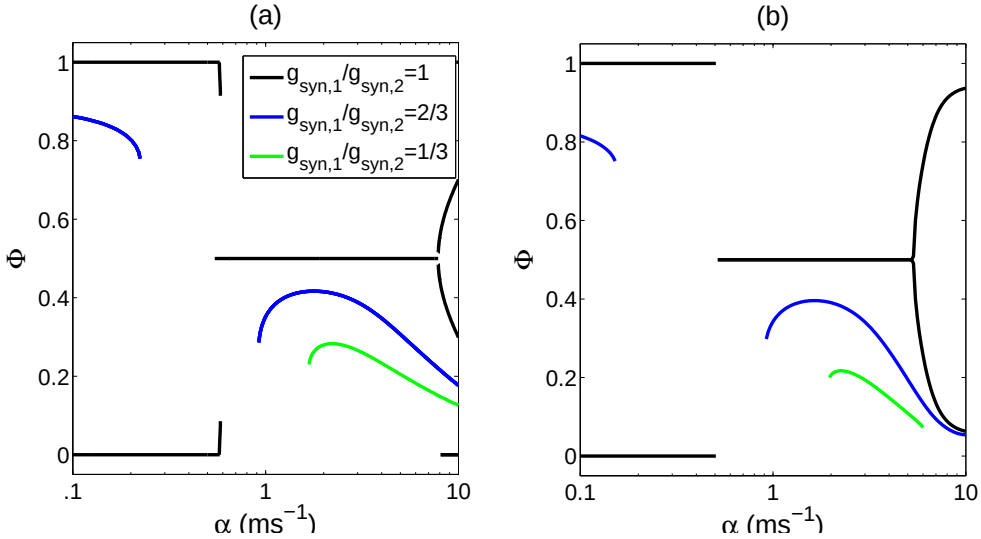

Figure 43: Numerically calculated bifurcation diagram of equilibrium phase-difference versus synaptic time constant for excitatory and coupled Wang-Buzsaki neurons compared with the weak coupling approximation results. The solid lines are the results of full numerical simulations, the dashed lines are results from the weak coupling approximation. All the points shown are stable fixed points of equilibrium phase-difference.

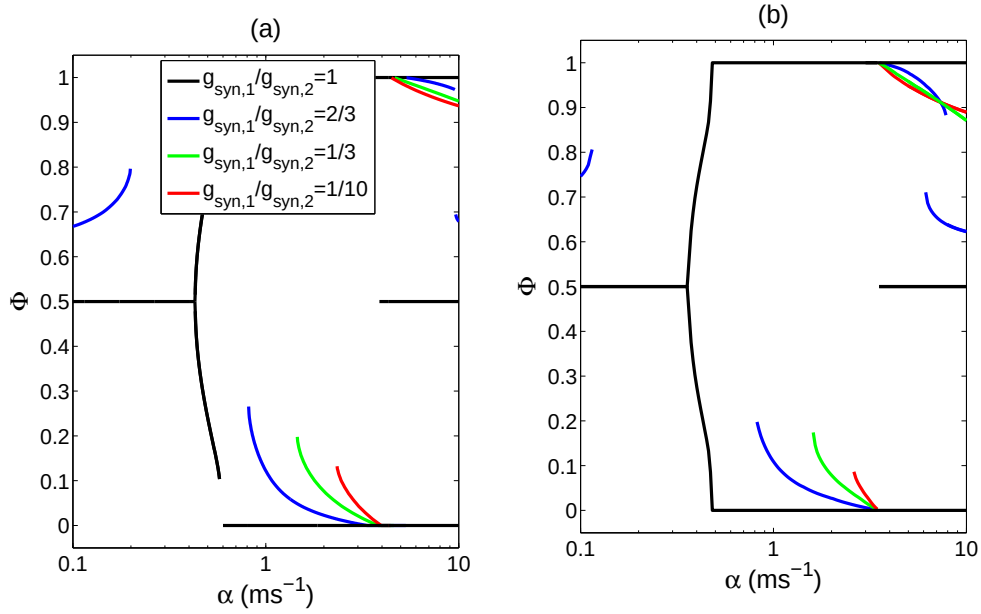

Figure 44: Bifurcation diagrams of equilibrium phase-difference versus synaptic time constant for inhibitory coupled Wang-Buzsaki neurons calculated (a) using the weak coupling approximation and (b) by solving the full set of equations numerically. Only stable fixed points are plotted.

identical. Therefore, exchanging the coupling (i.e. $h = 3/2$ instead of $h = 2/3$) yields a reflection of the former bifurcation diagram about the anti-phase ($\Phi = 0.5$) axis. The bifurcation diagram of any value of h (Fig. 45) is a reflection about the $\Phi = 0.5$ axis of the bifurcation diagram for $1/h$ (Fig. 46). Earlier we described the cusp bifurcation point as being the point where two branches of saddle-node points meet. In order to show this occurring in our systems we must consider both data for $h > 1$ and $h < 1$. In Fig. 41 and 42 we observe for a given value of h there are a pair of saddle-node bifurcation points. As we change h these points move. Plotting a number of these moving points in succession will establish a branch of saddle-node points that is a function of h. As we described in introductory material, we identify the saddle-node points as the points where $G(\Phi) = 0$ and $\frac{dG(\Phi)}{d\Phi} = 0$. At the cusp point $\frac{d^2G(\Phi)}{d\Phi^2} = 0$ in addition to the conditions for the saddle-node point. Varying both α and h allows us to "unfold the cusp" bifurcation. What we find is that the underlying structure of all 4 systems studied in this section is multiple cusp bifurcations [15].

When we plot both branches of the saddle-node points (one branch for $h \leq 1$ and the second for $h \geq 1$), they intersect at the point in phase space where the pitchfork bifurcation occurred ($h = 1$) (Fig. 47). This provides a qualitative description of the role of heterogeneity in the bifurcation structure, the viewer need not be concerned with the exact value of heterogeneity but more importantly the direction on each branch which heterogeneity is increasing and decreasing. The different bifurcation diagrams observed for individual values of h (Fig. 34, 37, 41, 42) occur because the branches of saddle-node points are crossed at distinct locations (Fig.48) in the (h, α) parameter space. The special case where $h = 1$ passes, symmetrically through all the cusp points of the system. Any value of $h \neq 1$ will not intersect any cusp point, and will intersect branches of saddle-node points individually.

In all four of the cases with identical coupling we study there is a similar bifurcation

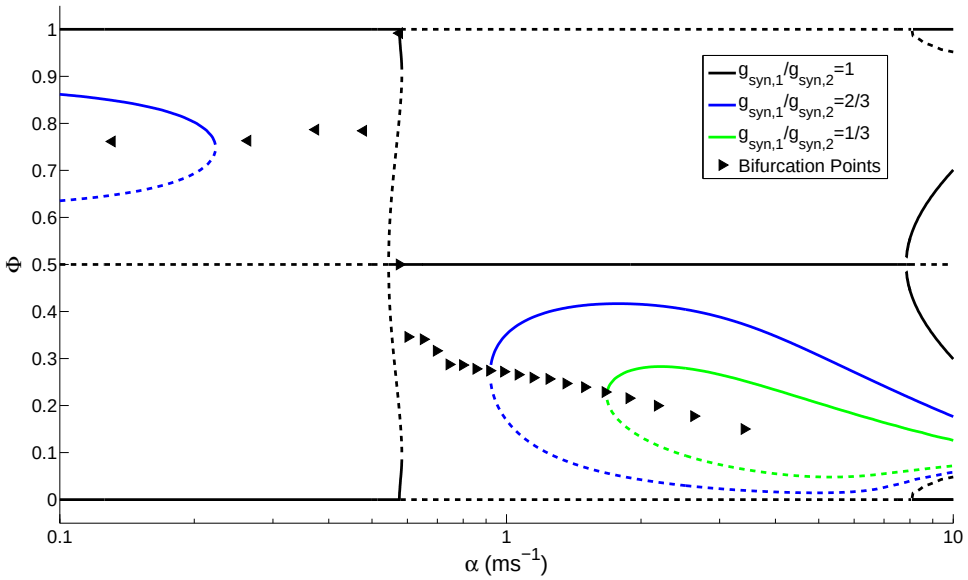

Figure 45: Bifurcation diagram showing equilibrium phase-difference as a function of the synaptic rate constant for excitatory coupled Wang-Buzsaki neurons with $h \leq 1$. There is a symmetry between heterogeneities of h and $1/h$. As h is varied the saddle-node bifurcation points move. The black triangles indicate saddle-node points; the vertex pointing in the horizontal direction indicates the direction of increasing heterogeneity.

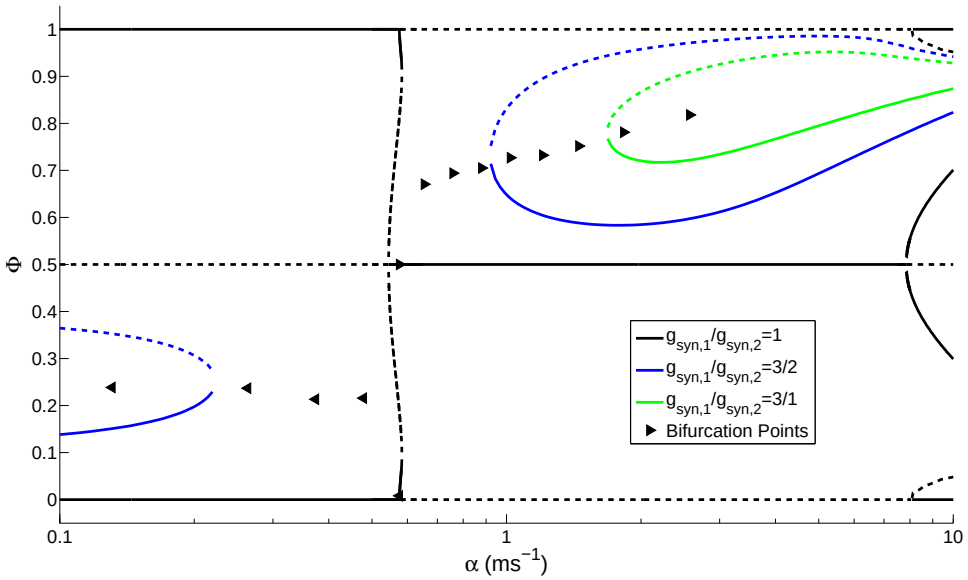

Figure 46: Bifurcation diagram showing equilibrium phase-difference as a function of the synaptic rate constant for excitatory coupled Wang-Buzsaki neurons with $h \geq 1$. There is a symmetry between heterogeneities of h and $1/h$. As h is varied the saddle-node bifurcation points move. The black triangles indicate saddle-node points; the vertex pointing in the horizontal direction indicates the direction of increasing heterogeneity.

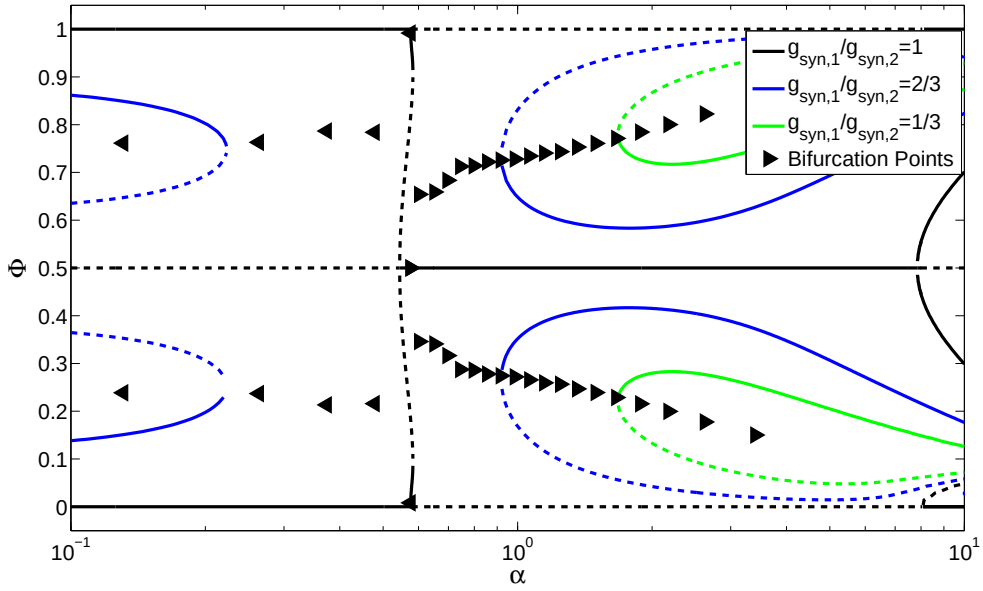

Figure 47: Bifurcation diagram of weakly excitatory coupled Wang-Buzsaki neurons with several branches of saddle-node bifurcation points highlighted. We have combined the cases with $h > 1$ and $h < 1$ on a single plot to illustrate the interaction of the branches of saddle-node points. The black triangles numerically track the branches of saddle-node points as h is varied. Heterogeneity is being varied to create the saddle-node branches and the vertex of the triangles point in the direction of increasing heterogeneity.

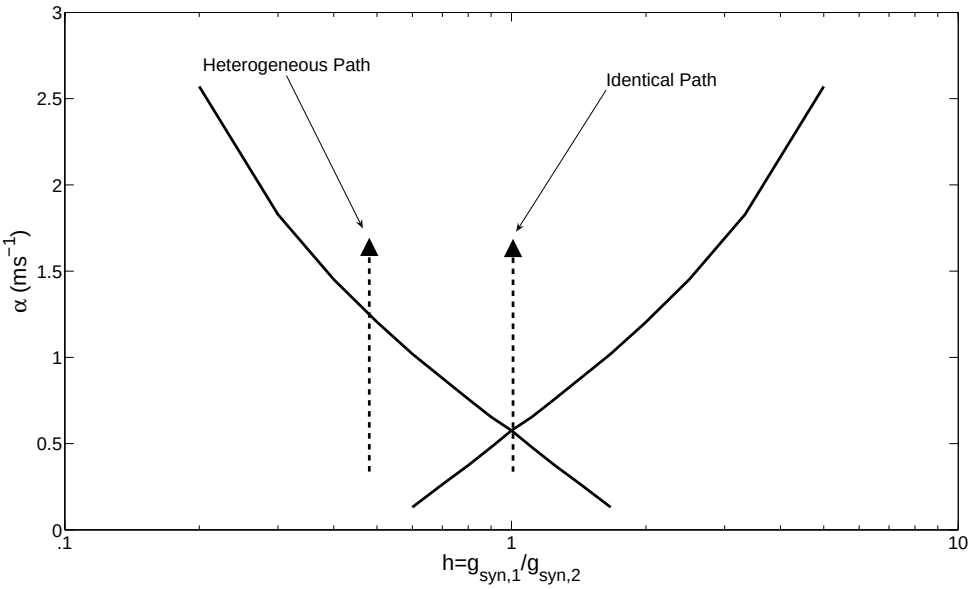

Figure 48: Saddle-node bifurcation points plotted as a function of α and h for the same system as Fig. 47. The dotted lines show two possible paths, the first path is when $h = 1$ or the identical case. When $h = 1$ the system passes symmetrically through all the cusp points as α is varied. When only plotting α vs. Φ this would appear as a series of pitchfork bifurcations. The other path is an example heterogeneous path where neither cusp point is encountered, a series of saddle-node bifurcations occur as α is varied.

structure, all having three pitchfork bifurcations (Fig. 22, 23, 26, 27). The pitchfork bifurcations occur at values of $\Phi = 0.5, 1$ or 0, and 0.5 again as we increase α. When the coupling is identical and we vary α, the system passes through the different cusp points in a symmetric way with respect to the branches of saddle-node points which converge at the cusp, producing the series of pitchfork bifurcations observed. When we have heterogeneities in g_{syn} and vary α, the system no longer moves over the cusp points and we observe the two branches of saddle-node points separately (Fig. 48).

By tracking the branches of saddle-node points and noting their intersections we show the more general form of the cusp bifurcations in our systems. This bifurcation diagram allows us to consider the identical and heterogeneous cases simultaneously.

The most significant change to the dynamics that we observe with heterogeneity in synaptic coupling is the loss of any phase locked solution in some regions of parameter space. For the Wang-Buzsaki model these regions come as a result of the cusp points being very close together. Usually a pitchfork bifurcation will split into a saddle node bifurcation and a branch of fixed points for any given value of h. Because of the close proximity the branch of fixed points from one cusp bifurcation intersects the branch of fixed points from the second cusp yielding another saddle-node bifurcation. For a given value of h, this produces a region of parameter space between the saddle-node points where no fixed point exists. The inhibitory coupled Hodgkin-Huxley case has another mechanism leading to a region of parameter space with no fixed points. In this case two saddle node bifurcations intersect at a transcritical bifurcation (Fig. 49). The transcritical bifurcation is different from a saddle-node or pitchfork bifurcations as fixed points are neither created nor destroyed [2]. As we discussed in the introductory section, they can be thought of as a point where branches of solutions exchange stability. If we think of the actual transcritical bifurcation as an "X" where two trajectories cross, varying h splits the "X" either horizontally ($h = 2/3$ curve in Fig. 49) or vertically ($h = 1/3$ curve in Fig. 49). We showed the effects

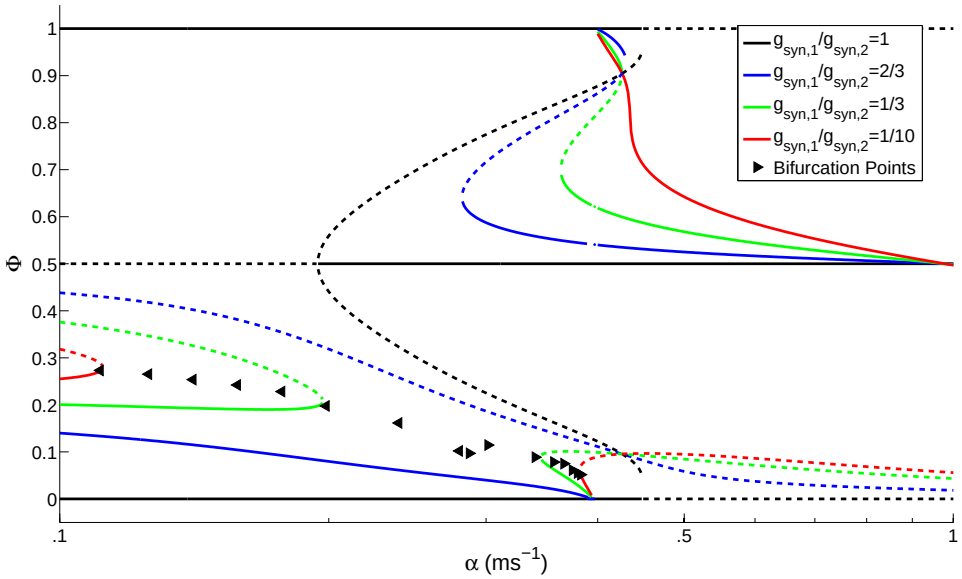

Figure 49: Transcritical bifurcation leading to the loss of phase locking for the inhibitory coupled Hodgkin-Huxley case. The magenta and cyan curves show the branches of saddle-node points which intersect at $\alpha \approx 0.28\text{ms}^{-1}$. The arrows on the lines indicate the direction of increasing heterogeneity.

that introducing a heterogeneity parameter into the normal form of the transcritical bifurcation (Fig. 8). In the current case we see that the transcritical bifurcation occurs when the coupling strengths are not identical. For the case of excitatory coupled Hodgkin-Huxley neurons we predict that increasing the heterogeneity greater than $h = 1/10$ we would also see a transcritical bifurcation occur. Clearly the trend towards this bifurcation is visible. In contrast we believe that this same mechanism leading to regions of parameter space with no phase locking also occurs in both the Wang-Buzsaki systems we studied, but at values of heterogeneity less than $h = 2/3$. The reason for the differences is the amount of separation in α between the two pitchfork bifurcations which occur for small values of α.

4.5 Discussion

We have shown there are qualitative changes to the behavior of coupled neurons when heterogeneity in synaptic conductance is present when compared to the identical case. Heterogeneity produces regions where no phase-locked solutions exist and even a modest amount of heterogeneity results in phase-locked solutions that are neither in-phase ($\Phi = 0, 1$) or anti-phase ($\Phi = 0.5$). In attempting to verify these predictions with real neurons it is necessary to take careful consideration of what will be observable. For example, the difference between in-phase and near in-phase synchronization is very difficult to differentiate in current experiments due to intrinsic network variability. When considering excitatory coupled Type II neurons as α is increased, one could observe the trend from nearer to anti-phase to in-phase and further it is predicted that the firing order will change (as Φ changes from near 0 to near 1 the firing order changes). Three of the four cases we studied predict regimes of parameter space where no phase-locking occurs. Verification of the existence of these regions would be a step to validating that this type of analysis is qualitatively describing the real system. Some regions of bi-stability are predicted, but again the question of observability must be considered. A useful future computational study would be determining the relative strength of attraction of different states in regions of bi-stability. In a region of bi-stability if one state has a much stronger attractor it is possible that the weaker attracting state will not be observed in an experiment.

In the previous paragraph we referenced predicted changes in firing order. For cases including heterogeneity, the weak coupling approximation does contain information about firing order. Identical neurons, coupled identically are interchangeable with no effect on the solution set. Bifurcation diagrams for the identically coupled case are symmetric under an exchange of neurons. For this reason every branch of fixed points has a corresponding branch reflected about the anti-phase ($\Phi = 0.5$) axis for the identical case. The symmetry breaking effects to the bifurcation diagrams occur

immediately when any heterogeneity is introduced. This symmetry breaking caused by heterogeneous coupling allows an additional prediction, that of firing order, to be made. When heterogeneity in synaptic conductance is present solutions are no longer found as symmetric pairs reflected about the anti-phase axis, only a single solution which specifies a firing order is found. For example, $\Phi(\alpha) = \Phi_1(\alpha) - \Phi_2(\alpha) = 0.1$ is a prediction of nearly in-phase synchrony with neuron 1 is firing at $0.1T$ before neuron 2, where T is the period. Since there is no symmetric solution, a phase-difference along with a firing order is predicted from the weak coupling approximation. Obviously no multi-period behavior, such as alternating firing order from one period to the next, will be captured by a straight forward application of this weak coupling technique.

The fact that we observe the multiple cusp bifurcation structure in all of the systems we studied leads us to speculate that multiple cusp bifurcations maybe the fundamental bifurcation structure of the dynamics of weakly coupled neurons with either mutual excitatory or inhibitory coupling. A second, related observation we have made is that qualitatively there is little difference between excitatory (inhibitory) coupled Hodgkin-Huxley neurons and inhibitory (excitatory) coupled Wang-Buzsaki neurons for the identical case. For the cases that are qualitatively different, the difference is simply a swapping of the stable and unstable fixed points. For the heterogeneous cases, the Type I Wang-Buzsaki neuron system shows a greater sensitivity to heterogeneity in conductance strength than the Type II Hodgkin-Huxley neuron system. We suspect that this sensitivity, particularly the regions of no-phase locking, occurs because of the close proximity of the cusp bifurcations on the α axis (Fig. 48). Less heterogeneity in synaptic conductance is required to cause branches of solutions from each cusp to intersect at a transcritical bifurcation point the closer in α the first two cusp points are located.

We used two different approaches to understanding the effects that heterogeneity

has on the mutual coupled neuron dynamics. A weak coupling approximation and an examination of the one dimensional function $G(\Phi)$ allowed us to track stable and unstable branches of solutions. From that we were able to observe what we recognized as imperfect pitchfork bifurcations. We then examined the system by tracking branches of saddle-node points. In this way we were able to unfold the multiple cusp bifurcation structure underlying each of the 4 systems studied,. This last approach yielded us a more fundamental understanding of the behavior of the systems and explained both the identical and heterogeneous cases simultaneously.

CHAPTER V

EXCITATORY TO INHIBITORY COUPLING

Heterogeneity in neural networks may arise from different types of coupling. A pair of mutually coupled neurons may have one excitatory synapse and one inhibitory synapse (E-I). In this section, we study both E-I coupled Hodgkin-Huxley and Wang-Buzsaki neurons. In both of these studies we apply the same weak coupling approximation and averaging procedure that we previously used to study E-E and I-I coupled neurons. Unlike studying heterogeneities in coupling strength, there is no "identical case" from which to start when examining E-I coupling. The weak coupling approximation is limited in the information that it can supply about a system. When we desire to know information which can be supplied by this approximation it is an efficient method to choose. Our final study is conducted on a system of E-I coupled theta neurons. We want to find $1:n$ coupled states, where n is an integer. This information could not be found by our straight forward application of the weak coupling approximation. We use return maps which we introduced earlier to locate various $1:n$ coupled states.

5.1 Excitatory to inhibitory coupled Hodgkin-Huxley neurons

We begin our study of E-I coupled pairs of neurons with a pair of weakly coupled Hodgkin-Huxley neurons. Aside from the synaptic reversal potentials (E_{syn}) all the parameters are the same as we described in the introductory portion of this thesis. The system is set up so that neuron 1 receives inputs from neuron 2 through an excitatory synapse ($E_{syn} = 35\,\text{mV}$) and neuron 2 receives inputs from neuron 1 via an inhibitory synapse ($E_{syn} = -77\,\text{mV}$).

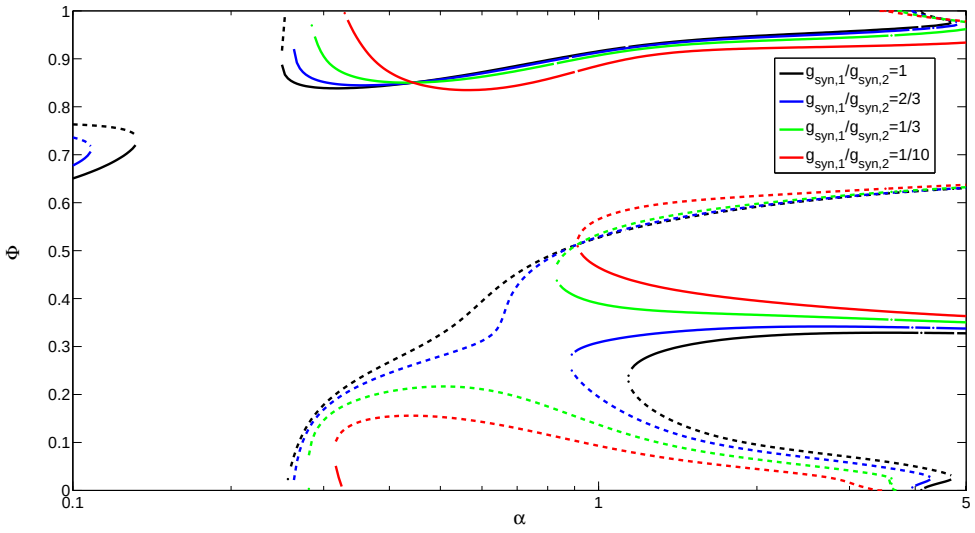

Figure 50: Bifurcation diagram of equilibrium phase-difference versus the synaptic rate constant for E-I coupled Hodgkin-Huxley neurons. The color coding is consistent with previous figures indicating the value of $h = g_{syn,1}/g_{syn,2}$.

As we expected we see no clear symmetry for E-I coupled Hodgkin-Huxley neurons as we vary the heterogeneity in coupling strength with similar values in the previous section (Fig. 50). We observe several saddle node bifurcations. For the case of identical coupling strength there are saddle-node bifurcations at $(\alpha = 0.13\,\mathrm{ms}^{-1}, \Phi = 0.74)$, $(\alpha = 0.25\,\mathrm{ms}^{-1}, \Phi = 0.89)$, $(\alpha = 1.15\,\mathrm{ms}^{-1}, \Phi = 0.21)$ and $(\alpha = 4.68\,\mathrm{ms}^{-1}, \Phi = 0.03)$. Qualitatively the case of $h = 2/3$ is the same as the identically coupled case with saddle-node bifurcations occurring at $(\alpha = 0.11\,\mathrm{ms}^{-1}, \Phi = 0.71)$, $(\alpha = 0.26\,\mathrm{ms}^{-1}, \Phi = 0.93)$, $(\alpha = 0.90\,\mathrm{ms}^{-1}, \Phi = 0.24)$, and $(\alpha = 4.27\,\mathrm{ms}^{-1}, \Phi = 0.03)$. We observe a qualitative difference between the $h = 2/3$ and $h = 1/3$ cases. If we zoom into the region surrounding the saddle-node point at $(\alpha = 0.90\,\mathrm{ms}^{-1}, \Phi = 0.24)$ for the $h = 2/3$ case and add in several other curves for $1/3 < h < 2/3$ we see that the saddle-node point for the $h = 2/3$ case gradually moves until it intersects the branch of unstable solutions (Fig. 51). As we continue to vary h the branch of unstable solutions not terminates at a saddle-node point where it meets the branch of stable solutions. We see the branch of unstable solutions that previously terminated at a

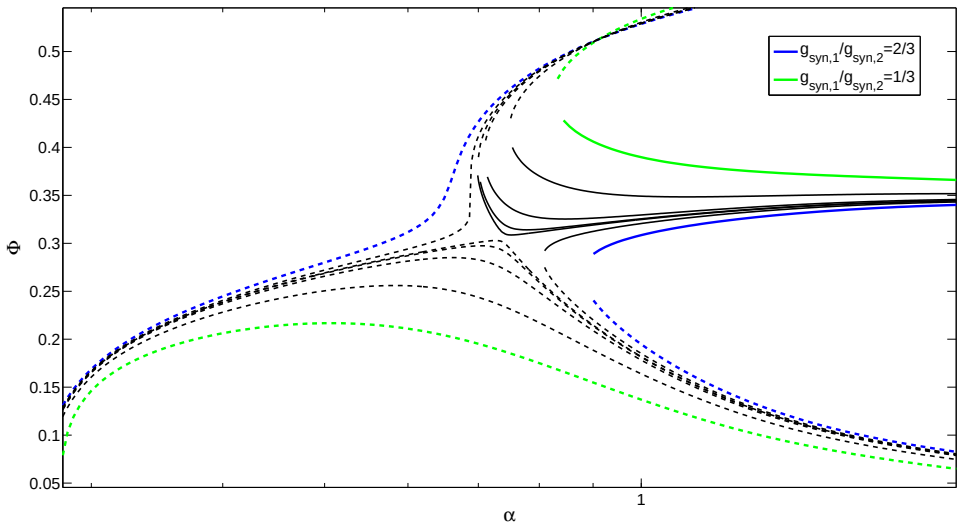

Figure 51: Zoomed in region for E-I coupled Hodgkin-Huxley neurons showing the intersection of a saddle-node point and an unstable branch of solutions. The black curves are for $1/3 < h < 2/3$.

saddle-node now continue with no bifurcation out of the zoomed in region. This is the behavior we expect to see around a cusp point. This bifurcation leaves us with two saddle-node points visible in the region of α we explored at $(\alpha = 0.28\,\text{ms}^{-1}, \Phi = 0.07)$ and $(\alpha = 0.84\ \text{ms}^{-1}, \Phi = 0.43)$. The $h = 1/10$ case is qualitatively the same as the $h = 1/3$ case with two saddle-node points at $(\alpha = 0.32\ \text{ms}^{-1}, \Phi = 0.10)$ and $(\alpha = 0.92\,\text{ms}^{-1}, \Phi = 0.49)$.

In our E-I study we wanted to explore a wider range of heterogeneities to see if there is a way that heterogeneity in synaptic conductance strength can balance the inherent heterogeneity in E-I coupling. Up to a value of $h = 1/1000$ we observed no such "balancing" of heterogeneity (Fig. 52). For heterogeneities stronger than $h = 1/1000$ there was little change. We plotted the case of $h = 0$ using $g_{syn,1} = 0\,\frac{\text{mS}}{\text{cm}^2}$ and $g_{syn,2} = 0.1\,\frac{\text{mS}}{\text{cm}^2}$ (Fig. 53). This one way coupling case had nearly identical results to the $h = 1/1000$ case, except it it contained only one saddle-node bifurcation at $(\alpha = 0.39\ \text{ms}^{-1}, \Phi = 0.03)$. We did, however, observe another qualitative change which occurred $1/10 < h < 1/100$. We examined more closely the region and found

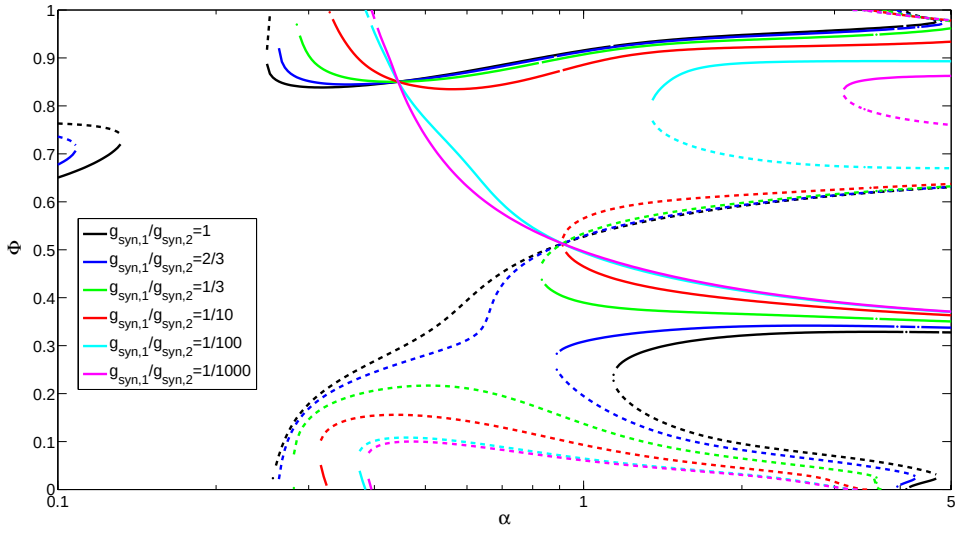

Figure 52: Bifurcation diagram of equilibrium phase-difference versus the synaptic rate constant for E-I coupled Hodgkin-Huxley neurons. The color coding is consistent with previous figures indicating the value of $h = g_{syn,1}/g_{syn,2}$ with the addition of a cyan curve for $h = 1/100$ and a magenta curve for $h = 1/1000$.

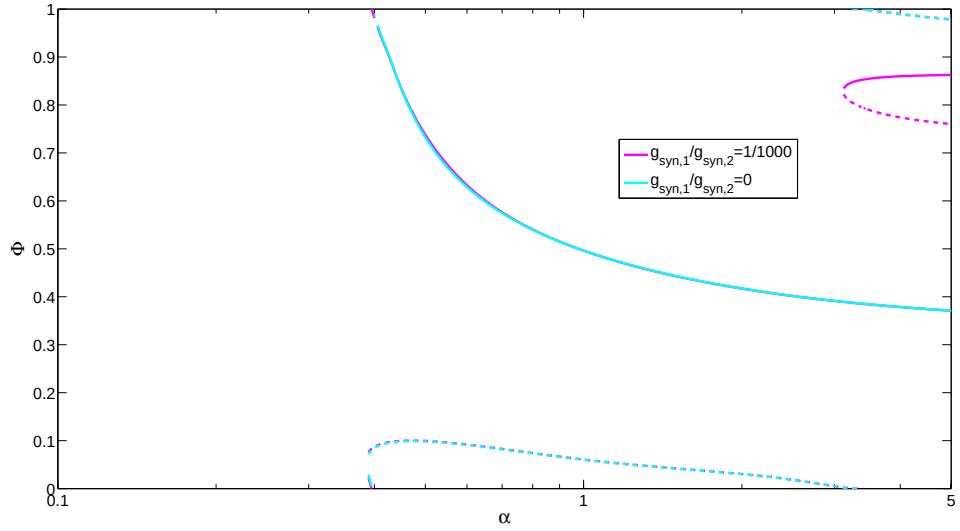

Figure 53: Bifurcation diagram of equilibrium phase-difference versus the synaptic rate constant for E-I coupled Hodgkin-Huxley neurons. We observe that the $h = 1/1000$ (magenta) and $h = 0$ (cyan) cases nearly overlap for the first saddle-node bifurcation. A second saddle-node bifurcation occurs in the $h = 1/1000$ case but not the $h = 0$ case.

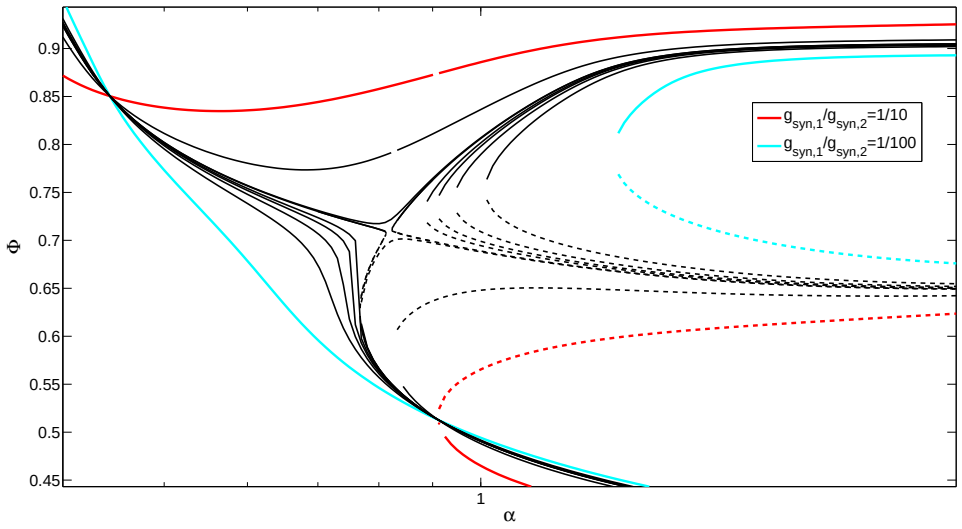

Figure 54: Zoomed in region for E-I coupled Hodgkin-Huxley neurons showing the intersection of a saddle-node point and a stable branch of solutions. The black curves are the results for $1/100 < h < 1/10$.

a very similar bifurcation as occurring between the $h = 2/3$ and $h = 1/3$ cases. We observe a saddle-node point intersecting a branch of solutions, this time stable (Fig. 54). Overall we see that there is a region of no phase-locking for all values of $h \geq 1$. This region exists at smaller values of the synaptic rate constant (slower synapses). For the identical and $h = 2/3$ cases we do see a stable, phase-locked solution return at the saddle-node bifurcations that occur at the smallest value of α. As expected we see no symmetry in any of the bifurcation diagrams.

In the E-I cases the bifurcation diagrams of equilibrium phase-difference versus the synaptic rate constant for h and h^{-1} are not simply reflections about the anti-phase axis as we saw in the E-E and I-I coupled systems. We plot the bifurcation diagram for $h = 1, 3/2, 3$ and 10 (Fig. 55). For the identical case we observe 4 saddle-node bifurcations at $(\alpha = 0.13\,\mathrm{ms}^{-1}, \Phi = 0.72)$, $(\alpha = 0.25\,\mathrm{ms}^{-1}, \Phi = 0.89)$, $(\alpha = 1.16\,\mathrm{ms}^{-1}, \Phi = 0.21)$ and $(\alpha = 4.68\,\mathrm{ms}^{-1}, \Phi = 0.03)$. For the $h = 3/2$ case we observe three saddle-node bifurcations with the fourth seemingly occurring at α just greater than $5\,\mathrm{ms}^{-1}$. The three saddle-node points are located at $(\alpha = 0.15\,\mathrm{ms}^{-1}, \Phi =$

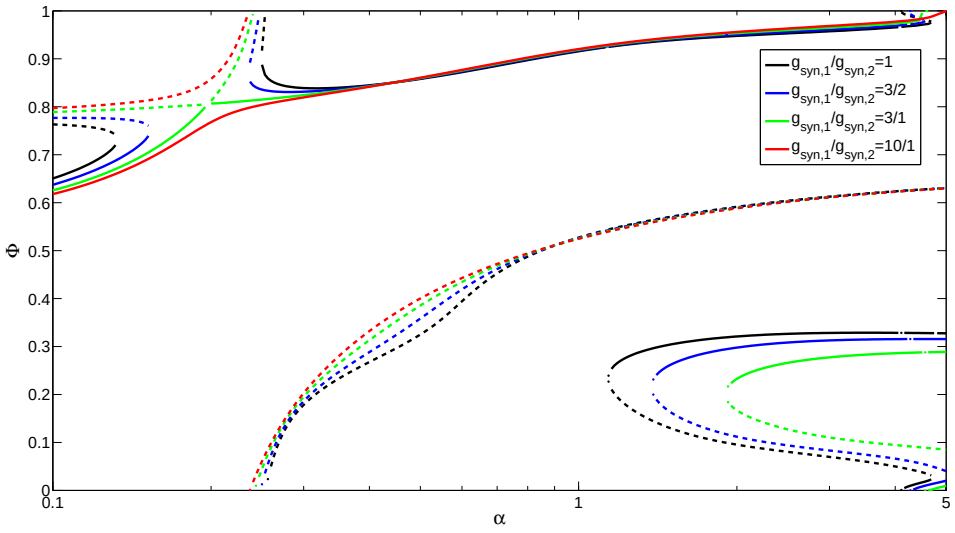

Figure 55: Bifurcation diagram of equilibrium phase-difference versus the synaptic rate constant for E-I coupled Hodgkin-Huxley neurons. The color coding in this figure represents the inverse of what we generally used throughout the thesis. In this case all values of $h \geq 1$. Since there is no obvious "identical" case we have to explore a wide spectrum of h to understand how the equilibrium is effected by coupling strength.

0.75), ($\alpha = 0.24\,\mathrm{ms}^{-1}, \Phi = 0.85$) and ($\alpha = 1.41\,\mathrm{ms}^{-1}, \Phi = 0.24$). We see similar qualitative results for $h = 3$ with saddle-node points at ($\alpha = 0.19\,\mathrm{ms}^{-1}, \Phi = 0.80$), ($\alpha = 0.20\,\mathrm{ms}^{-1}, \Phi = 0.81$) and ($\alpha = 1.95\,\mathrm{ms}^{-1}, \Phi = 0.18$). The $h = 10$ case contains no bifurcations over the entire region of α that we studied. There is simply a two branches of solutions, one stable and one unstable. This qualitative change is the result of a transcritical bifurcation that occurs at a value of h very near to 3. We can see that the two saddle-node points almost intersect when $h = 3$. The $h = 10$ case is the only case where we observe a stable, phase-locked solution predicted over the entire range of α. Values of $h > 10$ all resulted in nearly identical bifurcation diagrams. We calculated the bifurcation diagram for truly one-way coupling and found that it nearly overlapped the $h = 10$ case (Fig. 56). From this we conclude that one way coupling is more stable when the coupling is inhibitory. In fact, the bifurcation diagram with the largest region of no phase-locked solution was the case

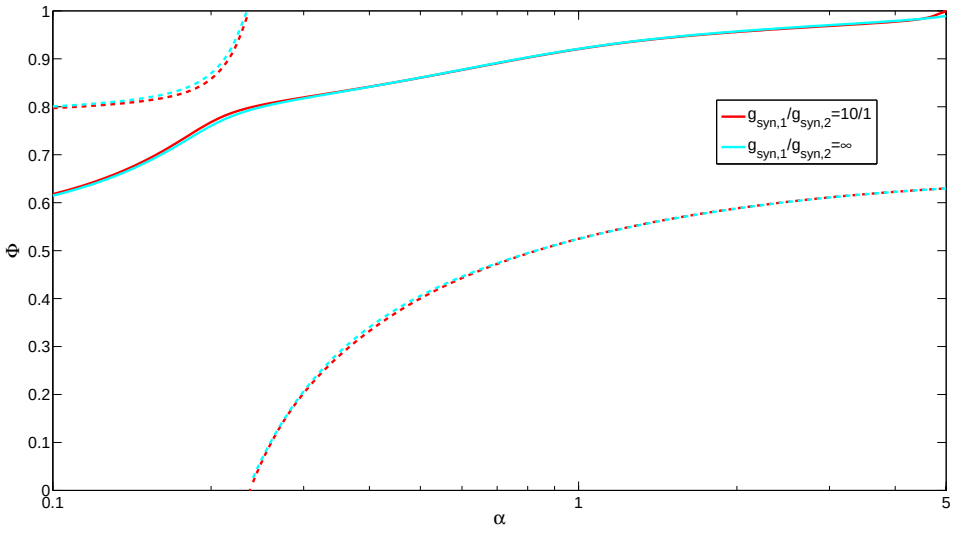

Figure 56: Bifurcation diagram of equilibrium phase-difference versus the synaptic rate constant for E-I coupled Hodgkin-Huxley neurons. We see that the case of $h = 10$ (red) is nearly one way coupling as it is almost completely overlapped by the truly one way coupling case (cyan) where $h = \infty$ or specifically $g_{syn,1} = 0.1\ \frac{\text{mS}}{\text{cm}^2}$ and $g_{syn,2} = 0\ \frac{\text{mS}}{\text{cm}^2}$.

where we assume the coupling was one way and excitatory. For the type II, Hodgkin-Huxley neurons our observations lead to the conclusion that the inhibitory synapse leads to more robust synchronization than the excitatory synapse.

5.2 Excitatory to inhibitory coupled Wang-Buzsaki neurons

The second case we examine is that of an E-I coupled pair of Wang-Buzsaki neurons. We use the same approach as in the previous section studying E-I coupled Hodgkin-Huxley neurons. For $h = 1, 2/3, 1/3$, and $1/10$ we observed a region of no phase locking for all values of h and the regions of no phase locking were larger than both the E-E and I-I coupled cases (Fig. 57). For all four values of h a single saddle-node bifurcation was observed. For the $h = 1$ case a saddle-node bifurcation occurred at ($\alpha = 5.74\ \text{ms}^{-1}$, $\Phi = 1$). As we increase α a stable and unstable pair of solution branches emanate from the saddle-node point. The stable branch decreases in Φ from

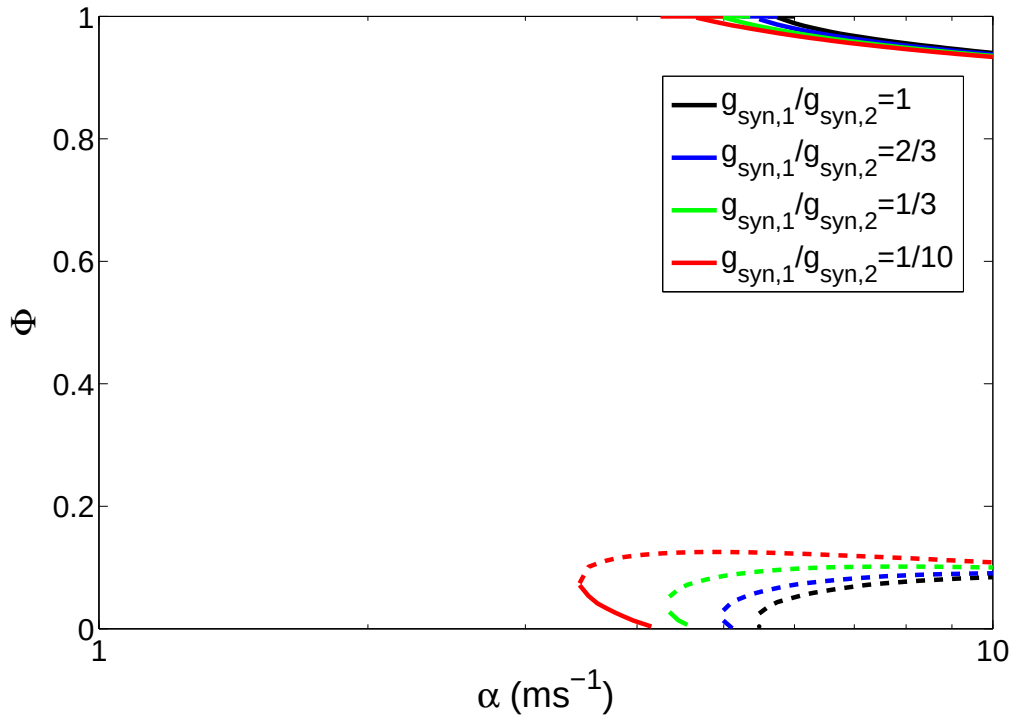

Figure 57: Bifurcation diagram of equilibrium phase-difference versus the synaptic rate constant for E-I coupled Wang-Buzsaki neurons. The color coding is consistent with previous figures indicating the value of $h = g_{syn,1}/g_{syn,2}$.

$\Phi = 1$ and the unstable branch increases in Φ from $\Phi = 0$. For $h = 2/3$ a saddle-node bifurcation occurs at ($\alpha = 5.00\,\mathrm{ms}^{-1}$, $\Phi = 0.01$). Increasing α from the saddle-node point results in a stable and unstable pair of solution branches. For $h = 1/3$ a saddle-node bifurcation occurs at ($\alpha = 4.35\,\mathrm{ms}^{-1}$, $\Phi = 0.03$). When we increase α from the saddle-node point results in a stable and unstable pair of solution branches. For $h = 1/10$ a saddle-node bifurcation occurs at ($\alpha = 3.45\,\mathrm{ms}^{-1}$, $\Phi = 0.07$). Increasing α from the saddle-node point results in a stable and unstable pair of solution branches. The stable and unstable pair of solution branches for each case approach the stable and unstable solution branches, respectively, of the $h = 1$ case as α is increased. We further examined the E-I coupled Wang-Buzsaki system with $h = 1/100$ and $h = 1/1000$ (Fig. 58). When $h = 1/100$ we again see a single saddle-node bifurcation which occurs at ($\alpha = 2.87\,\mathrm{ms}^{-1}$, $\Phi = 0.1$). When $h = 1/1000$ there is a saddle-node

bifurcation at ($\alpha = 2.80\,\mathrm{ms}^{-1}$, $\Phi = 0.11$). As in previous cases, a stable and unstable pair of solution branches are created at the saddle-node bifurcation point. As α is increased they approach the stable and unstable pair of solution branches for the $h = 1$ case. The position of the saddle-node bifurcation point hardly moves between the $h = 1/100$ and $h = 1/1000$ cases. The coupling has essentially become one way at this point.

In general E-I coupled Wang-Buzsaki neurons are less likely to synchronize over the same region of parameter space which we studied E-E and I-I cases. We conclude from this study that faster synapses synchronize E-I coupled type I neurons better than slow synapses. It is possible that other bifurcations occur at values of $\alpha > 10\,\mathrm{ms}^{-1}$ which may lead to a more rich bifurcation structure. We have restricted our region of study to be consistent with previous cases. From the data we have produced, a single saddle-node bifurcation is the fundamental bifurcation of E-I coupled Wang-Buzsaki neurons.

As in the E-I Hodgkin-Huxley system, we also need to examine how values of $h > 1$ effect results. We plot results for $h = 1$, $3/2$, and 3 (Fig. 59). For all these values we see no qualitative difference from the bifurcation diagrams with $h \leq 1$. The only observable change is that the saddle-node point moves slightly to higher values of α. We did not observe any phase-locked solutions for $h = 10$. We assume that a saddle-node point does exist for a value of $\alpha > 10\,\mathrm{ms}^{-1}$. Overall we see that for the type I, Wang-Buzsaki neurons one way coupling via an excitatory synapse is somewhat more robust in synchronizing the pair than via an inhibitory synapse.

5.3 Mammalian respiration

Identifying and understanding the neuronal mechanism controlling breathing in mammals is an active area of research in neuroscience today. There is a great deal of debate

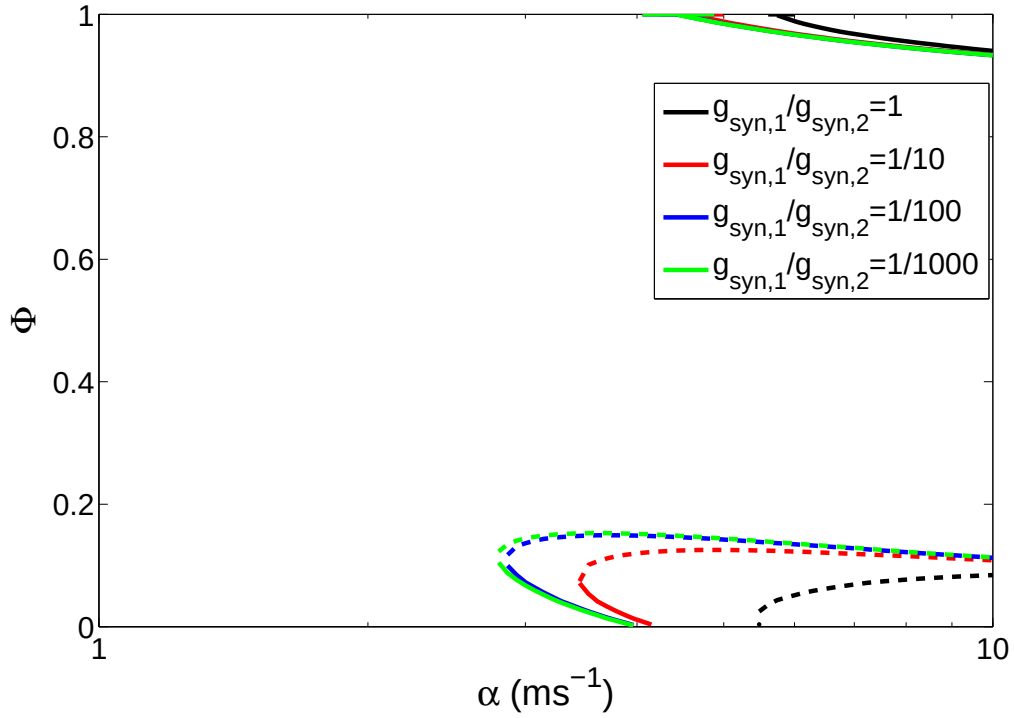

Figure 58: Bifurcation diagram of equilibrium phase-difference versus the synaptic rate constant for E-I coupled Wang-Buzsaki neurons. The color coding indicating the value of $h = g_{syn,1}/g_{syn,2}$ is different than in previous figures. The color coding is $h = 1$ (black), $h = 1/10$ (red), $h = 1/100$ (blue), $h = 1/1000$ (green). Solid lines indicate stable fixed points of equilibrium phase, dashed lines indicate unstable, fixed points of equilibrium phase-difference.

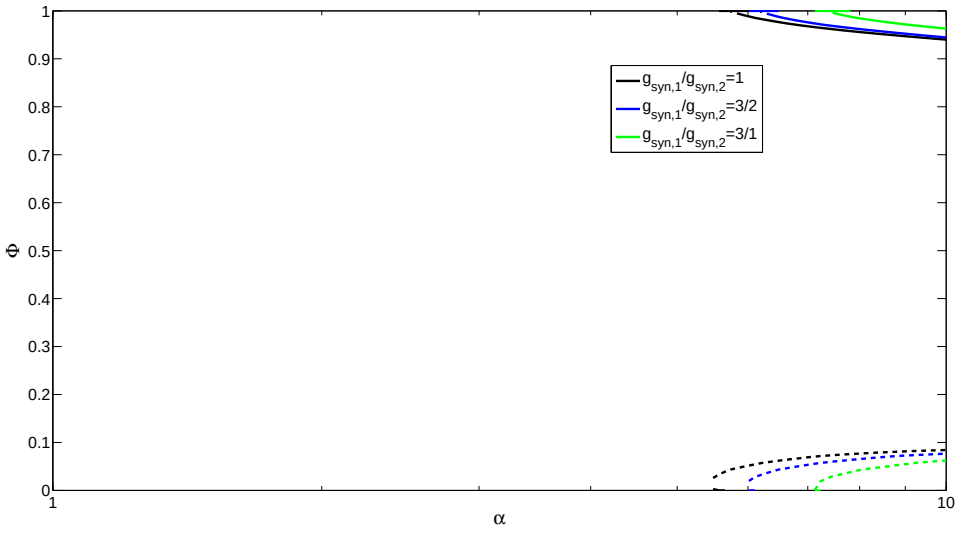

Figure 59: Bifurcation diagram of equilibrium phase-difference versus the synaptic rate constant for E-I coupled Wang-Buzsaki neurons. We plot three cases all for $h \geq 1$.

ongoing about exactly which complexes of neurons are important in respiratory control and the nature of the synchronous relationships between them. We focus on one specific aspect of the problem.

Two distinct regions of the brain, the pre-Bötzinger complex (pre-BötC) [33] and the parafacial respiratory group (pFRG) [27, 28] have been identified to contain pacemaker neurons involved in respiratory control. These regions show synchronized bursting behavior with respect to one another. An effect known as quantal slowing has been observed with the introduction of μ-opiates which effect the excitability and the intrinsic frequency of the pre-BötC [24]. Quantal slowing refers to changes from $1:1$ synchrony to $1:n$ synchrony where n is an integer.

> Opioids slow I (pre-BötC) but not pre-I (pFRG), neuronal burst periods. In slices opioids gradually lengthened respiratory periods, whereas in more intact preparations, periods jumped nondeterministically to integer multiples of the control period (quantal slowing). [24].

The "slice" that is referred to only contains the pre-BötC. The "more intact preparation" contains the pre-BötC and pFRG. Each population may be considered as an oscillator in isolation.

We wish to capture quantal slowing behavior as a result of parameter changes which are similar to the effects to the opioids using a simple coupled phase model. By reducing the complexity of the problem to a coupled phase model it maybe possible to flush out the truly important parts of these complex networks. In this thesis we show that many 1:n synchronous states exist in our phase model and depend on the parameters in a way that is consistent with the experimental application of the opiate. We model the two rhythm generating regions of the brain as a coupled pair of theta oscillators with excitatory to inhibitory coupling.

$$\dot{\theta_1} = \omega_1\{(1-\cos\theta_1) + [\beta_1 + s_{21}H(\Theta_A - \theta_2)](1+\cos\theta_1)\} \tag{61}$$

$$\dot{\theta_2} = \omega_2\{(1-\cos\theta_2) + [\beta_2 + s_{12}H(\Theta_A - \theta_1)](1+\cos\theta_2)\} \tag{62}$$

The phase of the pre-BötC is given by θ_1 and the phase of the pFRG by θ_2. For oscillator i, ω_i is the intrinsic frequency, β_i is the excitability, $s_{i,j}$ is the coupling strength and Θ_A is the duty cycle (the amount of time during the period that the population is firing spikes) assuming the cycle starts at $\theta_i = 0$. The introduction of the opiate is modeled by a reduction of the parameter β_1 or ω_1.

Searching for $1:n$ coupled states is beyond the scope of the weak coupling approximation that we have used for most of this thesis. In order to determine the existence of various m:n synchronous states we analyze the return maps of the coupled phase oscillators. We show some example time series data (Fig. 60, 61, 62) and examples of a first return map (Fig. 63) and a second return map (Fig. 64). We summarize the results in the table (Table 1). We found that reducing the excitability and/or frequency which mimics the results of the application of the μ-opiates in the experiments, does indeed result in a quantal slowing effect. This is a first step showing

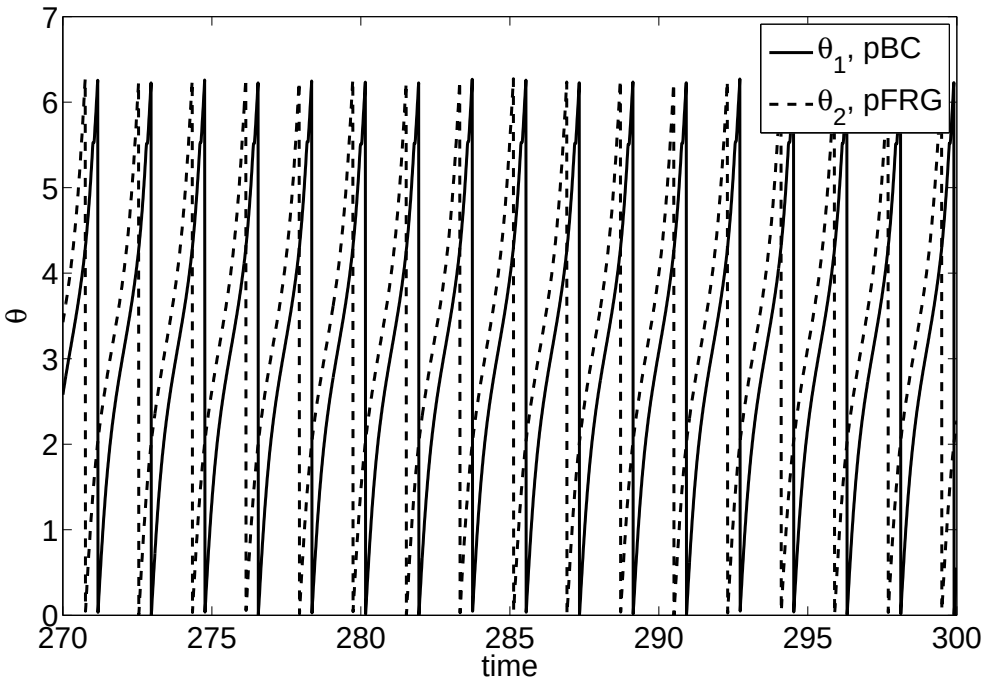

Figure 60: An example time series plot of θ_1 and θ_2 showing a 1:1 stable, synchronous state. $\omega_1 = \omega_2 = 1$, $\beta_1 = \beta_2 = 3.1$.

that this phase model can produce similar phase relationships to what is observed between the pre-BötC and pFRG.

5.4 Discussion

In our studies of E-I coupled Hodgkin-Huxley and Wang-Buszaki neurons we found that no amount of heterogeneity in synaptic coupling yielded symmetric bifurcation diagrams of equilibrium phase-difference versus synaptic rate constant. For the Hodgkin-Huxley system we observed that we could move the system around two cusp points that occurred for $1/3 < h < 2/3$ and $1/100 < h < 1/10$. Although there are still multiple cusp points in the system they do not occur simultaneously at a single value of h as with the E-E and I-I coupled systems. The inherent heterogeneity of the E-I coupling is not able to "balanced" or "canceled out" by any amount of heterogeneity in coupling strength. In general, for the E-I coupled, type II Hodgkin-Huxley

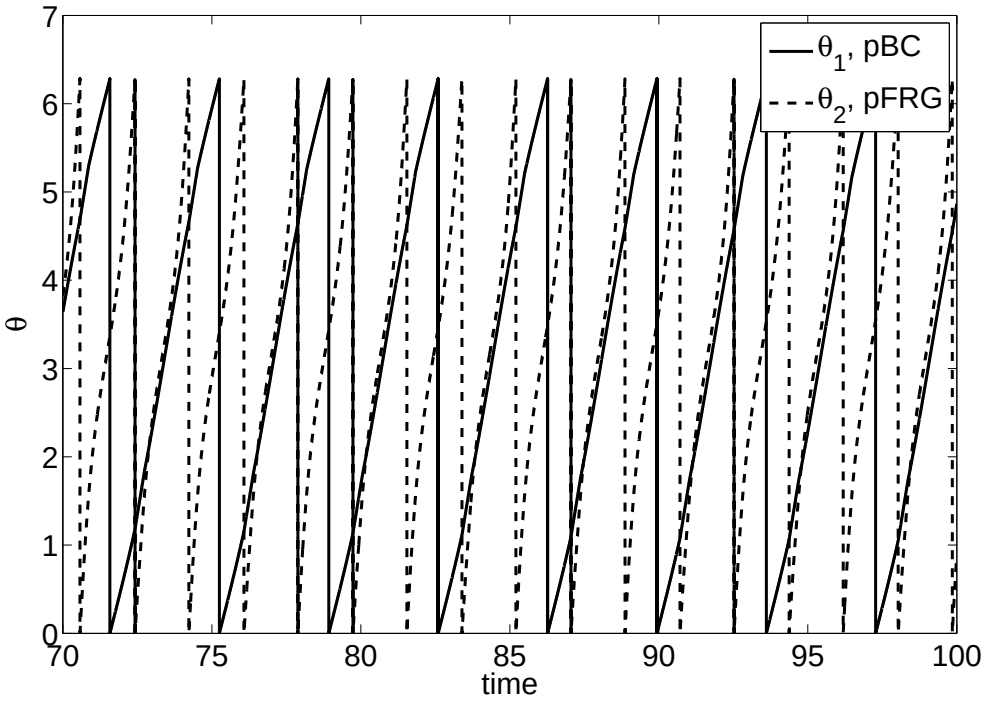

Figure 61: An example time series plot of θ_1 and θ_2 showing a 1:2 stable, synchronous state. $\omega_1 = \omega_2 = 1$, $\beta_1 = 0.6665$ and $\beta_2 = 3.1$.

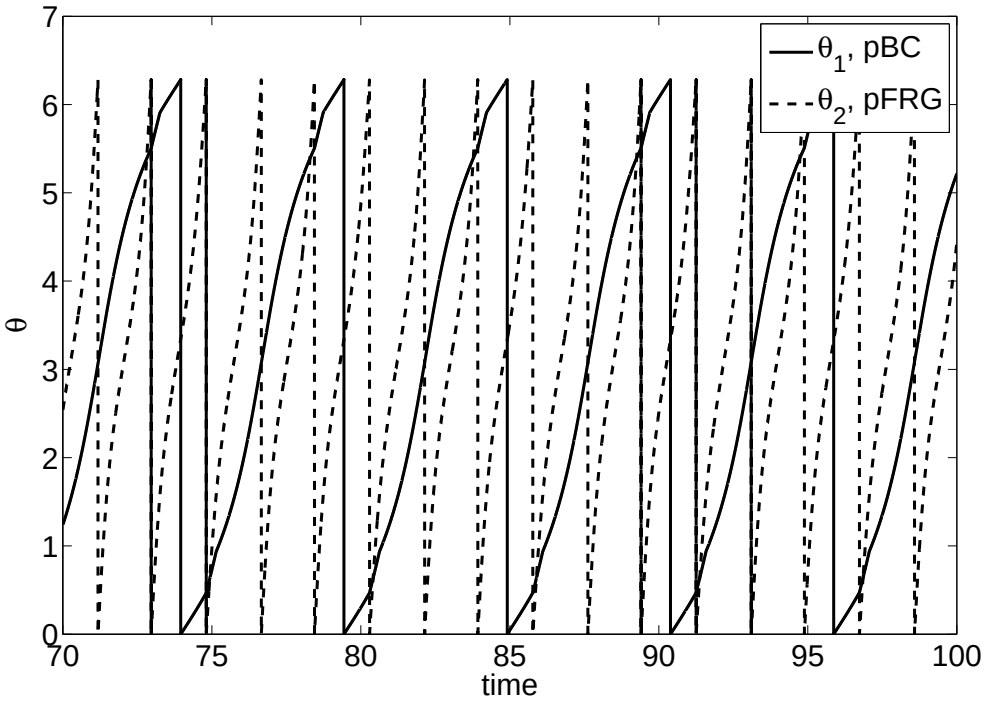

Figure 62: An example time series plot of θ_1 and θ_2 showing a 1:3 stable, synchronous state. $\omega_1 = \omega_2 = 1$, $\beta_1 = 0.2604$ and $\beta_2 = 3.1$.

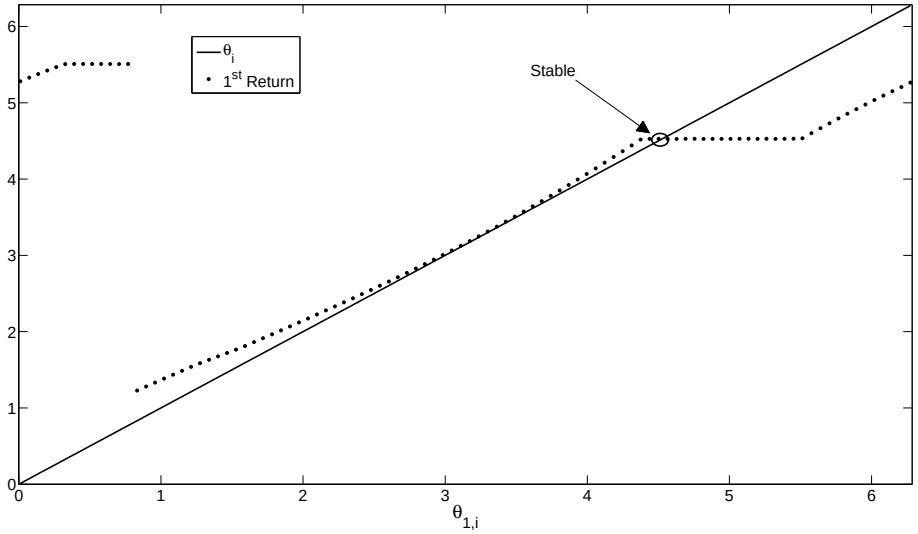

Figure 63: An example return map which shows a stable, 1:1 synchronous state exists. $\omega_1 = \omega_2 = 1$, $\beta_1 = \beta_2 = 3.1$.

n (θ_1)	m (θ_2)	ω_1	ω_2	β_1	β_2
1	1	1	1	3.1	3.1
1	2	1	1	0.6665	3.1
1	3	1	1	0.2604	3.1
1	4	1	1	0.1147	3.1
1	5	1	1	0.04867	3.1
1	1	1	1	1.8	2
1	2	1	1	0.38	2
1	3	1	1	0.123	2
1	2	1	1	0.055	0.5
1	7	1	1	0.00445	0.5
1	9	1	1	0.0026	0.5
1	15	1	1	0.00095	0.5
1	16	1	1	0.000825	0.5
1	2	0.46	1	0.23	0.5
1	3	0.34	1	0.17	0.5
1	4	0.27	1	0.135	0.5
1	5	0.23	1	0.115	0.5
1	6	0.2	1	0.1	0.5
1	7	0.175	1	0.0875	0.5
1	9	0.14	1	0.07	0.5
1	1	0.9	1	0.45	0.5
1	1	0.45	0.5	0.25	0.5

Table 1: n:m synchronization data from analyzing return maps for Eq. 62. $s_{21} = 0.4 = -s_{12}$ for all the data shown.

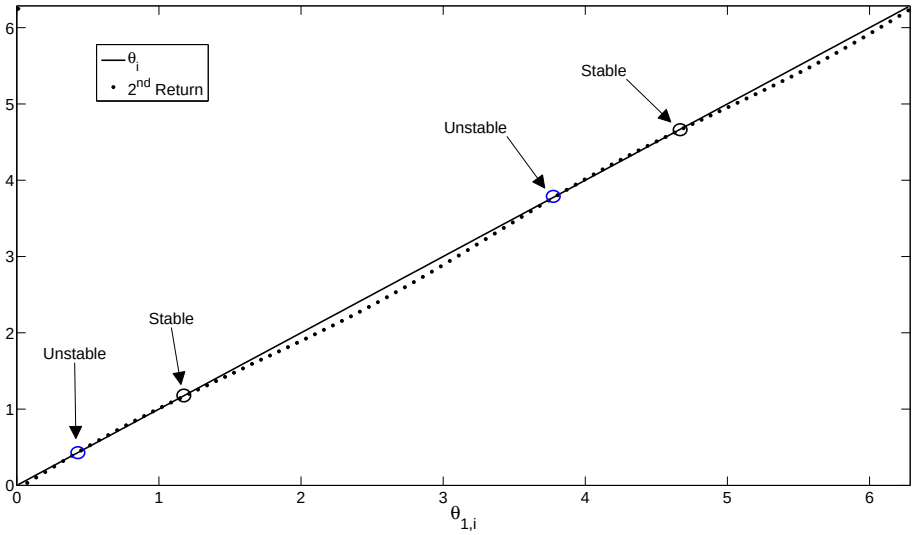

Figure 64: An example return map which shows a stable, 1:2 synchronous state exists. $\omega_1 = \omega_2 = 1$, $\beta_1 = 0.6665$ and $\beta_2 = 3.1$.

systems we always saw regions of no phase-locking until the coupling became one way inhibitory coupling. For the Wang-Buzsaki cases we saw large regions with no phase-locked solutions. No amount of heterogeneity caused these regions to disappear. We saw no evidence of any cusp points in the E-I coupled Wang-Buzsaki system over the entire range of α and h that we studied. We observed the region of no phase-locking to be minimized for the E-I coupled, type I Wang-Buzsaki system when we essentially were in a one way coupling situation with an excitatory synapse. Mutually coupled Hodgkin-Huxley neurons with one excitatory and one inhibitory synapse synchronize much more robustly than Wang-Buzsaki neurons.

We also examined another E-I coupled system consisting of coupled theta oscillators. These oscillators were used to model the behavior of two populations of neurons exhibiting periodic bursting behavior. Our goal was to show that various $1 : n$ coupled states exist in the system, which is necessary to support phenomena known as quantal slowing. In our quantal slowing study, we have shown that our coupled phase model has various stable 1:n synchronous states. We have also shown by varying parameters

which have an effect in our coupled phase model similar to introducing opiates in [24] that we can change between different 1:n synchronous states. Multistability of different 1:n states would need to be shown in order for our coupled phase model to more qualitatively match the dynamics of the quantal slowing experiments. Jumping between 1:n states was observed when the amount of opiate was unchanged.

CHAPTER VI

CONCLUSION

This thesis was an exhaustive study of heterogeneously coupled neurons. We studied a wide range of heterogeneities in coupling strength. We also explored neurons mutually coupled by excitatory to excitatory (E-E), inhibitory to inhibitory (I-I) and excitatory to inhibitory synapses (E-I).

We found a great deal of symmetry when comparing cases of E-E coupled Hodgkin-Huxley neurons and I-I coupled Wang-Buzsaki neurons as well as I-I coupled Hodgkin-Huxley neurons with E-E coupled Wang-Buzsaki neurons. This lead us to speculate that qualitatively E-E (I-I) coupled Type II neurons had the same bifurcation structure of equilibrium phase-difference versus the synaptic rate constant as I-I (E-E) coupled Type I neurons. This speculation is an area where future research could be performed. We showed that in all cases with the same type of synapse coupling the two neurons together, a multiple cusp bifurcation structure existed. Understanding why this structure results from the coupling of these types of neurons would help us to say with more confidence what we previously speculated.

Now that we understand a multiple cusp structure underlies the various E-E and I-I cases, we have a better understanding of what is observed in experiments of mutually coupled pairs of neurons. If the experimenter calculates a phase response curve (PRC) for both neurons, they are able to estimate h for their system. They can do this because in the weak coupling regime the PRC linearly depends upon the coupling strength [30]. If they are using similar neurons, ratios of the peak values of the calculated PRC's are roughly the same as ratios of synaptic conductance.

Numerical verification of the results of using the weak coupling approximation

through solving the full set of equations for a system has been lacking in most published literature using this technique. We showed good agreement between the results of the weak coupling approximation and those from full numerical simulations for all the E-E and I-I coupled cases that we studied.

In our studies of E-I coupled Hodgkin-Huxley neurons we found that two cusp points existed. We also found that only when the coupling had essentially become one way with an inhibitory synapse was there a stable solution of equilibrium phase-difference for the entire range of α studied. The E-I coupled Wang-Buzsaki system had a large region of no phase-locked solution and had only a single saddle-node bifurcation as it's entire bifurcation structure. As in the previous E-E and I-I coupled systems the coupled Wang-Buzsaki system exhibited a greater sensitivity to the heterogeneity imposed by E-I coupling, shown by a much larger region with no phase-locked solution when compared to the E-I coupled Hodgkin-Huxley system.

Our final study did not use the weak coupling approximation. We wanted to show that various $1 : n$ coupled states exist in a system of E-I coupled theta oscillators. This system was used to model two coupled populations of neurons that exhibit periodic bursting behavior. A phenomena known as quantal slowing was observed in experiments when an opiate was applied reducing the excitability of one of the populations [19]. By changing the parameters of our system in a way similar to how the opiate effects the neuron populations *in vitro* we observed various $1 : n$ states. Using this simple two dimensional model in future studies may allow us to understand what are the fundamental and important parts of these complex networks involved in respiratory control in mammals.

REFERENCES

[1] Amitabha, B., Kopell, N., and Terman, D., "Almost-synchronous solutions for mutually coupled excitatory neurons," *Physica D*, pp. 69–94, 2000.

[2] Crawford, J., "Introduction to bifurcation theory," *Rev. Mod. Phys.*, vol. 63, no. 4, pp. 991–1037, 1991.

[3] Cvitanovic, P., Artuso, R., Mainieri, R., Tanner, G., and Vattay, G., *Chaos: Classical and Quantum*. Niels Bohr Institute, 2009. www.ChaosBook.org.

[4] Ermentrout, G., *Simulating, Analyzing, and Animating Dynamical systems: A guide to XPPAUT for Researchers and Students*. SIAM, 2002.

[5] Ermentrout, G. and Kopell, N., "Oscillator death in systems of coupled neural oscillators," *SIAM J. Appl. Math.*, vol. 50, no. 1, pp. 125–146, 1990.

[6] Hansel, D. and Mato, G., "Patterns of synchrony in a heterogeneous hodgkin-huxley neural network with weak coupling," *Physica A*, pp. 662–669, 1993.

[7] Hansel, D., Mato, G., and Meunier, C., "Phase dynamics for weakly coupled hodgkin-huxley neurons," *Europhys. Lett.*, vol. 23, pp. 367–372, 1993.

[8] Hansel, D., Mato, G., and Meunier, C., "Synchrony in excitatory neural networks," *Neural Computation*, no. 7, pp. 307–337, 1995.

[9] Hodgkin, A., "The local electric changes associated with repetitive action in a non-medulated axon," *Journal of Physiology*, vol. 107, pp. 165–181, 1948.

[10] Hodgkin, A. and Huxley, A., "The components of membrane conductance in the giant axon of *Loligo*," *Journal of Physiology*, vol. 116, pp. 473–496, 1952.

[11] Hodgkin, A. and Huxley, A., "Currents carried by sodium and potassium ions through the membrane of the giant axon of *Loligo*," *Journal of Physiology*, vol. 116, pp. 449–472, 1952.

[12] Hodgkin, A. and Huxley, A., "The dual effect of membrane potential on sodium conductance in the giant axon of *Loligo*," *Journal of Physiology*, vol. 116, pp. 497–506, 1952.

[13] Hodgkin, A. and Huxley, A., "A quantitative description of membrane current and its application to conduction and excitation in nerve," *Journal of Physiology*, vol. 116, pp. 507–544, 1952.

[14] Hodgkin, A., Huxley, A., and Katz, B., "Measurement of current-voltage relations in the membrane of the giant axon of *Loligo*," *Journal of Physiology*, vol. 116, pp. 424–448, 1952.

[15] Izhikevich, E., "Multiple cusp bifurcations," *Neural Networks*, vol. 11, pp. 495–508, 1998.

[16] Izhikevich, E., *Dynamical Systems in Neuroscience*. The MIT Press, 2007.

[17] Izhikevich, E. and Hoppensteadt, F., *Weakly connected neural networks*. Springer, 1997.

[18] Izhikevich, E., "Phase equations for relaxation oscillators," *SIAM Journal on Applied Mathematics*, vol. 60, no. 5, 2000.

[19] Janczewski, W. and Feldman, J., "Distinctive rhythm generators for inspiration and expiration in the juvenile rat," *J Physiol*, vol. 570, no. 2, pp. 407–420, 2006.

[20] Kuramoto, Y., *Checmical Oscillations, Waves and Turbulence*. Springer, New York, 1984.

[21] Li, Y., Wang, Y., and Miura, R., "Clustering in small networks of excitatory neurons with heterogeneous coupling strengths," *Journal of Computational Neuroscience*, no. 14, pp. 139–159, 2003.

[22] Malkin, I., "Methods of poincare and liapunov in theory of non-linear oscillations," 1949.

[23] Malkin, I., "Some problems in nonlinear oscillation theory," 1956.

[24] Mellen, N., Janczewski, W., Bocchiaro, C., and Feldman, J., "Opiod induced quantal slowing reveals dual networks for repiratory rhythm generation," *Neuron*, vol. 37, pp. 821–826, 2003.

[25] Moler, C., *Numerical computing with Matlab*. SIAM, 2004.

[26] Morris, C. and Lecar, H., "Voltage oscillations in the barnacle giant muscle fiber," *Biophysics Journal*, vol. 35, pp. 193–213, 1981.

[27] Onimaru, H., Arata, A., and Homma, I., "Localization of respiratory rhythm-generating neurons in the medulla of brainstem-spinal cord preparations from newborn rats.," *Neuroscience Letters*, vol. 78, pp. 151–155, 1987.

[28] Onimaru, H. and Homma, I., "A novel funtional neuron group for respiratory rhythm generation innn the ventral medulla," *Journal of Neuroscience*, vol. 23, pp. 1478–1486, 2003.

[29] Prescott, S., Koninck, Y., and Sejnowski, T., "Mechanisms of action potential initiation," *PLoS Biology*, vol. 4, no. 10, 2008.

[30] Preyer, A. and Butera, R., "Neuronal oscillators in *Aplysia californica* that demonstarate weak couplin *In Vitro*," *Physical Review Letters*, vol. 95, no. 138103, 2005.

[31] Rinzel, J. and Ermentrout, G., *Methods in neuronal modeling*, ch. Analysis of neural excitability and oscillations, pp. 135–169. MIT Press, 1989.

[32] Sieling, F., Canavier, C., and Prinz, A., "Predictions of phase-locking in excitatory hybrid networks: excitation does not promote phase-locking in pattern-generating networks as reliably as inhibition," *Journal of Neurophysiology*, vol. 102, pp. 69–84, 2009.

[33] Smith, J., Ellenberger, H., Ballanyi, K., Richter, D., and Feldman, J., "Pre-botzinger complex: a brainstem region that may generate respiratory rhythm in mammals," *Science*, vol. 254, pp. 726–729, 1991.

[34] Song, S., Sjöström, P. J., Reigl, M., Nelson, S., and Chklovskii, D., "Highly nonrandom features of synaptic connectivity in local cortical circuits," *PLoS Biology*, vol. 3, no. 3, p. e68, 2005.

[35] Strogatz, S., *Nonlinear Dynamics and Chaos*. Perseus Books, 1994.

[36] Terman, D., Kopell, N., and Bose, A., "Dynamics of two mutually coupled slow inhibitory neurons," *Physica D*, vol. 117, pp. 241–275, 1998.

[37] Van Vreeswijk, C., Abbott, L., and Ermentrout, G., "When inhibition not excitation synchronizes neural firing," *J. Computat. Neurosci.*, vol. 1, pp. 313–321, 1994.

[38] Wang, X. and Buzsaki, G., "Gamma oscillation by synaptic inhibition in a hippocampal interneuronal network model," *Journal of Neuroscience*, vol. 16, pp. 6402–6413, 1996.

[39] White, J., Chow, C., Ritt, J., Soto-Tervino, C., and Kopell, N., "Synchronization and oscillatory dynamics in heterogeneous, mutually inhibited neurons," *J. Computat. Neurosci.*, vol. 5, pp. 5–16, 1998.

VITA

Patrick Justin Bradley was born in Philadelphia, Pennsylvania and grew up in Ambler, Pennsylvania. Patrick attended Wissahickon High School and graduated in 1995. He received an A.S. in Physical Science from Montgomery County Community College in Blue Bell, Pennsylvania in December 1999. In June 2003 Patrick was awarded a B.S. in Physics from Drexel University in Philadelphia. He started graduate school in August 2003 and completed his Ph.D. in Physics in Spring 2010.